Application of Phosphoproteomics in Glioma

– A targeted mass spectrometric analysis of phosphopeptides –

Lona Moradi - Zeneyedpour

ISBN: 978-94-6419-600-9
Cover : Ilse Modder – www.ilsemodder.nl
Lay-out: Ilse Modder – www.ilsemodder.nl
Printing: Gildeprint – www.gildeprint.nl

Application of Phosphoproteomics in Glioma

– A targeted mass spectrometric analysis of phosphopeptides –

Toepassing van phosphoproteomics in glioma

– Een gerichte massaspectrometrische analyses van fosfopeptide –

Proefschrift

Ter verkrijging van de graad van doctor aan de
Erasmus Universiteit Rotterdam
op gezag van de
rector magnificus
prof.dr. A.L. Bredenoord

en volgens besluit van het college voor promoties.
De openbare verdediging zal plaatsvinden op
dinsdag 22 november 2022 om 13.00 uur
door

Lona Moradi-Zeneyedpour
geboren te Ahvaz, Iran

Erasmus University Rotterdam

Promotiecommissie:

Promotor:
Prof. dr. P.A.E. Sillevis Smitt

Overige leden:
Prof. dr. J.M. Kros
Prof. dr. C.R. Jimenez
Prof. dr. C.M.F. Dirven

Copromotor:
Dr. T.M. Luider

TABLE OF CONTENTS

1

INTRODUCTION

MASS SPECTROMETRY

Over the last two decades, proteomics has become an important technique in biological research due to improvements in sample preparation and liquid chromatography-mass spectrometry instrumentation. The introduction of high-resolution mass spectrometers with quadrupole functionality – such as the Orbitrap Fusion series – enabled sensitive targeting of proteins with high-resolution MS/MS fragmentation methods [1, 2]. Recent studies showed also large improvement in the sensitivity for targeted detection of phosphopeptides using parallel reaction monitoring, even outperforming data-dependent acquisition experiments with two-dimensional fractionation [1, 3]. Proteomics and phosphoproteomics analyses have, therefore, become a powerful tool to analyze clinical samples [4, 5].

PHOSPHOPROTEOMICS

The workflow of phosphoproteomics applied for studying specific phospho-sites is important to study dysregulation in cancer [6, 7]. Most phosphopeptides are low-abundant and still can be successfully measured with MS. An enrichment method such as metal oxide affinity chromatography or immobilized metal affinity chromatography is needed to identify these low-abundant phosphopeptides. These enrichment methods are often combined with fractionation methods such as strong cation or anion exchange chromatography, electrostatic repulsion–hydrophilic interaction chromatography, or high-pH reversed-phase chromatography [8].

MUTATED AND POST-TRANSLATIONALLY MODIFIED TUMOR ANTIGENS

Autoantibodies are generated against epitopes of self-antigens. In cancer, autoantibodies can be generated against tumor antigens, which can stem from mutations and post-translational modifications (PTM) [9]. Amino-acid mutated and post-translationally modified antigens can have similar reactivity [10]. However, post-translationally modified antigens are less investigated [11, 12]. These mutations and post-translational modifications may potentially have great value for the diagnosis, prognosis, and targeted therapy of cancers [3, 13]. Mutations can have impact on protein structure and stability, protein function, subcellular localization and protein-protein interactions [3, 14]. These mutations can have a direct effect in oncogenesis, and progression of cancer and drug resistance in cancer treatment [15].

Phosphorylation is one of the most common and best studied PTM in proteins [16, 17]. Up to 30% of all human proteins can be phosphorylated [18, 19]. Most phosphorylation events are observed in the serine, threonine, and tyrosine amino acid moieties of a protein. Phosphorylation regulates for instance cell growth, differentiation, apoptosis and cell signaling in eukaryotes. Studies have shown that dysregulation of protein phosphorylation can play an important role in cancer development [19-22]. A few studies have shown that a specific phosphopeptide site can be seen as a tumor-specific antigen. This type of tumor antigen can be derived from dysregulated cell signaling pathways in various cancers, and has the potential to be beneficial in cancer immunotherapy developments [23-25].

ISOLATION OF ANTIBODIES

There are several techniques to isolate antibodies from body fluids; e.g., ammonium sulfate precipitation and affinity purification using protein A, protein G or ion exchange chromatography [26, 27]. Alternatively, Melon Gel resin can be used also for immunopurification. In this way, non-immunoglobulin proteins bind to the Melon Gel resin and immunoglobulins can be collected directly in the flow-through. Several research groups have successfully used Melon Gel resin to purify IgG from body fluids in combination with MS [28-30].

SCOPE OF THIS THESIS

The goal of this thesis is detection and quantification using MS of phosphopeptides in glioma. To realize this goal, we applied phosphoproteomics and state-of-the-art MS to clinical samples. **Chapter 2** describes the detection of a protein coding mutation using MS. Detecting somatic mutation-derived neoantigens in early disease stages can be valuable for diagnostic purpose. PTM-derived-antigens have been less well studied than amino acid mutation neoantigens. These PTM-derived antigens can be detected with MS. The available phosphoproteomics approaches to detect these phosphopeptide antigens are discussed and investigated in **Chapter 3**. We introduced an MS-based method to accurately and precisely determine phosphorylation levels for specific phosphorylation sites in a sensitive, relatively fast, and reproducible way in glioma-derived cell lines. Next, this method was applied in brain tumor tissue samples obtained from glioma patients. Using this MS-based method, we were able to quantify phosphorylation ratios of specific phospho-sites in formalin-fixed paraffin embedded (FFPE) and fresh-frozen brain tissue (**Chapter 4**). **Chapter 5** describes an MS-based approach to determine if a tumor-specific phosphopeptide can raise autoantibodies in glioma patients. Using a novel application of Melon Gel resin, we could demonstrate the presence of EGFR autoantibodies, reactive

with a tumor-specific phosphopeptide, in plasma from patients with high-grade glioma. Implications of the results of the studies in this thesis are addressed in the general discussion in **Chapter 6**.

REFERENCES

1. Lawrence, R. T.; Searle, B. C.; Llovet, A.; Villen, J., Plug-and-play analysis of the human phosphoproteome by targeted high-resolution mass spectrometry. *Nat Methods* **2016,** 13, (5), 431-4.
2. Osinalde, N.; Aloria, K.; Omaetxebarria, M. J.; Kratchmarova, I., Targeted mass spectrometry: An emerging powerful approach to unblock the bottleneck in phosphoproteomics. *J Chromatogr B Analyt Technol Biomed Life Sci* **2017,** 1055-1056, 29-38.
3. Lin, T. T.; Zhang, T.; Kitata, R. B.; Liu, T.; Smith, R. D.; Qian, W. J.; Shi, T., Mass spectrometry-based targeted proteomics for analysis of protein mutations. *Mass Spectrom Rev* **2021**, e21741.
4. The path of biomolecular mass spectrometry into open research. *Nature Communications* **2019,** 10, (1), 4029.
5. Iwamoto, N.; Shimada, T., Recent advances in mass spectrometry-based approaches for proteomics and biologics: Great contribution for developing therapeutic antibodies. *Pharmacology & Therapeutics* **2018,** 185, 147-154.
6. Gerritsen, J. S.; White, F. M., Phosphoproteomics: a valuable tool for uncovering molecular signaling in cancer cells. *Expert Rev Proteomics* **2021,** 18, (8), 661-674.
7. Ruprecht, B.; Lemeer, S., Proteomic analysis of phosphorylation in cancer. *Expert Review of Proteomics* **2014,** 11, (3), 259-267.
8. Low, T. Y.; Mohtar, M. A.; Lee, P. Y.; Omar, N.; Zhou, H.; Ye, M., Widening the Bottleneck of Phosphoproteomics: Evolving Strategies for Phosphopeptide Enrichment. *Mass Spectrom Rev* **2021,** 40, (4), 309-333.
9. Benvenuto, M.; Mattera, R.; Masuelli, L.; Tresoldi, I.; Giganti, M. G.; Frajese, G. V.; Manzari, V.; Modesti, A.; Bei, R., The crossroads between cancer immunity and autoimmunity: antibodies to self antigens. *Front Biosci (Landmark Ed)* **2017,** 22, 1289-1329.
10. Hogan, K. T.; Eisinger, D. P.; Cupp Iii, S. B.; Lekstrom, K. J.; Deacon, D. D.; Shabanowitz, J.; Hunt, D. F.; Engelhard, V. H.; Slingluff Jr, C. L.; Ross, M. M., The peptide recognized by HLA-A68.2-restricted, squamous cell carcinoma of the lung-specific cytotoxic T lymphocytes is derived from a mutated elongation factor 2 gene. *Cancer Research* **1998,** 58, (22), 5144-5150.
11. Solleder, M.; Guillaume, P.; Racle, J.; Michaux, J.; Pak, H.-S.; Müller, M.; Coukos, G.; Bassani-Sternberg, M.; Gfeller, D., Mass Spectrometry Based Immunopeptidomics Leads to Robust Predictions of Phosphorylated HLA Class I Ligands*. *Molecular & Cellular Proteomics* **2020,** 19, (2), 390-404.
12. Zeneyedpour, L.; Sten-van, T. H. J.; Luider, T., Using phosphoproteomics and next generation sequencing to discover novel therapeutic targets in patient antibodies. *Expert Rev Proteomics* **2020,** 17, (9), 675-684.
13. Wang, Q.; Chaerkady, R.; Wu, J.; Hwang, H. J.; Papadopoulos, N.; Kopelovich, L.; Maitra, A.; Matthaei, H.; Eshleman, J. R.; Hruban, R. H.; Kinzler, K. W.; Pandey, A.; Vogelstein, B., Mutant proteins as cancer-specific biomarkers. *Proc Natl Acad Sci U S A* **2011,** 108, (6), 2444-9.
14. Reva, B.; Antipin, Y.; Sander, C., Predicting the functional impact of protein mutations: application to cancer genomics. *Nucleic Acids Res* **2011,** 39, (17), e118.
15. Tan, Z.; Zhu, J.; Stemmer, P. M.; Sun, L.; Yang, Z.; Schultz, K.; Gaffrey, M. J.; Cesnik, A. J.; Yi, X.; Hao, X.; Shortreed, M. R.; Shi, T.; Lubman, D. M., Comprehensive Detection of Single Amino Acid Variants and Evaluation of Their Deleterious Potential in a PANC-1 Cell Line. *J Proteome Res* **2020,** 19, (4), 1635-1646.
16. Duan, G.; Walther, D., The roles of post-translational modifications in the context of protein interaction networks. *PLoS computational biology* **2015,** 11, (2), e1004049.
17. Ramazi, S.; Zahiri, J., Post-translational modifications in proteins: resources, tools and prediction methods. *Database* **2021,** 2021, baab012.
18. Cohen, P., The origins of protein phosphorylation. *Nature Cell Biology* **2002,** 4, (5), E127-E130.
19. Ardito, F.; Giuliani, M.; Perrone, D.; Troiano, G.; Lo Muzio, L., The crucial role of protein phosphorylation in cell signaling and its use as targeted therapy (Review). *Int J Mol Med* **2017,** 40, (2), 271-280.
20. Singh, V.; Ram, M.; Kumar, R.; Prasad, R.; Roy, B. K.; Singh, K. K., Phosphorylation: Implications in Cancer. *Protein J* **2017,** 36, (1), 1-6.
21. Jhaveri, K.; Burris Rd, H. A.; Yap, T. A.; Hamilton, E.; Rugo, H. S.; Goldman, J. W.; Dann, S.; Liu, F.; Wong, G. Y.; Krupka, H.; Shapiro, G. I., The evolution of cyclin dependent kinase inhibitors in the treatment of cancer. *Expert Rev Anticancer Ther* **2021,** 21, (10), 1105-1124.
22. Garcia-Garcia, T.; Poncet, S.; Derouiche, A.; Shi, L.; Mijakovic, I.; Noirot-Gros, M.-F., Role of Protein

Phosphorylation in the Regulation of Cell Cycle and DNA-Related Processes in Bacteria. *Frontiers in Microbiology* **2016,** 7, (184).

23. Cobbold, M.; De La Peña, H.; Norris, A.; Polefrone, J. M.; Qian, J.; English, A. M.; Cummings, K. L.; Penny, S.; Turner, J. E.; Cottine, J.; Abelin, J. G.; Malaker, S. A.; Zarling, A. L.; Huang, H. W.; Goodyear, O.; Freeman, S. D.; Shabanowitz, J.; Pratt, G.; Craddock, C.; Williams, M. E.; Hunt, D. F.; Engelhard, V. H., MHC class I-associated phosphopeptides are the targets of memory-like immunity in leukemia. *Sci Transl Med* **2013,** 5, (203), 203ra125.
24. Mahoney, K. E.; Shabanowitz, J.; Hunt, D. F., MHC Phosphopeptides: Promising Targets for Immunotherapy of Cancer and Other Chronic Diseases. *Mol Cell Proteomics* **2021,** 20, 100112.
25. Engelhard, V. H.; Obeng, R. C.; Cummings, K. L.; Petroni, G. R.; Ambakhutwala, A. L.; Chianese-Bullock, K. A.; Smith, K. T.; Lulu, A.; Varhegyi, N.; Smolkin, M. E.; Myers, P.; Mahoney, K. E.; Shabanowitz, J.; Buettner, N.; Hall, E. H.; Haden, K.; Cobbold, M.; Hunt, D. F.; Weiss, G.; Gaughan, E.; Slingluff, C. L., Jr., MHC-restricted phosphopeptide antigens: preclinical validation and first-in-humans clinical trial in participants with high-risk melanoma. *J Immunother Cancer* **2020,** 8, (1).
26. Bergmann-Leitner, E. S.; Mease, R. M.; Duncan, E. H.; Khan, F.; Waitumbi, J.; Angov, E., Evaluation of immunoglobulin purification methods and their impact on quality and yield of antigen-specific antibodies. *Malaria Journal* **2008,** 7, (1), 129.
27. Grodzki, A. C.; Berenstein, E., Antibody purification: ammonium sulfate fractionation or gel filtration. *Methods Mol Biol* **2010,** 588, 15-26.
28. Singh, V.; Stoop, M. P.; Stingl, C.; Luitwieler, R. L.; Dekker, L. J.; van Duijn, M. M.; Kreft, K. L.; Luider, T. M.; Hintzen, R. Q., Cerebrospinal-fluid-derived immunoglobulin G of different multiple sclerosis patients shares mutated sequences in complementarity determining regions. *Mol Cell Proteomics* **2013,** 12, (12), 3924-34.
29. Broodman, I.; de Costa, D.; Stingl, C.; Dekker, L. J.; VanDuijn, M. M.; Lindemans, J.; van Klaveren, R. J.; Luider, T. M., Mass spectrometry analyses of κ and λ fractions result in increased number of complementarity-determining region identifications. *Proteomics* **2012,** 12, (2), 183-91.
30. Barnidge, D. R.; Dasari, S.; Botz, C. M.; Murray, D. H.; Snyder, M. R.; Katzmann, J. A.; Dispenzieri, A.; Murray, D. L., Using mass spectrometry to monitor monoclonal immunoglobulins in patients with a monoclonal gammopathy. *J Proteome Res* **2014,** 13, (3), 1419-27.

2

NEOANTIGENS IN CHRONIC OBSTRUCTIVE PULMONARY DISEASE AND LUNG CANCER, A POINT OF VIEW

Lona Zeneyedpour[1], Lennard J.M. Dekker[1], Jenny J.M. van Sten-van `t Hoff[1], Peter C. Burgers[1], Nick H.T. ten Hacken[2], Theo M. Luider[1]

[1)] Department of Neurology, Erasmus Medical Center, Rotterdam, The Netherlands
[2)] Department of Pulmonology, University Medical Center Groningen (UMCG)/ University of Groningen (RUG).

Proteomics Clinical Applications. 2019, 13(2):e1800093

ABSTRACT

The goal of this manuscript is to explore the role of clinical proteomics for detecting mutations in COPD and lung cancer by mass spectrometry technology. COPD and lung cancer caused by smoking are most likely linked by challenging the immune system via partly shared pathways. GWAS have identified several single nucleotide polymorphisms (SNPs) which predispose an increased susceptibility to COPD and lung cancer. In lung cancer this leads to coding mutations in the affected tissues, development of neoantigens and different functionality and abundance of proteins in specific pathways. If a similar reasoning can also be applied in COPD is discussed. The Technology of Mass spectrometry has developed into an advanced technology for proteome research detecting mutated peptides or proteins and finding relevant molecular mechanisms which will enable predicting the response to immunotherapy in COPD and lung cancer patients.

INTRODUCTION

The importance of neoantigens for lung cancer (LC) is well-acknowledged. However, it is interesting to research a possible role of neoantigens in COPD by using mass spectrometry technology. This manuscripts starts with describing the role of neoantigens, followed by an introduction of COPD and lung cancer and an analysis of the link between COPD and LC.

Some statistics on mortality on COPD and LC give insight differences in developing and underdeveloped regions. A section on genomics is followed by an analysis of how to detect neoantigens by mass spectrometry.

Neoantigens

Neoantigens are antigens that deviate from own structures that change into protein structures that can be recognized by the immune system. They can be linked to DNA repair mutations and generate increased tumor infiltrating lymphocytes (TILs). Neoantigens correlate with increased expression of multiple pro-inflammatory cytokines and immune-related genes, MI-polarized macrophage genes, PD-L1 and PD-1[1]. Identifying individual mutations by exosome-sequencing is desirable for developing neoantigen-targeted cancer immunotherapies that aim to activate cytotoxic T cells and control tumor progression by major histocompatibility complex (MHC) molecules[2]. T cells can recognize neoantigens and can mediate immune responses against tumor cells containing these neoantigens[3]. To identify candidate neoantigens high-throughput next generation sequencing (NGS) and whole-exome sequencing (WES) is used[4, 5]. The use of WES combined with in silico peptide translation has become a promising approach to detect patient-specific neoantigens[6].

Chronic Obstructive Pulmonary Disease (COPD)

COPD is a leading cause of death worldwide, smoke being widely accepted as one of the most important causes. COPD is characterized by airflow obstruction in the lung and symptoms related to decreased expiratory volume.

An important modulator of the immune system is the regulatory T cell (Treg). Tregs are involved in the suppression of smoke induced specific immune response and a diminished presence or function of these cells may underlie the development of specific humoral immune response in COPD [7]. Damage in the lung by COPD is caused by oxidative stress, inflammatory cytokine release, protease activity and auto-antibody expression[6]. Shorter telomeres are associated with COPD and short telomere length may contribute to inflammation in COPD and increases susceptibility to emphysema[6]. Systematic inflammation associated with COPD might cause an increase in Apo M expression and there are two single nucleotide polymorphisms (SNPs) flanking the Apo M gene involved

that are associated with altered lung function[8]. COPD is identified with an elevated ROS (reactive oxygen species) level and ROS are able to change biological molecules, signaling pathways and anti-oxidant molecule functions and a decrease in the level of PTEN and SIRT1 in COPD. This can lead to activation in COPD of the mTOR-aging pathway via P13K activation by ROS, resulting in reduced antioxidant defense by FOXO3A inhibition and a loss of autophagy[9].

GWAS have identified several single nucleotide polymorphisms (SNPs) which predispose an increased susceptibility to COPD and lung cancer (LC) such as SERPIN2, HHIP, FAM13A, IREB2, CHRNA3 and CHRNA5[10].

Single nucleotide variants in COPD observed in GWAS studies are for a part missense mutations, that generate differences in proteins that are hardly investigated on the protein level. The impracticality to measure large numbers of missense mutated peptides chosen from these GWAS studies hampers an assessment from a technical point of view. Also the possible presence of neo-antigens, i.e. antigens that originate from own structures that change into protein structures that can be recognized by the immune system [11], in COPD and lung cancer is hampered by the sensitivity of mass spectrometry to detect and identify peptides derived of neo-antigens and it is even debated if neo-antigens exist in COPD [12].

Lung Cancer

Lung cancer (LC) has become one of the leading causes of death with smoke as the main etiologic factor [13, 6]. Lung cancer is caused by mutations in oncogenes [6], leading to the proliferation of mutated cells and the formation of a tumor. Genome-wide association studies (GWAS) identified over 500 SNPs influencing cancer risk and downstream targets for at least three genes were enriched by cell cycle genes involved in G1/S transition. A history of emphysema is the highest risk factor for long cancer among_smokers [14]. Molecular profiles in non-small cell lung cancer generate ideas to develop molecular targeting agents that inhibit the growth signals resulting from driver mutations. EGFR and anaplastic lymphoma kinase inhibitors, such as PD1 immunotherapy, become the key drugs for long cancer treatment [2]. Immunological checkpoint blockade therapies targeting cytotoxic T-lymphocyte antigen-4 (CTLA-4), programmed cell death-1 (PD-1 and programmed death ligand-1 (PD-L1)) have been shown to have remarkable benefits for the treatment of lung cancer [2]. Research by Chae and co-workers[1] showed that the immunophenotype of lung adenocarcinoma can be seen as a primary infiltration by activated CD4 and CD8 cells.

The link between COPD and Lung Cancer

COPD and lung cancer are interrelated diseases with substantial mortality and most

probably an immunological link may exist between the two diseases [15]. However, their pathophysiologic mechanisms are not yet fully understood [16]. The increased risk of lung cancer in COPD patients suggests the existence of a two-fold altered cell-mediated immune response in COPD patients: dysregulation of T-cells in the lungs and T-cell exhaustion [16]. Activation of nuclear transcription factor (NF)-kB may have a crucial role in the development of lung cancer from COPD. NF-kB activation increases the release from inflammatory mediators that can induce COPD, and also inhibits apoptosis, induces proliferation and accelerates cancer development [14].The high prevalence of lung cancer in COPD suggests that there may be common mechanisms, such as premature aging in lung tissue, genetic predispositions to either disease or common pathogenic factors such as growth factors, activation of intracellular pathways or epigenetics [6]. Various mechanisms to explain the association between COPD and lung cancer include genetic susceptibility, deoxyribonucleic acid (DNA) damage and repair, epigenetics, downregulation of specific microRNA, expression of pro-inflammatory genes induced by hypoxia, tumor growth factor-B and integrins, telomere length and dysfunction[17]. Telomere shortening is a risk factor in COPD and lung cancer[6].

Chronic inflammation through the induction of several interleukins and cyclooxygenase-2 activity may be an important player in the lung tumor formation among patients with COPD. For instance, CCL21 may favor cancer cell migration in the lungs of patients with COPD [13]. Oxidative damage and antioxidant depletion may contribute to a greater risk to lung carcinogenis, especially in patients with underlying COPD [13]. An epigenome wide association study identified that DNA methylation and repression of 2 genes,CCDC37 and MAP1B, was significantly associated with both COPD and lung cancer [6]. COPD leads to changes in lipid profiles including increased ceramide levels in lung tissue by high density lipoprotein [8]. These changes in lipid metabolism in turn may alter other physiological responses, including the hypoxia response and EGFR signaling and may play a role in the link between COPD and lung cancer [6].

STAT3 and its downstream genes , such as CBLN1, CBLN2, FGL1, FOX03, GJB1, HNF4α,TMEM27 and TTR, are differentially changed in both lung adenocarcinoma and COPD [18]. The tumor suppressor protein p53 is a general inhibitor of inflammation; its gene, TP53, is often mutated by cigarette smoke and may be suppressed by oxidant activation of NF-kB mediated inflammation [14]. Exposing human bronchial epithelial cells to PM2.5 (particulate matter 2.5, the mass per cubic meter of air of particles with a size of less than 2.5 micrometres) induces a significant upregulation of vascular endothelial growth factor A (VEGA) production. Macroautophagy/autophagy is induced upon PM2.5 exposure and then mediates VEGA upregulation by activating the SRC-CTA3 pathway in bronchial epithelial cells[19]

Mutational signature analysis in a study by Xiao and co-workers[10] suggests that there was no specific mutation pattern during the development of LC associated with COPD. The high concordance in the mutational burden and spectra further suggests that the inflammatory environment surrounding the tumor cells does not generate new mutations in lung adenocarcinoma (LUAD) patients, but integrative analysis of DNA methylation and transcriptome profiling demonstrates that the presence of COPD is associated with changes in methylation and expression in genes involved in immune response in NSCLC. Loss of PARK2 (encoding Parkin) increases the expression of proinflammation factors as well as nuclear NF-kB localization, suggesting a role of PARK2 loss in inflammation, and PARK2 deficiency promotes genomic instability and cell transformation, so PARK 2 might have a tumor suppressor role in the development of COPD and lung cancer [20].

SNP variation-associated inflammatory genes identified between COPD and lung cancer may play critical roles in a COPD-LC transformation; activated nAchRs (nicotinic acetylcholine receptor gene) in COPD may cause mutation and down-regulates the expression of the crucial tumor suppressor gene TP53 and P53-related signaling pathways, causing lung tumorigenesis [21, 22].

Saber and co-workers[23] showed that COPD is not associated with the presence of KRAS mutations as observed in lung cancer, whereas presence of EGFR mutations was more frequent in non-COPD as compared to COPD lung patients. Their findings that EGFR mutations are more common in non-COPD lung patients might indicate that lung cancer development depends on activating EGFR mutations in non-COPD patients. Lim and co-workers[24] argue that COPD is not a prognostic factor in advanced NSCLC patients, however, COPD had a negative impact on the overall survival of NSCLC patients in the smoker and stage IV subgroup.

Genome-wide association studies (GWAS) have shown that large numbers of coding variants can have effects on the susceptibility of COPD [25-27]. Although these coding variants have a significant effect on the susceptibility for COPD, the heterogeneity of the disease does not allow yet to translate this knowledge into clinical applicable molecular tools to identify those individuals which are susceptible for COPD and will develop lung cancer. Very recently, therapeutic antibodies that effect the immune system such as atezolizumab for lung cancer have been introduced with considerable results in the treatment of NSCLC (non-small cell lung carcinoma) compared to classical chemotherapy treatment (docetaxel, cisplatinum, gemcitabine) in case of advanced disease (for review see[28, 29]). In general, for COPD no medication is available that cures the disease and the developed drugs for lung cancer have shown no effect in COPD although the number of studies on this topic is rather limited. It is suggested that an immunological link exists between the two diseases [15, 16], so detailed investigation can be highly rewarding for

developing knowledge on possible treatment of COPD.

Mortality for COPD and LC

COPD (chronic obstructive pulmonary disease) and lung cancer are heterogeneous diseases that are for a large part (85% (man) and 69% (female) for instance in the Dutch situation (2018)) linked causatively by the use of cigarettes (RIVM; www.jellinek.nl). [16, 30] In Table 1 the global situation and the situation in the continents is presented. From this table one can notice that in the developed world (Europe, Oceania and North America) similar ratios of mortality for COPD and LC can be observed. In developing and underdeveloped regions the cause of COPD and LC is much more linked to indoor pollution[31-34].

Table 1: Annual mortality in COPD (2010) and Lung Cancer (2015)

Number of deaths[a)]	COPD	Lung Cancer	Ratio COPD/Lung cancer
Global Continents	2,837,877	1,823,929	1.55
Europe	267,451	387,913	0.69
Oceania	10,256	11,822	0.87
North Amerika	167,299	173,278	0.96
South America	117,865	62,922	1.87
Asia	2,159,952	1,068,862	2.02
Africa	103,325	37,748	2.71

a) Source: For COPD – Burney et al. (2015).[35] . For lung cancer–WHO Globocan (http://www-dep.iarc.fr/WHOdb/WHOdb.htm)

Genomics

The recently published COPD Gene investigators study [36] indicates that rarely found genetic variants were enriched in specific pathways such as the transforming growth factor beta pathway, the hedgehog pathway and the cilia-related pathway in a relatively large cohort (n =2543) of COPD patients and controls who were not affected by smoking. The criteria used were GOLD grade 3 and 4 (https://goldcopd.org/); FEV< 50% post-bronchodilator age less than 65 for the patient group and for the control group frequency-matched pack years of cigarette smoking, FEV1 > 80%, age >65, no significant emphysema. For instance for proteins CTC1, OR5B12, GTF3C5, BLVRB, SLC7A7, SLC 26A7 and Notch2 coding mutations were found for COPD[36]. In general, GWAS studies until now do not result into a molecular or a genetic clinical test. Most ideally patients can be categorized for these missense mutations and treated for COPD in a much earlier phase besides prevention and assistance in the cessation of smoking in a very early stage.

The risk of developing lung cancer is 8 times higher if COPD has been diagnosed[30, 37]. Different molecular mechanisms related to inflammation, to innate immune responses and to carcinogenic processes are affected in COPD and lung cancer [38] These molecular

mechanisms are most likely defense mechanisms to the chemical exposure of smoke in the lung. Research by Lambrechts and co-workers showed that rs1051730 on chromosome 15q24/25 is associated with the presence and severity of emphysema and they discussed a shared pathogenic mechanism in COPD and lung cancer[22]. As mentioned above, anti-PD-L1 antibody (e.g. atezolizumab) has revolutionized the treatment of NSCLC patients and has been approved in 2016[39] by the FDA. For COPD such a treatment does not yet exist and therapeutic antibodies to proteins of the innate system (cytokines) have not proven to be successful [40]. However, a better understanding of mechanisms of the development of COPD can hopefully lead to the finding of key regulated molecules that can be effectively targeted by drugs or therapeutic antibodies. Research by Mark and co-workers [15] showed that PD1 expression was increased in tumors of COPD patients and the presence of COPD was associated with longer progression-free survival of patients treated with immune checkpoint inhibitors.

The enormous efforts in GWAS and cohort studies [8, 10, 20] in which NGS is performed on cellular materials of patients with COPD and lung carcinoma open ways to investigate these pathways on a protein level [41], especially, if specific coding mutations or neoantigens specific for COPD or lung cancer can be identified [36]. As a consequence the affected molecular mechanism (e.g. immune response or inflammation) can be targeted or modulated in a way beneficial for the patient.

Neoantigens and mass spectrometry of missense mutations

The presence of a high number of clonal neoantigens in homogeneous lung adenocarcinoma(LUAD) may favor immune surveillance, whereas in lung squamous cell carcinoma (LUSC) immune escape may be more prevalent through HLA downregulation and a high clonal neoantigen burden in LUAD is associated with an inflamed microenvironment with activated T cells, potentially regulated by inhibitory immune checkpoint molecules and their ligands [42]. Immune checkpoint inhibitors have shown significant therapeutic responses against tumors containing increased mutation-associated neoantigen load [43]. Direct proteomic analysis of MHC ligands by liquid chromatography and tandem mass spectrometry (LS-MS/MS) enables discovery of neoantigens directly from cancer cells [44]. The success of checkpoint inhibitor therapies underlines the notion that tumor-specific T cell responses pre-exist in patients with lung cancer and are kept under tight control via immune modulatory mechanisms [45]. In non-small lung cancer, smoking-related carcinogenesis are strongly associated with higher mutation rate and immunotherapy response, and the presence of neoantigen-specific T cells in the peripheral blood demonstrates that some neoantigens are capable of including T cell reactivity[3].

Recent proteomic approaches provide a comprehensive way to analyze whole HLA ligandomes containing various types of TAAs and direct peptide isolation from live cells using antibodies directed against HLA molecules followed by LC-MS/MS sequencing is an ideal strategy to map and screen natural T-cell epitopes presented by cancer cells [46].

Neoantigen loss occurs through elimination of tumor subclones or through deletion of chromosomal regions containing truncal alterations and were associated with changes in T cell receptor clonality. There could be two mechanisms of neoantigen loss in resistant tumor: 1) through the immune elimination of neoantigen-containing tumor cells that represent a subset of the tumor population, and 2) through the acquisition of one or more genetic events in a tumor cell that results in neoantigen loss, followed by selection and expansion of the resistant clone [43].

Frameshift neoantigens provide a unique opportunity to target common tumor-suppressor genes such as TP53 and BAP1, and frameshift indels trigger an increased quantity of neoantigens and greater mutant binding specificity [45].

Application of the epitope prediction approach to sequencing data from different cancer types reveals a range of predicted neoantigens per individual tumor, providing evidence that neoantigens are frequent in most human cancers [47].

Mass spectrometry has, in addition to the potential to identify proteins in the presence or absence of databases, the inherently present possibility of quantification of proteins and peptides in a relatively sensitive way[48]. This opens possibilities to detect missense mutations in antigens and even neo-antigens in biopsies and body fluids.

By mass spectrometry coding mutations can be detected and quantified on the protein level and in heterozygous patients the ratio of the wildtype and mutated protein can be determined.

It is particularly of interest if the abundance of these variants is influenced by the presence of COPD. Hereafter, an example is given of the detection of a mutation in isocitrate dehydrogenase (*IDH1*) on position 132 of this protein [49, 50] which is observed in various tumors including lung carcinoma. The example in figure 1 describes a mutation at positon 132, where an arginine (R) is replaced by a histidine (H). The difference in weight between the mutated and the normal peptide can be observed in the mass spectrum. However, the mutation dictates the size of the tryptic peptide and the composition of aminoacids in the peptide. Sometimes specific enzymes (Lys-N or chymotrypsin) ought to be applied to technically realize the visualization of these mutated and normal peptides [51]. Mass spectrometry allows to measure the ratio of mutated and the corresponding normal

peptides potentially associated to a specific disease. These ratios can be determined accurately if synthetic stable isotope labelled peptides are applied.

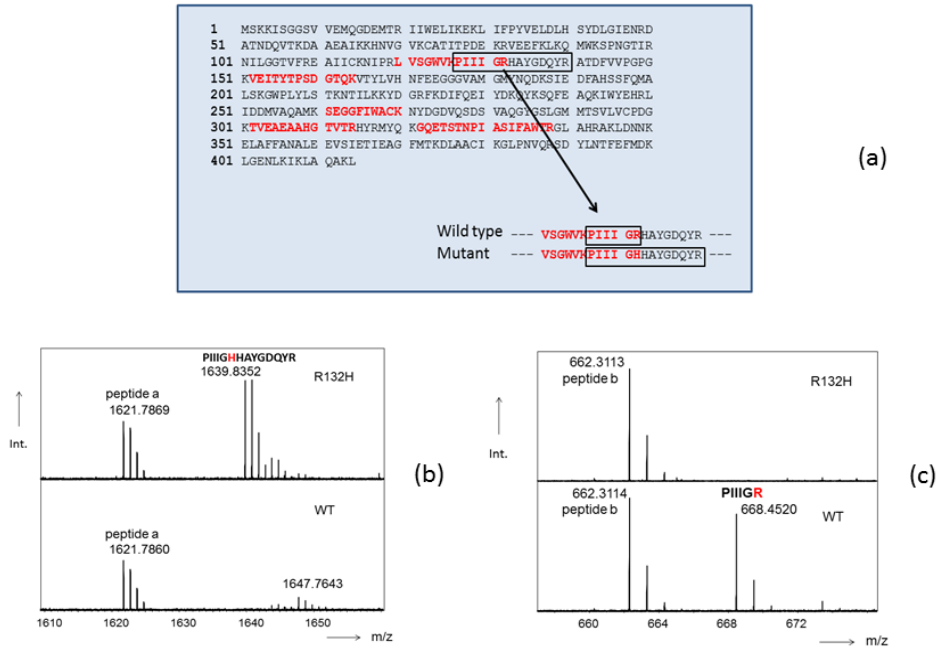

Fig. 1. ***a)*** *Primary structure of mutant IDH-1.* ***b)*** *and* ***c)*** *Partial mass spectra of mutated IDH-1(top) and wild type (WT) IDH1 digested proteins.*
Partial sequence of mutant ...RLVSGWVK **|** PIIIG**H**HAYGDQYR **|** ATDFVVPGPG... *Partial sequence wild type* ...RLVSGWVK **|** PIIIG**R|**HAYGDQYR**|** ATDFVVPGPG...*Trypsin cleavage sites are indicated with* **|**. *Peptides a and b are peptides from other proteins and they may serve as references for intensity variation observed between various samples.*

Although these missense mutations can be attractive targets for therapy, neoantigens presented on human leucocyte antigens (HLA) [52] might be even a more attractive way to find proteins that might be affected in COPD. Recently, Bassani-Sternberg and co-workers [53] have shown the possibility to detect neo-antigens in native human melanoma tissue. Neoantigens that are displayed by the MHC can be analysed by mass spectrometry (MS) and it is of interest to determine the immunopeptidome in lung tissue of COPD patients. The feasibility of this approach as described by Bassani-Sternberg and co-workers [54] shows that by MS mutated peptide ligands for HLA can be identified in relative small periods of time (three weeks) in contrast to immunological oriented studies. Intensive fractionation of peptides eluted from HLA makes it possible to identify

these neo-epitopes in proteins by mass spectrometry in a much faster way and can lead potentially to targeted approaches or specific antibody treatment for COPD, indicating that MS technology has major advantages for detecting relevant proteins.

For absolute quantitative mass spectrometric analysis of mutated proteins and mutated peptides, a stable isotope labelled peptide or protein needs to be synthesized. In this way a precise quantification can be reached for a mutated protein. Targeted mass spectrometry (SRM and PRM) allows the measurement of tens to hundreds of mutated proteins in a single analysis. A disadvantage of this technique is the sensitivity if no sample fragmentation is performed for serum or tissue samples. Without sample preparation, most often microgram/ ml biofluid can be reached. If affinity separations (e.g. by specific column chromatography materials, binders such as antibodies or affimers) are applied one can reach the ng/ml biofluid or pg protein/ gram tissue [41, 48]. These improved sample preparations and improved technology in quadrupole and high resolution detection in advanced mass spectrometers (hardware and software) will enable the large scale detection and quantitation of mutated proteins in the near future.

Specific binders for cancer associated pathways can be very instrumental to extract differentially expressed proteins from these pathways in lung biopsies. Mass spectrometry has the advantage that it is possible to define very accurately the ratios of mutated proteins in these pathways and may show proteins that can effectively modulate immunological processes involved in the induction and progression of COPD.

CONCLUSION

The idea that cancer has pre-stages is widely accepted (for reviews see [6, 55-57]). The same might hold for COPD and as the risk of lung cancer is 8 times higher in COPD patients one may assume that in a part of the COPD patients COPD is a pre-stage of lung cancer. If so, than neoantigens might also be present in COPD. Since the technology has been described, the chance to investigate this possibility in much more depth is of high interest.

GLOSSARY

CTLA-4	cytotoxic T-lymphocyte antigen-4
EGFR	epidermal growth factor receptor
GWAS	genome-wide association studies
HLA	human lymphocyte antigen
IDH1	isocitrate dehydrogenase.1
LC-MS/MS	liquid chromatography and tandem mass spectrometry
LUAD	lung adenocarcinoma
LUSC	lung squamous cell carcinoma
MHC	major histocompatibility complex
MS	mass spectrometry
nAchRs	nicotinic acetylcholine receptor gene
NGS	next-generation sequencing
NSCLC	non-small cell lung carcinoma
PD-1	programmed cell death-1
PD-L1	programmed death ligand-1
PM2.5	particulate matter 2.5
PRM	parallel reaction monitoring
ROS	reactive oxygen species
SNP	single nucleotide polymorphism
SOD	superoxide dismutase
SRM	selection reaction monitoring
STAT	signal transducer and activator of transcription
TAA	tumor associated antigen
TIL	tumor infiltrating lymphocites
VEGA	vascular endothelial growth factor A
WES	whole-exome sequencing

Acknowledgement

This work acknowledges the CliniMark e-COST (CA 16113) project.

REFERENCES

[1] Chae, Y. K., Anker, J. F., Bais, P., Namburi, S., *et al.*, Mutations in DNA repair genes are associated with increased neo-antigen load and activated T cell infiltration in lung adenocarcinoma. *Oncotarget* 2018, *9*, 7949-7960.

[2] Karasaki, T., Nagayama, K., Kawashima, M., Hiyama, N., *et al.*, Identification of Individual Cancer-Specific Somatic Mutations for Neoantigen-Based Immunotherapy of Lung Cancer. *J Thorac Oncol* 2016, *11*, 324-333.

[3] Desrichard, A., Snyder, A., Chan, T. A., Cancer Neoantigens and Applications for Immunotherapy. *Clin Cancer Res* 2016, *22*, 807-812.

[4] Gubin, M. M., Artyomov, M. N., Mardis, E. R., Schreiber, R. D., Tumor neoantigens: building a framework for personalized cancer immunotherapy. *J Clin Invest* 2015, *125*, 3413-3421.

[5] Karasaki, T., Nagayama, K., Kuwano, H., Nitadori, J. I., *et al.*, Prediction and prioritization of neoantigens: integration of RNA sequencing data with whole-exome sequencing. *Cancer Sci* 2017, *108*, 170-177.

[6] Durham, A. L., Adcock, I. M., The relationship between COPD and lung cancer. *Lung Cancer* 2015, *90*, 121-127.

[7] Brandsma, C. A., Hylkema, M. N., Geerlings, M., van Geffen, W. H., *et al.*, Increased levels of (class switched) memory B cells in peripheral blood of current smokers. *Respir Res* 2009, *10*, 108.

[8] Yu, Y., Zhang, J., Qiao, Y., Pan, L., *et al.*, Apolipoprotein M gene single nucleotide polymorphisms discovery in patients with chronic obstructive pulmonary disease and determined by the base-quenched probe technique. *Gene* 2017, *637*, 9-13.

[9] Aghasafari, P., George, U., Pidaparti, R., A review of inflammatory mechanism in airway diseases. *Inflamm Res* 2018.

[10] Xiao, D., Li, F., Pan, H., Liang, H., *et al.*, Integrative analysis of genomic sequencing data reveals higher prevalence of LRP1B mutations in lung adenocarcinoma patients with COPD. *Sci Rep* 2017, *7*, 2121.

[11] Secher, T., Guilleminault, L., Reckamp, K., Amanam, I., *et al.*, Therapeutic antibodies: A new era in the treatment of respiratory diseases? *Pharmacol Ther* 2018, *189*, 149-172.

[12] Greene, C. M., Low, T. B., O'Neill, S. J., McElvaney, N. G., Anti-proline-glycine-proline or antielastin autoantibodies are not evident in chronic inflammatory lung disease. *Am J Respir Crit Care Med* 2010, *181*, 31-35.

[13] Barreiro, E., Bustamante, V., Curull, V., Gea, J., *et al.*, Relationships between chronic obstructive pulmonary disease and lung cancer: biological insights. *J Thorac Dis* 2016, *8*, E1122-E1135.

[14] Sekine, Y., Katsura, H., Koh, E., Hiroshima, K., Fujisawa, T., Early detection of COPD is important for lung cancer surveillance. *Eur Respir J* 2012, *39*, 1230-1240.

[15] Mark, N. M., Kargl, J., Busch, S. E., Yang, G. H. Y., *et al.*, Chronic Obstructive Pulmonary Disease Alters Immune Cell Composition and Immune Checkpoint Inhibitor Efficacy in Non-Small Cell Lung Cancer. *Am J Respir Crit Care Med* 2018, *197*, 325-336.

[16] Chalela, R., Gea, J., Barreiro, E., Immune phenotypes in lung cancer patients with COPD: potential implications for immunotherapy. *J Thorac Dis* 2018, *10*, S2186-S2189.

[17] Gonzalez, J., Marin, M., Sanchez-Salcedo, P., Zulueta, J. J., Lung cancer screening in patients with chronic obstructive pulmonary disease. *Ann Transl Med* 2016, *4*, 160.

[18] Qu, P., Roberts, J., Li, Y., Albrecht, M., *et al.*, Stat3 downstream genes serve as biomarkers in human lung carcinomas and chronic obstructive pulmonary disease. *Lung Cancer* 2009, *63*, 341-347.

[19] Xu, X., Wang, H., Liu, S., Xing, C., *et al.*, TP53-dependent autophagy links the ATR-CHEK1 axis activation to proinflammatory VEGFA production in human bronchial epithelial cells exposed to fine particulate matter (PM2.5). *Autophagy* 2016, *12*, 1832-1848.

[20] Lee, S., She, J., Deng, B., Kim, J., *et al.*, Multiple-level validation identifies PARK2 in the development of lung cancer and chronic obstructive pulmonary disease. *Oncotarget* 2016, *7*, 44211-44223.

[21] Wang, D. C., Shi, L., Zhu, Z., Gao, D., Zhang, Y., Genomic mechanisms of transformation from chronic obstructive pulmonary disease to lung cancer. *Semin Cancer Biol* 2017, *42*, 52-59.

[22] Lambrechts, D., Buysschaert, I., Zanen, P., Coolen, J., *et al.*, The 15q24/25 susceptibility variant for lung cancer and chronic obstructive pulmonary disease is associated with emphysema. *Am J Respir Crit Care Med* 2010, *181*, 486-493.

[23] Saber, A., van der Wekken, A. J., Kerner, G. S., van den Berge, M., *et al.*, Chronic Obstructive Pulmonary Disease Is Not Associated with KRAS Mutations in Non-Small Cell Lung Cancer. *PLoS One* 2016, *11*, e0152317.

[24] Lim, J. U., Yeo, C. D., Rhee, C. K., Kim, Y. H., *et al.*, Overall survival of driver mutation-negative non-small cell lung cancer patients with COPD under chemotherapy compared to non-COPD non-small cell lung cancer patients. *Int J Chronic Obstr* 2018, *13*, 2139-2146.

[25] Yeo, J., Morales, D. A., Chen, T., Crawford, E. L., *et al.*, RNAseq analysis of bronchial epithelial cells to identify COPD-associated genes and SNPs. *BMC Pulm Med* 2018, *18*, 42.

[26] Wain, L. V., Shrine, N., Artigas, M. S., Erzurumluoglu, A. M., *et al.*, Genome-wide

association analyses for lung function and chronic obstructive pulmonary disease identify new loci and potential druggable targets. *Nat Genet* 2017, *49*, 416-425.

[27] Hobbs, B. D., de Jong, K., Lamontagne, M., Bosse, Y., *et al.*, Genetic loci associated with chronic obstructive pulmonary disease overlap with loci for lung function and pulmonary fibrosis. *Nat Genet* 2017, *49*, 426-432.

[28] Santini, F. C., Hellmann, M. D., PD-1/PD-L1 Axis in Lung Cancer. *Cancer J* 2018, *24*, 15-19.

[29] Santini, F. C., Rudin, C. M., Atezolizumab for the treatment of non-small cell lung cancer. *Expert Rev Clin Pharmacol* 2017, *10*, 935-945.

[30] Keller, A., Fehlmann, T., Ludwig, N., Kahraman, M., *et al.*, Genome-wide MicroRNA Expression Profiles in COPD: Early Predictors for Cancer Development. *Genomics Proteomics Bioinformatics* 2018, *16*, 162-171.

[31] Salvi, S. S., Barnes, P. J., Chronic obstructive pulmonary disease in non-smokers. *Lancet* 2009, *374*, 733-743.

[32] Salvi, S., Barnes, P. J., Is exposure to biomass smoke the biggest risk factor for COPD globally? *Chest* 2010, *138*, 3-6.

[33] Hu, G., Zhou, Y., Tian, J., Yao, W., *et al.*, Risk of COPD from exposure to biomass smoke: a metaanalysis. *Chest* 2010, *138*, 20-31.

[34] Kurmi, O. P., Semple, S., Simkhada, P., Smith, W. C., Ayres, J. G., COPD and chronic bronchitis risk of indoor air pollution from solid fuel: a systematic review and meta-analysis. *Thorax* 2010, *65*, 221-228.

[35] Burney, P. G., Patel, J., Newson, R., Minelli, C., Naghavi, M., Global and regional trends in COPD mortality, 1990-2010. *Eur Respir J* 2015, *45*, 1239-1247.

[36] Qiao, D., Ameli, A., Prokopenko, D., Chen, H., *et al.*, Whole exome sequencing analysis in severe chronic obstructive pulmonary disease. *Hum Mol Genet* 2018.

[37] Young, R. P., Hopkins, R. J., Chronic obstructive pulmonary disease (COPD) and lung cancer screening. *Transl Lung Cancer Res* 2018, *7*, 347-360.

[38] Berg, J., Halvorsen, A. R., Bengtson, M. B., Tasken, K. A., *et al.*, Levels and prognostic impact of circulating markers of inflammation, endothelial activation and extracellular matrix remodelling in patients with lung cancer and chronic obstructive pulmonary disease. *BMC Cancer* 2018, *18*, 739.

[39] Secher, T., Guilleminault, L., Reckamp, K., Amanam, I., *et al.*, Therapeutic antibodies: A new era in the treatment of respiratory diseases? *Pharmacol Ther* 2018.

[40] Brody, R., Zhang, Y., Ballas, M., Siddiqui, M. K., *et al.*, PD-L1 expression in advanced NSCLC: Insights into risk stratification and treatment selection from a systematic literature review. *Lung Cancer* 2017, *112*, 200-215.

[41] Guzel, C., Govorukhina, N. I., Wisman, G. B. A., Stingl, C., *et al.*, Proteomic alterations in early stage cervical cancer. *Oncotarget* 2018, *9*, 18128-18147.

[42] McGranahan, N., Furness, A. J., Rosenthal, R., Ramskov, S., *et al.*, Clonal neoantigens elicit T cell immunoreactivity and sensitivity to immune checkpoint blockade. *Science* 2016, *351*, 1463-1469.

[43] Anagnostou, V., Smith, K. N., Forde, P. M., Niknafs, N., *et al.*, Evolution of Neoantigen Landscape during Immune Checkpoint Blockade in Non-Small Cell Lung Cancer. *Cancer Discov* 2017, *7*, 264-276.

[44] Khodadoust, M. S., Olsson, N., Wagar, L. E., Haabeth, O. A., *et al.*, Antigen presentation profiling reveals recognition of lymphoma immunoglobulin neoantigens. *Nature* 2017, *543*, 723-727.

[45] Turajlic, S., Litchfield, K., Xu, H., Rosenthal, R., *et al.*, Insertion-and-deletion-derived tumour-specific neoantigens and the immunogenic phenotype: a pan-cancer analysis. *Lancet Oncol* 2017, *18*, 1009-1021.

[46] Kochin, V., Kanaseki, T., Tokita, S., Miyamoto, S., *et al.*, HLA-A24 ligandome analysis of colon and lung cancer cells identifies a novel cancer-testis antigen and a neoantigen that elicits specific and strong CTL responses. *Oncoimmunology* 2017, *6*, e1293214.

[47] Ward, J. P., Gubin, M. M., Schreiber, R. D., The Role of Neoantigens in Naturally Occurring and Therapeutically Induced Immune Responses to Cancer. *Adv Immunol* 2016, *130*, 25-74.

[48] Guzel, C., Govorukhina, N. I., Stingl, C., Dekker, L. J. M., *et al.*, Comparison of Targeted Mass Spectrometry Techniques with an Immunoassay: A Case Study for HSP90alpha. *Proteomics Clin Appl* 2018, *12*.

[49] Toth, L. N., de Abreu, F. B., Tafe, L. J., Non-small cell lung cancers with isocitrate dehydrogenase 1 or 2 (IDH1/2) mutations. *Hum Pathol* 2018, *78*, 138-143.

[50] Arita, H., Narita, Y., Yoshida, A., Hashimoto, N., *et al.*, IDH1/2 mutation detection in gliomas. *Brain Tumor Pathol* 2015, *32*, 79-89.

[51] Pastor, M. D., Nogal, A., Molina-Pinelo, S., Melendez, R., *et al.*, Identification of proteomic signatures associated with lung cancer and COPD. *J Proteomics* 2013, *89*, 227-237.

[52] Corbett, A. J., Eckle, S. B., Birkinshaw, R. W., Liu, L., *et al.*, T-cell activation by transitory neo-antigens derived from distinct microbial pathways. *Nature* 2014, *509*, 361-365.

[53] Bassani-Sternberg, M., Braunlein, E., Klar, R., Engleitner, T., *et al.*, Direct identification of clinically relevant neoepitopes presented on native human melanoma tissue by mass spectrometry. *Nat Commun* 2016, *7*, 13404.

[54] Bassani-Sternberg, M., Mass Spectrometry Based Immunopeptidomics for the Discovery of Cancer Neoantigens. *Methods Mol Biol* 2018, *1719*, 209-221.

[55] Scambler, T., Holbrook, J., Savic, S., McDermott, M. F., Peckham, D., Autoinflammatory disease in the lung. *Immunology* 2018.
[56] Brown, S. D., Warren, R. L., Gibb, E. A., Martin, S. D., *et al.*, Neo-antigens predicted by tumor genome meta-analysis correlate with increased patient survival. *Genome Res* 2014, *24*, 743-750.
[57] Peckham, D., Scambler, T., Savic, S., McDermott, M. F., The burgeoning field of innate immune-mediated disease and autoinflammation. *J Pathol* 2017, *241*, 123-139.

3

DETERMINATION OF SITE SPECIFIC PHOSPHORYLATION RATIOS IN PROTEINS WITH TARGETED MASS SPECTROMETRY

Lennard J. M. Dekker[1], Lona Zeneyedpour[1], Sandor Snoeijers[2], Jos Joore[2], Sieger Leenstra[3], Theo M. Luider[1]

1. Erasmus MC, Department of Neurology, Rotterdam, The Netherlands
2. Pepscope, Utrecht, The Netherlands
3. Erasmus MC, Department of Neurosurgery, Rotterdam, The Netherlands

Journal of Proteome Research. 2018, 17(4):1654-1663
The Supporting Information is available on the ACS Publications website at DOI: 10.1021/acs.jproteome. 7b00911.

ABSTRACT

We show that parallel reaction monitoring (PRM) can be used for exact quantification of phosphorylation ratios of proteins using stable isotope labelled peptides. We have compared two different PRM approaches on a digest of a U87 cell culture, namely direct-PRM (tryptic digest measured by PRM without any further sample preparation) and TiO2-PRM (tryptic digest enriched with TiO2 cartridges, followed by PRM measurement); these approaches are compared for the following phosphorylation sites: Neuroblast differentiation-associated protein (AHNAK S5480-p), Calcium/calmodulin-dependent protein kinase type II subunit delta (CAMK2D T337-p) and Epidermal growth factor receptor (EGFR S1166-p). A reproducible percentage of phosphorylation could be determined (CV 6-13%) using direct-PRM or TiO2-PRM. In addition, we tested the approaches in a cell culture experiment in which U87 cells were deprived of serum. As a "gold standard" we included immune precipitation of EGFR followed by PRM (IP-PRM). For EGFR (S1166) and AHNAK (S5480), a statistical significant change in the percentage of phosphorylation could be observed as a result of serum deprivation; for EGFR (S1166) this change was observed for both TiO2-PRM and IP-PRM. The presented approach has the potential to multiplex and to quantify the ratio of phosphorylation in a single analysis.

Keywords
Phosphoproteomics, PRM, Targeted mass spectrometry, Quantitative proteomics and Phosphorylation ratio

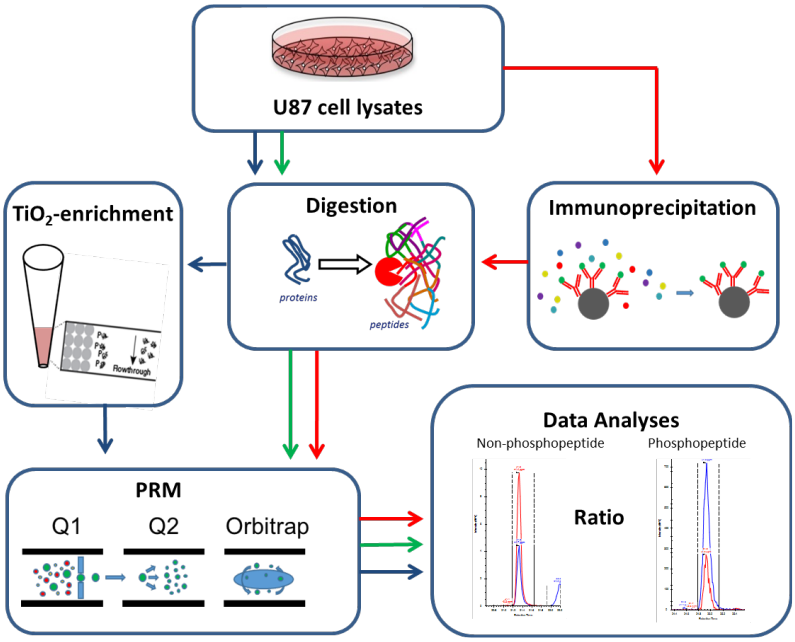

INTRODUCTION

Phosphorylation is a reversible post-translational modification (PTM) which regulates many cellular processes [1, 2] and as such plays an important role in cell signaling. In healthy organisms, phosphorylation is well-regulated but in diseases and especially in cancer this process is derailed. For this reason, there is a large interest in studying changes that occur in the phosphoproteome as a result of various diseases [3, 4].

Phosphoproteomics has resulted in complementary knowledge about new phosphorylation sites compared to antibodies directed to specific phosphosites [5]. A disadvantage of phosphoproteomics is that the identification of less abundant phosphopeptides by mass spectrometry still requires enrichment methods such as metal oxide affinity chromatography (MOAC) or immobilized metal affinity chromatography (IMAC); these are often combined with fractionation methods such as strong cation exchange chromatography (SCX), strong anion exchange chromatography (SAX), electrostatic repulsion-hydrophilic interaction chromatography (ERLIC) or high-pH reversed-phase chromatography (HpH) [6-12]. These quite lengthy procedures result in relatively long analyses time per sample. Techniques using antibodies are restricted by the relatively low number of phosphorylation site specific antibodies [13]. In addition, the specificity of antibodies remains a problem in tissue and cell lysates [14].

Knowledge about new phosphorylation sites detected by mass spectrometry are often publically available in databases, for instance Phosphopedia and PhosphoSitePlus [15]. The availability of information on large numbers of phosphorylation sites has opened possibilities for label-free targeted screening of phosphorylation using mass spectrometry. The merits of targeted mass spectrometry in terms of increased sensitivity, analytical precision and accuracy have been recognized for over a decade [16]. Using targeted MS methods it is possible to quantify the absolute or relative amount of a phosphorylated peptide in a sensitive way [17-19]. The introduction of high resolution mass spectrometers with quadrupole functionality such as the Orbitrap Q-Exactive and Orbitrap Fusion makes it possible to use targeted high resolution MS/MS-methods like Parallel Reaction Monitoring (PRM) [15, 20-23]. The higher resolution of MS2 spectra has resulted in lower noise levels in a PRM approach compared to conventional Selected Reaction Monitoring (SRM) approaches with triple quadrupole instruments. The reduced noise levels result in significantly lower limits of detection in complex samples compared to lower resolution SRM approaches [24]. Recently, Lawrence et al. [15] showed large improvement in sensitivity for targeted detection by PRM of phosphopeptides even outperforming DDA experiments with deep fractionation.

A disadvantage of most phosphoproteomics methods is that only the abundance of the

phosphopeptide is determined. The percentage phosphorylation of a phosphorylation site is not determined because the total protein abundance of the protein of interest is not measured. The importance of using protein abundance to calculate the degree of phosphorylation has been earlier underlined by Wu et al [25]. These authors showed, in a large scale study with SILAC labeling in yeast strains, that 25% of the phosphopeptides with a differential expression was related to a change in protein abundance. To determine the percentage of phosphorylation in phosphoproteins, a number of techniques have been described in literature, most of which include a labeling approach and / or a phosphatase treatment of the protein sample [26-30]. A SILAC labelling approach is used by Olsen et al. in which three SILAC ratios (phosphopeptide, nonphosphopeptide and protein ratio) are used to calculate phosphorylation levels [29]. Wu et al. and Tsai et al. use an approach in which the sample is divided in two equal aliquots, one aliquot is treated with phosphatase and the other aliquot is untreated. After digestion of the sample, a peptide labeling technique is performed after which the aliquots are combined again. The combined sample is measured using an LC-MS approach in which the ratio of the labeled and unlabeled form of peptides are determined. The determined ratios can be used to calculate the phosphorylation percentage of a peptide [26, 28]. These methods are quite complex and time-consuming d, in addition, absolute quantitation of the amount of phosphorylated protein remains difficult or impossible.

We describe a method to absolute quantify phosphopeptides and to determine their percentage of phosphorylation using PRM in combination with stable isotope labelled peptides. To develop and validate this method, U87 cells (a glioblastoma multiforme cell line) were used as a model. First, a phosphoproteome profile is created by performing a data dependent LC-MS measurement on enzymatic digested cell lysates which are enriched by TiO_2 and subsequently fractionated by a High-pH reversed-phase method. Second, a number of phosphopeptides were selected from this data set and used for a PRM approach with stable isotopic labeled peptides. In this PRM approach not only phosphorylated peptides but also the non-phosphorylated counterparts including their stable isotope labelled standards are targeted. This combination of techniques allows for a very precise determination of the percentage of phosphorylation for the investigated phosphosites. A thorough evaluation of the technology for this purpose has not been presented before. The aim of the current study is to show that it is feasible, with targeted proteomics, to accurately and precisely determine phosphorylation levels for specific phosphorylation sites in a sensitive, relatively fast and reproducible way.

MATERIALS AND METHODS

Unless otherwise noted, all chemicals were purchased from Sigma-Aldrich, (Saint Louis, MO) and all solvents were purchased from Biosolve, (Valkenswaard, The Netherlands).

Cell culture

U87 cells were cultured until 80% confluence in DMEM (Gibco, Invitrogen, Carlsbad, CA) with 10 % fetal bovine serum (FCS) and 100 µg/mL Pen Strep (Gibco, Thermo Fisher Scientific, Waltham, MA) in T75 flasks. Subsequently, the cells were washed with PBS (Lonza, Basel, Switzerland) and the cells were scraped on ice with cold 500 µl lysis buffer (0.1% SDS, 50 mM TEAB (triethyl ammonium bicarbonate) and 5 µl Halt™ phosphatase inhibitor (Thermo Fisher Scientific). The scraped cells were further disrupted by external sonification for 2 min at 70% amplitude at a maximum temperature of 25°C (Branson, Ultrasonic, Danbury, CT). Cell lysates were divided into two aliquots and stored at -80 °C. One aliquot was used for in-solution digest and one aliquot for immunoprecipitation.

Serum starvation

U87 cells were cultured until 80% confluence as mentioned above in 14.5 cm Petri dishes. Subsequently, the culture medium was deprived of FCS for 3 hours after which the cell cultures were incubated for two different durations with medium containing 10% FCS (10 and 15 minutes). We used two conditions as controls: a) cells that were not deprived of FCS and b) cells that were deprived of FCS for three hours but which were not subsequently incubated with FCS. Finally, cells were lysed and stored as mentioned above.

In-solution-digestion

Five µl of 200 mM TCEP (tris(2-carboxyethyl)phosphine was added to cell lysate (~500 ug total protein) and incubated for 1 hour at 55°C. Subsequently, 5 µl of 375 mM IAA (iodoacetamide) was added and incubated at room temperature for 30 min. Next, samples were precipitated by adding 600 µl cold acetone and incubated for 2 h at -20°C. Subsequently, samples were centrifuged for 10 min at 8,000 g at 4°C and supernatants were discarded. Pellets were washed twice with cold acetone and dissolved in 100 µl 50 mM TEAB that contained 25 µg trypsin (Promega, Madison, WI) and incubated overnight at 37°C. After overnight incubation, to each sample 4 µl 5% TFA was added and centrifuged at 20,000 g. Four µl of the digest was used to perform a quantitative colorimetric peptide assay (Pierce, Thermo Fisher Scientific, Rockford, IL) to determine the peptide concentration of each sample. The assay was performed according to the manufacturer's protocol. The rest of the digested sample was dried using a vacuum centrifuge (Savant SC210A, Thermo Fisher Scientific) and stored at -80 °C.

Immunoprecipitation of EGFR and on-bead digestion

Thawed lysates were centrifuged at 4°C at 20,000 g for 10 min and the supernatants were used. Subsequently, IP buffer (20 mM Tris/HCl pH 7.2, 10 mM sodium phosphate and 50 mM NaCl) was added to the supernatant and protein A Dyna beads (Thermo Fisher Scientific) were used for IP. Dyna beads (1.5 mg) were loaded with 5 µg of anti-EGFR (MABF119, Merck Millipore, Billerica, MA) and incubated for 10 min. According to the instructions of the manufacturer, the beads were washed and then the complete supernatant in the IP buffer was added to the beads and incubated at 4°C for 2 hours. After incubation, the beads were washed three times with 200 µl PBS-0.01% Tween 20. Subsequently, the beads were re-suspended into 100 µl PBS and transferred to a clean tube and PBS was removed. For digestion of the proteins bound to the beads, 50 µl 0.1% Rapigest (Waters) was added. After adding 2.5 µl 0.1 M dithiothreitol (DTT), the sample was incubated for 30 min at 60 °C. Subsequently, 2.5 µl 375 mM IAA was added and incubated at room temperature for 30 min. This was followed by addition of 0.5 µg trypsin and incubation overnight at 37°C. After adding 6 µl 5% TFA and centrifugating at 20,000 g the supernatants were stored at 4 °C.

Automated phosphopeptide enrichment and fractionation

For the automated sample processing an AssayMAP Bravo platform (Agilent technologies, Santa Clara, CA) was used. For the phosphopeptide enrichment, TiO_2 cartridges were used. For HpH (High pH) fractionation, reversed phase cartridges (Agilent technologies, Santa Clara, CA) were used. Manufacturer's protocols were applied for all cartridges as described briefly below.

Desalting of peptides

C18 cartridges were primed with 100 µl 50% ACN /0.1% TFA and equilibrated with loading buffer (0.1% TFA / water). Hundred twenty µg of dried digested U87 cells were re-suspended in 120 µl loading buffer. Hundred µl of the re-suspended sample was loaded onto the C18 cartridge. After washing the cartridges with 100 µl loading buffer, the desalted peptides were eluted in 25 µl elution buffer 70% ACN/0.1% TFA.

TiO_2 phosphopeptide enrichment

To the 25 µl desalted U87 peptide digests, 95 µl 40% ACN/2.5% TFA was added. TiO_2 cartridges were primed with 100 µl 5% ammonia/ 50% ACN and equilibrated with equilibration buffer (50% ACN/ 2% TFA). The desalted digests of the U87 cells were loaded onto the cartridges. Phosphopeptides were eluted with 25 µl 5% ammonia /15% ACN after washing the cartridges with 100 µl of the equilibration buffer. The eluted phosphopeptides were dried directly using a vacuum centrifuge. The dried sample was dissolved in 12 µl 0.1% TFA/ 2% ACN and measurement by LC-MS.

High pH reversed-phase fractionation

Hundred µg of dried digested U87 cells or the dried eluate of TiO_2 enrichment was re-suspended in 120 µl loading buffer (0.1% TFA/water). The reversed-phase (RP) cartridges were primed with 100 µl 80% ACN /0.1% TFA and equilibrated with loading buffer. The re-suspended sample was loaded onto an RP cartridge. After washing the cartridges with 100 µl of loading buffer, the peptides were eluted by applying a step gradient of increasing acetonitrile concentration in trimethylamine (0.1%/ water), 10, 15, 25, 30, 35 and 50%, respectively. Eluted peptide fractions were dried directly using vacuum centrifugation. The dried peptide fractions were dissolved in 25 µl 0.1% TFA prior to LC-MS analyses.

Sample preparation for Parallel Reaction Monitoring (PRM)

For PRM analyses, 3 peptide pairs were selected, a phosphopeptide and its non-phosphorylated counterpart. For quantification, a stable isotope labeled (SIL) version of these 3 pairs were purchased (Pepscan, Lelystad, The Netherlands) labeled with lysine-$^{13}C_{6,}$ $^{15}N_2$. The purity of the obtained peptides was >95% and the variation in the concentration is specified as less than 5%. The spiking level of SIL-peptides in the digested samples was determined based on the ratio to the endogenous peptide in an untreated U87 digest, see Table 1. The spiking levels have been selected to obtain a ratio close to one, ratios exceeding a factor 10 resulted in incorrect quantitative results for some of the peptides. For the immuno-precipitated samples, other spiking concentrations were used to not exceed a factor of 10, see Table 1.

Table 1: Targeted peptides

Protein	Sequence*	Precursor mass MH+	Charge	Extracted fragments	Amount of spiked peptide fmol /100 µg total peptide	
					Direct-PRM &TiO_2-PRM	IP-PRM
AHNAK (S5448)	ISAPNVDFNLEGPK	750.8883	2	y8[+],y11[+],y12[+],y11[++]	-	-
	ISAPNVDFNLEGP**K**	754.8954			1000	-
	I**S**APNVDFNLEGPK	790.8714			-	-
	I**S**APNVDFNLEGP**K**	794.8714			400	-
CAMK2D (T337)	ESTESSNTTIEDEDVK	892.3894	2	y6[+],y8[+],y10[+],y11[+],y12[+]	-	-
	ESTESSNTTIEDEDV**K**	896.3965			400	-
	ESTESSNT**T**IEDEDVK	932.3726		y6[+],y8[+],y9[+],y11[+],y12[+]	-	-
	ESTESSNT**T**IEDEDV**K**	936.3797			100	-
EGFR (S1166)	GSHQISLDNPDYQQDFFPK	746.015	3	y6[+],y7[+],y10[++],b9[+]	-	-
	GSHQISLDNPDYQQDFFP**K**	748.6864			1000	100
	GSHQI**S**LDNPDYQQDFFPK	772.6705			-	-
	GSHQI**S**LDNPDYQQDFFP**K**	775.3419			50	4

*__Bold and underlined__ phosphorylated residue, **Bold** lysine-$^{13}C_{6,}$ $^{15}N_2$

NanoLC data dependent mass spectrometry measurements

Samples were analyzed by nano-LC (Ultimate 3000RS, Thermo Fisher Scientific, Germering, Germany). After preconcentration and washing of the samples on a C18 trap column (1 mm × 300 µm i.d., Thermo Fisher Scientific), they were loaded onto a C18 column (PepMap C18, 75 mm ID × 250 mm, 2 µm particle and 100 Å pore size, Thermo Fisher Scientific) using a linear 90 minutes gradient (4-38% ACN/H20; 0.1% formic acid) at a flow rate of 250 nL/min. The separation of the peptides was monitored by a UV detector (absorption at 214 nm). The nano-LC was coupled to a nanospray source of a Q Exactive HF mass spectrometer (Thermo Fisher Scientific, Bremen, Germany) which was operated in the data dependent acquisition (DDA) mode. Full scan MS spectra (m/z 375-1500) in profile mode were acquired in the Orbitrap with a resolution of 60,000 after accumulation of an AGC (Automatic Gain Control) target of 3×10^6. The top 20 peptide signals (charge-state 2+ and higher) were isolated (1.4 m/z window) and fragmented by HCD (Higher-energy collision, normalized collision energy, NCE, 28.0) and measured in the Orbitrap with an AGC target of 50,000 and a resolution of 15,000. Maximum fill times were 60 ms for the full scans and 50 ms for the MS/MS scans. The dynamic exclusion was activated; after the first time a precursor was selected for fragmentation it was excluded for a period of 40 seconds using a relative mass window of 10 ppm. Lock mass correction was activated to improve mass accuracy of the survey scan.

PRM measurements

PRM was performed on the same nano-LC Orbitrap Q Exactive HF system as the DDA measurements. A shorter 30 minute gradient is used on the nanoLC system under similar LC conditions as for the DDA measurements. A targeted MS/MS method was developed for 12 peptides, see Table 1. A quadrupole isolation window of 0.7 m/z units, an AGC target of 1e6 ions, a maximum fill time of 250 ms and an Orbitrap resolving power of 120,000 at 200 m/z were used. The normalized collision energy was optimized and retention time was determined for each peptide, using the SIL-peptides. An optimal NCE of 20 for all peptides and a retention time window of 3 minutes for each peptide was used.

Data Processing and Analysis

From the DDA data files the MS/MS spectra were extracted and converted into mgf files by using MSConvert of ProteoWizard (version 3.0.06245). All mgf files were analyzed using Mascot (version 2.3.02; the Matrix Science, London, UK). Mascot was used to perform database searches against the human subset of the uniprot_sprot_2015-10 database; Homo sapiens species restriction; 20,194 sequences) of the extracted MS/MS data. For the database search the following settings were used: a maximum of two miss cleavages, oxidation as a variable modification of methionine, carbamidomethylation as a fixed modification of cysteine and phosphotyrosine, phosphoserine and phosphothreonine as a variable modification. Trypsin was set as enzyme. A peptide mass tolerance of 10

ppm and a fragment mass tolerance of 0.02 Da were allowed. In additional also an error tolerant search in Mascot using the same database and parameters as above is performed. Scaffold software (version 4.8.3, Portland, OR) was used to summarize and filter MS/MS based peptides and protein identifications at an FDR of 1% (peptide level). Proteins that contained similar peptides and could not be differentiated based on MS/MS analysis alone were grouped.

PRM data analysis

The PRM data was analyzed using Skyline version 3.5.0.9320 MacCoss Lab Software, Seattle, WA; https://skyline.gs.washington.edu/labkey/project/home/software/Skyline/begin.view), fragment ions for each targeted mass were extracted and peak areas were integrated. Based on the peak areas, ratio between the endogenous peptide and the SIL peptide were calculated in excel. The ratios, spiking level of the peptide and the total peptide concentration determined by the peptide assay were used to calculate for each peptide the respective protein amount per 100 µg total peptide. In addition, the phosphorylation ratios were calculated using the formula:

$$\frac{\text{Amount of phosphorylated protein*100}}{\text{amount of phosphorylated protein* + amount of non-phosphorylated protein* = ratio phosphorylation (\%)}}$$

*For the targeted phosphorylation site.

Statistical comparison between methods and experimental conditions are performed using a t-test in Excel.

RESULTS

Phosphopeptide enrichment was performed in triplicate on 100 µg of tryptic digests of a lysate of U87 cells using TiO_2 enrichment and high-pH reversed-phase fractionation measured by LC-MS. This resulted in the identification of 7,774 unique phosphopeptides, see Table 2 and supplementary Table S1a. This corresponded to a total of 4,270 unique phosphosites of which 3,908 were phosphorylated at serine, 335 at threonine and 27 at tyrosine. In addition, the same sample was also measured without phospho-peptide enrichment resulting in the identification of in total 5,519 proteins at an FDR <1% and 41,341 unique peptides, see Table 2 and supplementary Table S1b.

All phosphopeptides in the dataset that were also present in the non-phosphorylated state were selected. A total of 1,980 pairs could be observed in the complete dataset (see supplementary Table S1c). From this list a selection was made based on biological

relevance, related to pathways that are known to be affected in glioma [31]. In addition, the intensity of the observed pairs was taken into account and peptides with different intensities levels were selected: high, medium and low. This resulted in three peptide pairs originating from three different proteins, AHNAK S5448 (ISAPNVDFNLEGPK) (high intensity), CAMK2D T337 (ESTESSNTTIEDEDVK) (medium intensity) and EGFR S1166 (GSHQISLDNPDYQQDFFPK) (low intensity), see Table 1. The six selected peptides were used to establish and validate a PRM method for quantification of the phosphorylated and non-phosphorylated forms of these peptides. To accurately quantify the six selected peptides, stable isotopically labeled variants were used as internal standard in the PRM measurements, see Table 1. In addition a database search was performed to check for additional modifications of the selected peptides, this to prevent errors in the phosphorylation ratio calculations. In the results of this database search for none of the selected peptides additional modifications besides phosphorylation were identified.

Table 2: Identification of peptides and proteins present in U87 cell line

Sample preparation	# Non-Phosphorylated Proteins	#Phosphoproteins	#Non-phosphopeptides	#Phosphopeptides
Not fractionated	1563	34	6404	37
TiO_2 enrichment	2125	1568	4311	4267
HpH fractionation	5329	372	32640	595
TiO_2 and HpH combined	3153	2076	9643	5487
Total	5519	2444	41341	7774
Overlap	778		1980	

Two different sample preparation strategies were used: a) an in-solution digestion measured by LC-MS in PRM mode (direct-PRM), b) an in-solution digestion followed by TiO_2 enrichment. Both the TiO_2 enriched and the non-enriched digest are measured by LC-MS in PRM mode (TiO_2-PRM) . The different strategies are depicted in Figure 1. The same settings for the PRM measurements were used for all strategies. The strategies were performed in triplicate using three U87 lysates of 100 µg total peptide; all lysates were obtained from a single cell culture procedure. The amount in ng protein per 100 µg of total peptide for all three proteins was calculated for both the phosphorylated and non-phosphorylated fraction. In addition, the percentage of phosphorylation was calculated. For each of the strategies all samples were measured in triplicate to determine the technical variation. The measured concentrations, the CV values and the phosphorylation ratios are summarized in Table 3 from which it can be observed, that using direct-PRM, the phosphorylated peptide of EGFR cannot be detected.

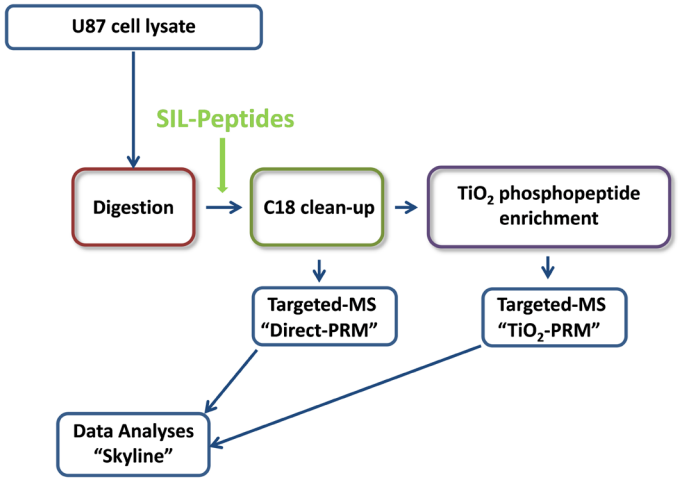

Figure 1: Flowchart of the PRM strategies: Direct-PRM and TiO_2-PRM.
The spiked SIL-peptides were selected from the list of peptide pairs (phosphorylated and non-phosphorylated) resulting from the screening measurement in U87, see table 2. From this list AHNAK S5448 (ISAPNVDFNLEGPK), CAMK2D T337 (ESTESSNTTIEDEDVK) and EGFR S1166 (GSHQISLDNPDYQQDFFPK) were selected. SIL-peptides of both the phosphorylated and non-phosphorylated peptide were added to the trypsin digested sample.

Table 3: Comparison and reproducibility of Direct-PRM and TiO_2–PRM

		Non-phosphorylated protein		Phosphorylated protein				Phosphorylation			
		Direct-PRM		**Direct-PRM**		**TiO_2-PRM**		**Direct-PRM**		**TiO_2-PRM****	
	Reproducibility	Amount ng*	CV (%)	Amount ng*	CV (%)	Amount ng*	CV (%)	%	CV (%)	%	CV (%)
AHNAK	PRM measurement	2672	1.7	253	3.7	232	1.5	8.65	2.0	7.98	2.3
(S5448)	Complete approach***	2537	7.3	220	11.2	200	14	7.98	6.0	7.34	12.0
CAMK2D	PRM measurement	42.7	1.6	0.78	2.4	1.08	1.8	1.80	2.6	2.46	2.0
(T337)	Complete approach***	40.4	6.4	0.78	5.8	1.03	2.6	1.89	2.2	2.49	6.4
EGFR	PRM measurement	81.6	3.0	ND	ND	11.8	0.3	ND	ND	12.6	2.9
(S1166)	Complete approach***	81.5	8.9	ND	ND	10.5	10.8	ND	ND	11.5	13.1

* ng protein / 100 µg total peptide
** Phosphorylation percentage calculated based on non-phosphorylated protein amounts from the Direct-PRM approach and phosphorylated protein amounts from TiO_2-PRM
*** Including all sample preparation steps (digestion and TiO_2 enrichment) on a U87 cell lysate coming from the same culture
ND = not detectable

For the other two peptide pairs AHNAK and CAMK2D all peptides could be detected, the phosphorylation percentages were determined, CV values of 2.0% and 2.3%, respectively for the PRM measurement and 6.0 and 2.2%, respectively for the entire approach (including trypsin digestion) were obtained. For CAMK2D the signal intensity for the phosphorylated peptide is quite low and a reliable integration of the fragment

peaks was difficult to perform in the extracted ion chromatograms. This resulted in a possible underestimation of the amount of phosphorylated CAMK2D. Using the TiO_2-PRM approach, all three phosphopeptides AHNAK, CAMK2D and EGFR could be reliably quantified. CV values for the phosphorylation percentage of 2.3%, 2.0% and 2.9%, for the PRM measurement and 12.0%, 6.4% and 13.1% for the entire approach were obtained, respectively. Surprisingly, also two out of three non-phosphorylated peptides could be measured in the TiO_2 enriched sample, see Supplementary Table S2. The measured amounts of these peptides do not differ from the measurements obtained with the direct-PRM method, also resulting in comparable phosphorylation percentages. The calculated percentages of phosphorylation were not significantly different between the PRM strategies (p-value >0.05), paired t-test for AHNAK, see Supplementary Table 2. For the CAMK2D, the PRM strategies are statically significantly different, p-value <0.05, paired t-test, see Supplementary Table S2. This is likely related to the lower amount of phosphorylated CAMK2D detected in the direct-PRM approach resulting in a larger variation and less reliable measurements.

For CAMK2D multiple possible phosphorylation forms of the targeted peptide in this study exist including CAMK2D (T337) and (T336). In the screening of the U87 digest, a number of additional phosphorylation sites besides (T337) for this peptide were observed, see Supplementary Table S1a. We checked the PRM data to see if also other phosphorylated forms could be observed. The presence of the T336 phosphorylation site was monitored by the y8 fragment that differentiates between the (T337) and (T336) forms. For the y8 fragment of the (T337) a clear signal is observed in contrast to the y8 fragment of (T336) which is not observed, see supplementary Figure 1. For the other possible phosphorylation forms of the peptide also no spectral evidence was obtained so either they were not present in the measured samples or at very low intensities.

We performed a cell culture experiment to validate the PRM strategies in a larger sample set. In this cell culture experiment we compared the direct-PRM and TiO_2-PRM strategies also with "the gold standard" immunoprecipitation of EGFR, followed by an in-solution digestion measured by LC-MS in PRM mode (IP-PRM), see Figure 2. For the IP-PRM approach only the concentration and phosphorylation percentage for EGFR was determined. In the cell culture experiment on U87 cells, we deprived the culture of fetal bovine serum (FCS) for 3 hours and subsequently incubated the cell cultures for two different durations with FCS, i.e. 10 and 15 minutes. In such an experiment a large change in phosphorylation is expected [32-34]. As controls we used cells that were not deprived of FCS and cells that were deprived of FCS for three hours but which were not subsequently incubated with FCS, see Figure 2 for a flowchart of the experiment. Each experimental condition was performed in triplicate to determine the biological variation in the experiment. In supplementary Table S3 an overview of the resulting measured

concentrations of the peptides and the percentage of phosphorylation is displayed for all strategies.

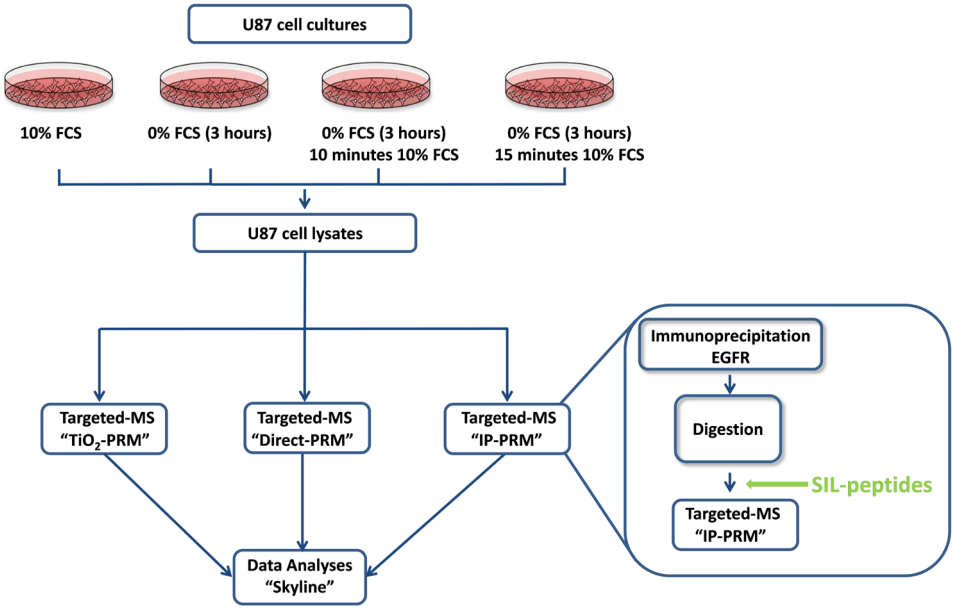

Figure 2: Flowchart of the experimental procedure.
The effect of FCS starvation on the phosphorylation of AHNAK S5448 (ISAPNVDFNLEGPK), CAMK2D T337 (ESTESSNTTIEDEDVK) and EGFR S1166 (GSHQISLDNPDYQQDFFPK) is measured with three PRM strategies.

In Figure 3 the measured concentrations and the percentages of phosphorylation are displayed for the different proteins and time points using the TiO_2-PRM approach (A, B and C), for EGFR also the IP-PRM approach is shown (D). We observed that for both EGFR and AHNAK statistical significant changes in phosphorylation levels occur as a result of FCS starvation (p-value < 0.01 and p-value < 0.05, respectively). For EGFR the level of the phosphorylated peptide increases as an effect of serum starvation and the non-phosphorylated peptide remains at a constant level. For AHNAK the level of the phosphorylated peptide remains constant but the non-phosphorylated peptide increases. These examples show that changes in phosphorylation percentage can be the result of changes in the amount of phosphorylated peptide or changes of the non-phosphorylated peptide. When comparing the phosphorylation percentages for the TiO_2-PRM and IP-PRM approach a comparable trend between the measured samples was observed. The absolute phosphorylation values obtained by the IP-PRM method are however consequently lower as measured by TiO_2-PRM, see Table S3 supplementary

data. In addition the amounts of both the phosphorylated and the non- phosphorylated protein are much lower in the IP-PRM method, indicating a low recovery for the IP-PRM method. The recovery was calculated by using the amounts as determined for non-phosphorylated EGFR by the direct-PRM as 100%. In this way recoveries ranging from 4-13% were determined for the EGFR immunoprecipitation, see Table S3 supplementary data. In addition, also the recovery for the TiO_2-PRM was determined by comparing the intensities of internal standards for samples which were spiked before and after the TiO_2 procedure. The recovery for the complete procedure including the C18 clean-up ranged from (16%-36%). The difference in recovery between the peptides was larger compared to the difference in recovery for the replicates of the individual peptides.

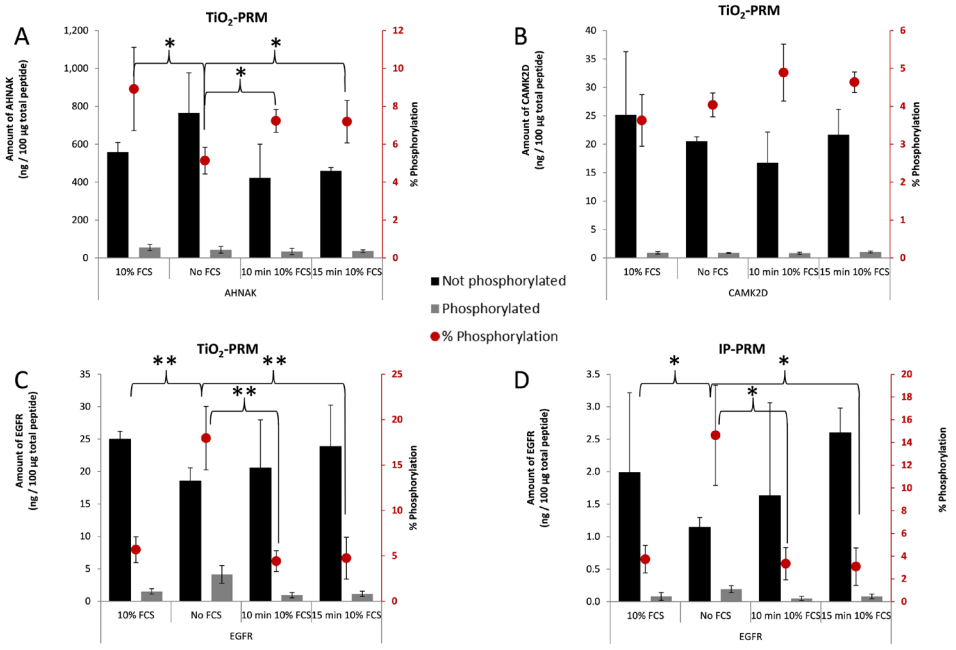

Figure 3: Changes in phosphorylated and non-phosphorylated protein abundance and phosphorylation ratio in U87 cell as a result of FCS deprivation.
Each plot shows the results of four culture conditions used in this experiment. 10% FCS, (Standard culture conditions), No FCS, (Cells cultured for 3 hours on medium without FCS), Ten minutes 10% FCS (Three hours cultured without FCS and subsequent incubation with 10% FCS for 10 minutes), 15 minutes 10% FCS, (3 hours cultured without FCS and subsequent incubation with 10% FCS for 15 minutes). All measurements have been performed in triplicate and error bars indicate standard deviation. A statistical comparison of the different culture conditions is performed, t-test, * = p-value <0.05, ** = p-value <0.01. The following proteins are displayed in the plot, A) AHNAK using the TiO_2-PRM approach, B) CAMK2D using the TiO_2-PRM approach, C) EGFR using the TiO_2-PRM approach and D) EGFR using the IP-PRM approach.

DISCUSSION

We developed a method that uses targeted mass spectrometry with high resolution to accurately determine the phosphorylation percentage of protein phosphorylation-sites in cell lysates. We investigated if the use of isotopically labeled standards for targeted quantitation of phosphorylation sites in combination with measuring the non- phosphorylated peptide can be used to reliably determine the phosphorylation percentages. Our results show that by using a PRM approach, targeted phosphorylated peptides could be measured with a high degree of reproducibility, CV < 10%. Two strategies described in this manuscript (direct-PRM and TiO_2-PRM) were comparable in terms of reproducibility and quantitative performance. For CAMK2D slightly lower concentrations of the phosphorylated form are obtained using the direct-PRM approach in comparison to the TiO_2-PRM approach. Closer inspection of the raw data revealed that in the direct-PRM method intensity levels of phosphorylated CAMK2D are low and that not all extracted ions produce peaks that can be reliably integrated. This resulted in an underestimation of the amount of phosphorylated CAMK2D.

The direct-PRM method is the easiest and quickest method and can potentially be used for larger numbers of more abundant phosphorylation sites. In cases were sensitivity issues are observed, the TiO_2-PRM approach is essential. We have shown that using a combination of PRM with a phosphopeptide enrichment procedure can clearly increase the sensitivity of the method. The phosphorylated EGFR peptide could in the direct-PRM approach be only barely observed while it gave an intense and reproducible signal using the TiO_2-PRM approach. A disadvantage of the TiO_2-PRM method is that two PRM measurements are required to determine the percentage of phosphorylation, non-enriched and enriched sample. We have however observed that for two of the three selected peptides the non-phosphorylated peptide could be measured in the enriched fraction. Most of the non-phosphorylated peptide is lost during the enrichment procedure but since the same holds true for the non-phosphorylated internal standard, still a reliable quantitation can be performed. The results obtained by this approach were not different from the quantitative results obtained using an additional measurement on the not enriched sample.

The direct-PRM and TiO_2-PRM approach require a minimal sample preparation that can be automated and performed for a large batch of samples simultaneously. The enrichment for up to 96 samples can be performed in less than 2 hours using the robotic-platform described. The PRM measurements are performed using a short LC-gradient of only 30 minutes, this allows the sample preparation and analyses of relative large sample cohorts, ~25 samples a day. This increased throughput is a clear advantage in comparison to existing methods that require more complex sample preparation strategies (labeling,

phosphatase treatment or extensive fractionation) [26-30]. An additional advantage of using a targeted method is the increase in sensitivity which allows the detection of lower abundant species without additional fractionation. A disadvantage of a targeted approach is that prior knowledge about the sample is required to select targets. We combined for this reason an untargeted screening (for target selection) with subsequent targeted measurements.

The IP-PRM method was used as a "gold standard" to validate the result of the two other strategies. The results show that in a relative clean immune purified cell lysate, similar percentages of phosphorylation are measured indicating that the effect of the matrix on the quantitation of the phosphorylation levels is minimal for these peptides. The IP-PRM method is potentially the most sensitive method and could have its use when many phosphorylation sites in a single protein are investigated. Limitations of this approach are that an antibody is required for which the binding to the target protein is not affected by the phosphorylation of the target. In addition, also the sensitivity of this method is largely influenced by the recovery of the target protein. In the experiments performed in this study a recovery between 5-13% was obtained. This limits the use for absolute quantitation of the phosphorylated and non-phosphorylated protein. The relatively low recovery can have a number of reasons, e.g. the solubility of the target protein, the binding constant and specificity of the antibody. For membrane proteins like EGFR, the solubility could be a problem and further optimization of IP-buffers could potentially increase the recovery. This shows a drawback of IP based method were, besides the choice of the antibody, also the optimization of IP procedure plays an important role. This makes the development and testing of such an approach for a large number of target proteins costly and complicated. The recovery of the TiO_2 procedure ranged from 16-36% depending on the selected peptide and this is lower compared to earlier published recoveries [35] but does in our study include the complete approach including the C18 purification and vacuum evaporation steps. In addition, also the lower recovery can be related to the complexity of the cell lysate. The variable recovery for different phospho-peptides underlines once more the importance of the use of internal standards to correct for losses and variations in the sample preparation.

In this study six peptides are targeted. The advantage of a PRM approach is that a larger number of peptides can be measured in parallel. However, the number of peptides that can be monitored simultaneously using PRM has its limits. The used measurement conditions in combination with retention time scheduling would allow the measurement of 30-40 peptides in a single run. The increased retention time reproducibility of LC systems and developments in mass spectrometry acquisition and analyses software (automated retention time adjustments or triggered-PRM methods [36, 37]) can even further increase this number. A number of recent publications showed that both SRM

and PRM approaches can be applied to quantify large numbers of peptides in a single measurement [17, 36, 38-40]. For this reason, we anticipate that it is feasible to monitor phosphorylation in a selected pathway using the described PRM strategies.

A number of limitations exist in phosphoproteomics as reviewed by Olsen et al. and Osinalde et al. [8, 18]. One of the main limitations is that the phospho site dictates which peptide should be used for quantification in a standard trypsin digest. This is in contrast to quantitative proteomics for proteins were the best performing peptides can be selected for quantitation. This inflexibility in quantitative phosphoproteomics can result in not optimal target peptides for quantitation. For this reason a judicious selection of key phosphorylation sites based on biological knowledge and existing databases of phosphoproteomics data is required to enable the monitoring of a selected pathway. In addition, also peptides with multiple possible phosphorylation sites can be challenging such as for example the targeted peptide ESTESSNTTIEDEDVK of CAMK2D in our analyses. CAMK2D (T-337) and (T-336) both exist and can only be differentiated by a single fragment ion y8. In this case, the presence of the T-336 phosphorylation could be excluded because only the fragment specific for the T-337 form was observed .

The FCS starvation experiment shows the importance of quantifying both the phosphorylated and non-phosphorylated peptide for a specific phosphorylation site. For the phosphorylation sites studied in EGFR and AHNAK, changes in phosphorylation percentages were observed as an effect of FCS deprivation of the cell culture. For EGFR the change in phosphorylation is related to an increase in phosphorylation as a result of FCS deprivation. In AHNAK the amount of phosphorylated AHNAK does not change but the amount of non-phosphorylated AHNAK increases as a result of FCS deprivation. This results in a net decrease in phosphorylation of AHNAK. This change in phosphorylation percentage would not have been detected when only the phosphorylated form was measured.

All three targeted phosphorylation sites EGFR (S1166), AHNAK (S5448) and CAMK2D (T337) have been earlier observed by mass spectrometry in a number of phosphoproteomics studies, see PhosphoSitePlus database. For both EGFR (S1166) and AHNAK (S5448) a relation to EGF stimulation has been described [33, 41]. This supports our observation that changes in the phosphorylation level for these two phosphorylation sites occur as a result of serum starvation.

In conclusion, we have developed a relatively fast approach for absolute quantification of phosphopeptides and for the determination of the phosphorylation ratios of specific peptides. The direct-PRM and TiO_2-PRM methods are relatively quick and do not require antibodies, labeling strategies, phosphatase treatment or complex fractionation

methods. These methods can be multiplexed as demonstrated. This technology can potentially be used for studies in which the activity of a specific pathway is monitored by protein abundance and site specific phosphorylation ratios of key proteins of the chosen pathway.

Supporting information

Supplementary Table S1a: List of identified phosphorylated proteins and peptides
Supplementary Table S1b: List of identified non-phosphorylated proteins and peptides
Supplementary Table S1c: List of identified proteins and peptides that occur in non-phosphorylated and phosphorylated state
Supplementary Table S2: Comparison and reproducibility of Direct-PRM, TiO2-PRM
Supplementary Table S3: Overview of protein concentrations, phosphopeptide concentrations and percentage of phosphorylation in FCS deprived U87 cells for EGFR, AHNAK and CAMK2D
Supplementary Figure S1: Extracted ion chromatograms from a PRM measurement of a U87 digest of the phosphorylated peptide ESTESSNTTIEDEDVK

Acknowledgement

This work is part of the research programme Open Technology with project number 12778 which is financed by the Netherlands Organisation for Scientific Research (NWO).

REFERENCES

1. Burkhart, J. M.; Gambaryan, S.; Watson, S. P.; Jurk, K.; Walter, U.; Sickmann, A.; Heemskerk, J. W. M.; Zahedi, R. P., What Can Proteomics Tell Us About Platelets? *Circulation Research* **2014,** 114, (7), 1204-1219.
2. Manning, G.; Whyte, D. B.; Martinez, R.; Hunter, T.; Sudarsanam, S., The Protein Kinase Complement of the Human Genome. *Science* **2002,** 298, (5600), 1912-1934.
3. Reimand, J.; Wagih, O.; Bader, G. D., The mutational landscape of phosphorylation signaling in cancer. *Sci Rep* **2013,** 3, 2651.
4. Xu, X.; Li, A.; Wang, M., Prediction of human disease-associated phosphorylation sites with combined feature selection approach and support vector machine. *IET Syst Biol* **2015,** 9, (4), 155-63.
5. Liu, Y.; Chance, M. R., Integrating phosphoproteomics in systems biology. *Comput Struct Biotechnol J* **2014,** 10, (17), 90-7.
6. Batth, T. S.; Francavilla, C.; Olsen, J. V., Off-Line High-pH Reversed-Phase Fractionation for In-Depth Phosphoproteomics. *Journal of Proteome Research* **2014,** 13, (12), 6176-6186.
7. Beausoleil, S. A.; Jedrychowski, M.; Schwartz, D.; Elias, J. E.; Villén, J.; Li, J.; Cohn, M. A.; Cantley, L. C.; Gygi, S. P., Large-scale characterization of HeLa cell nuclear phosphoproteins. *Proceedings of the National Academy of Sciences of the United States of America* **2004,** 101, (33), 12130-12135.
8. Olsen, J. V.; Mann, M., Status of Large-scale Analysis of Post-translational Modifications by Mass Spectrometry. *Molecular & cellular proteomics : MCP* **2013,** 12, (12), 3444-3452.
9. Zhou, H.; Ye, M.; Dong, J.; Corradini, E.; Cristobal, A.; Heck, A. J. R.; Zou, H.; Mohammed, S., Robust phosphoproteome enrichment using monodisperse microsphere–based immobilized titanium (IV) ion affinity chromatography. **2013,** 8, (3), 461-480.
10. Montoya, A.; Beltran, L.; Casado, P.; Rodríguez-Prados, J.-C.; Cutillas, P. R., Characterization of a TiO(2) enrichment method for label-free quantitative phosphoproteomics. *Methods (San Diego, Calif)* **2011,** 54, (4), 370-378.
11. Villén, J.; Gygi, S. P., The SCX/IMAC enrichment approach for global phosphorylation analysis by mass spectrometry. *Nature protocols* **2008,** 3, (10), 1630-1638.
12. Fukuda, I.; Hirabayashi-Ishioka, Y.; Sakikawa, I.; Ota, T.; Yokoyama, M.; Uchiumi, T.; Morita, A., Optimization of Enrichment Conditions on TiO2 Chromatography Using Glycerol As an Additive Reagent for Effective Phosphoproteomic Analysis. *Journal of Proteome Research* **2013,** 12, (12), 5587-5597.
13. van der Mijn, J. C.; Labots, M.; Piersma, S. R.; Pham, T. V.; Knol, J. C.; Broxterman, H. J.; Verheul, H. M.; Jiménez, C. R., Evaluation of different phospho-tyrosine antibodies for label-free phosphoproteomics. *Journal of Proteomics* **2015,** 127, Part B, 259-263.
14. Engholm-Keller, K.; Larsen, M. R., Technologies and challenges in large-scale phosphoproteomics. *Proteomics* **2013,** 13, (6), 910-31.
15. Lawrence, R. T.; Searle, B. C.; Llovet, A.; Villen, J., Plug-and-play analysis of the human phosphoproteome by targeted high-resolution mass spectrometry. *Nat Methods* **2016,** 13, (5), 431-4.
16. Anderson, L.; Hunter, C. L., Quantitative mass spectrometric multiple reaction monitoring assays for major plasma proteins. *Mol Cell Proteomics* **2006,** 5, (4), 573-88.
17. Narumi, R.; Murakami, T.; Kuga, T.; Adachi, J.; Shiromizu, T.; Muraoka, S.; Kume, H.; Kodera, Y.; Matsumoto, M.; Nakayama, K.; Miyamoto, Y.; Ishitobi, M.; Inaji, H.; Kato, K.; Tomonaga, T., A Strategy for Large-Scale Phosphoproteomics and SRM-Based Validation of Human Breast Cancer Tissue Samples. *Journal of Proteome Research* **2012,** 11, (11), 5311-5322.
18. Osinalde, N.; Aloria, K.; Omaetxebarria, M. J.; Kratchmarova, I., Targeted mass spectrometry: An emerging powerful approach to unblock the bottleneck in phosphoproteomics. *J Chromatogr B Analyt Technol Biomed Life Sci* **2017,** 1055-1056, 29-38.
19. Jin, L. L.; Tong, J.; Prakash, A.; Peterman, S. M.; St-Germain, J. R.; Taylor, P.; Trudel, S.; Moran, M. F., Measurement of protein phosphorylation stoichiometry by selected reaction monitoring mass spectrometry. *J Proteome Res* **2010,** 9, (5), 2752-61.
20. Kelstrup, C. D.; Jersie-Christensen, R. R.; Batth, T. S.; Arrey, T. N.; Kuehn, A.; Kellmann, M.; Olsen, J. V., Rapid and Deep Proteomes by Faster Sequencing on a Benchtop Quadrupole Ultra-High-Field Orbitrap Mass Spectrometer. *Journal of Proteome Research* **2014,** 13, (12), 6187-6195.
21. Gallien, S.; Bourmaud, A.; Kim, S. Y.; Domon, B., Technical considerations for large-scale parallel reaction monitoring analysis. *Journal of Proteomics* **2014,** 100, 147-159.
22. Rauniyar, N., Parallel Reaction Monitoring: A Targeted Experiment Performed Using High Resolution and High Mass Accuracy Mass Spectrometry. *International Journal of Molecular Sciences* **2015,** 16, (12), 28566-28581.
23. Peterson, A. C.; Russell, J. D.; Bailey, D. J.; Westphall, M. S.; Coon, J. J., Parallel Reaction Monitoring for High Resolution and High Mass Accuracy Quantitative, Targeted Proteomics. *Molecular & Cellular Proteomics : MCP* **2012,** 11, (11), 1475-1488.
24. Guzel, C.; Govorukhina, N. I.; Stingl, C.; Dekker, L. J. M.; Boichenko, A.; van der Zee, A. G. J.;

Bischoff, R. P. H.; Luider, T. M., Comparison of Targeted Mass Spectrometry Techniques with an Immunoassay: A Case Study for HSP90alpha. *Proteomics Clin Appl* **2018,** 12, (1).
25. Wu, R.; Dephoure, N.; Haas, W.; Huttlin, E. L.; Zhai, B.; Sowa, M. E.; Gygi, S. P., Correct interpretation of comprehensive phosphorylation dynamics requires normalization by protein expression changes. *Mol Cell Proteomics* **2011,** 10, (8), M111 009654.
26. Li, X.; Cox, J. T.; Huang, W.; Kane, M.; Tang, K.; Bieberich, C. J., Quantifying Kinase-Specific Phosphorylation Stoichiometry Using Stable Isotope Labeling In a Reverse In-Gel Kinase Assay. *Anal Chem* **2016,** 88, (23), 11468-11475.
27. Tsai, C. F.; Wang, Y. T.; Yen, H. Y.; Tsou, C. C.; Ku, W. C.; Lin, P. Y.; Chen, H. Y.; Nesvizhskii, A. I.; Ishihama, Y.; Chen, Y. J., Large-scale determination of absolute phosphorylation stoichiometries in human cells by motif-targeting quantitative proteomics. *Nat Commun* **2015,** 6, 6622.
28. Wu, R.; Haas, W.; Dephoure, N.; Huttlin, E. L.; Zhai, B.; Sowa, M. E.; Gygi, S. P., A large-scale method to measure absolute protein phosphorylation stoichiometries. *Nat Methods* **2011,** 8, (8), 677-83.
29. Olsen, J. V.; Vermeulen, M.; Santamaria, A.; Kumar, C.; Miller, M. L.; Jensen, L. J.; Gnad, F.; Cox, J.; Jensen, T. S.; Nigg, E. A.; Brunak, S.; Mann, M., Quantitative phosphoproteomics reveals widespread full phosphorylation site occupancy during mitosis. *Sci Signal* **2010,** 3, (104), ra3.
30. Curran, T. G.; Zhang, Y.; Ma, D. J.; Sarkaria, J. N.; White, F. M., MARQUIS: a multiplex method for absolute quantification of peptides and posttranslational modifications. *Nat Commun* **2015,** 6, 5924.
31. Brennan, C. W.; Verhaak, R. G.; McKenna, A.; Campos, B.; Noushmehr, H.; Salama, S. R.; Zheng, S.; Chakravarty, D.; Sanborn, J. Z.; Berman, S. H.; Beroukhim, R.; Bernard, B.; Wu, C. J.; Genovese, G.; Shmulevich, I.; Barnholtz-Sloan, J.; Zou, L.; Vegesna, R.; Shukla, S. A.; Ciriello, G.; Yung, W. K.; Zhang, W.; Sougnez, C.; Mikkelsen, T.; Aldape, K.; Bigner, D. D.; Van Meir, E. G.; Prados, M.; Sloan, A.; Black, K. L.; Eschbacher, J.; Finocchiaro, G.; Friedman, W.; Andrews, D. W.; Guha, A.; Iacocca, M.; O'Neill, B. P.; Foltz, G.; Myers, J.; Weisenberger, D. J.; Penny, R.; Kucherlapati, R.; Perou, C. M.; Hayes, D. N.; Gibbs, R.; Marra, M.; Mills, G. B.; Lander, E.; Spellman, P.; Wilson, R.; Sander, C.; Weinstein, J.; Meyerson, M.; Gabriel, S.; Laird, P. W.; Haussler, D.; Getz, G.; Chin, L.; Network, T. R., The somatic genomic landscape of glioblastoma. *Cell* **2013,** 155, (2), 462-77.
32. Tari, A. M.; Lopez-Berestein, G., Serum predominantly activates MAPK and akt kinases in EGFR- and ErbB2-over-expressing cells, respectively. *Int J Cancer* **2000,** 86, (2), 295-7.
33. Olsen, J. V.; Blagoev, B.; Gnad, F.; Macek, B.; Kumar, C.; Mortensen, P.; Mann, M., Global, in vivo, and site-specific phosphorylation dynamics in signaling networks. *Cell* **2006,** 127, (3), 635-48.
34. Levin, V. A.; Panchabhai, S. C.; Shen, L.; Kornblau, S. M.; Qiu, Y.; Baggerly, K. A., Different changes in protein and phosphoprotein levels result from serum starvation of high-grade glioma and adenocarcinoma cell lines. *J Proteome Res* **2010,** 9, (1), 179-91.
35. Yu, L. R.; Zhu, Z.; Chan, K. C.; Issaq, H. J.; Dimitrov, D. S.; Veenstra, T. D., Improved titanium dioxide enrichment of phosphopeptides from HeLa cells and high confident phosphopeptide identification by cross-validation of MS/MS and MS/MS/MS spectra. *J Proteome Res* **2007,** 6, (11), 4150-62.
36. Gallien, S.; Kim, S. Y.; Domon, B., Large-Scale Targeted Proteomics Using Internal Standard Triggered-Parallel Reaction Monitoring (IS-PRM). *Mol Cell Proteomics* **2015,** 14, (6), 1630-44.
37. Escher, C.; Reiter, L.; MacLean, B.; Ossola, R.; Herzog, F.; Chilton, J.; MacCoss, M. J.; Rinner, O., Using iRT, a normalized retention time for more targeted measurement of peptides. *Proteomics* **2012,** 12, (8), 1111-21.
38. Wu, C.; Shi, T.; Brown, J. N.; He, J.; Gao, Y.; Fillmore, T. L.; Shukla, A. K.; Moore, R. J.; Camp, D. G., 2nd; Rodland, K. D.; Qian, W. J.; Liu, T.; Smith, R. D., Expediting SRM assay development for large-scale targeted proteomics experiments. *J Proteome Res* **2014,** 13, (10), 4479-87.
39. Martinez-Garcia, E.; Lesur, A.; Devis, L.; Cabrera, S.; Matias-Guiu, X.; Hirschfeld, M.; Asberger, J.; van Oostrum, J.; Casares de Cal, M. L. A.; Gomez-Tato, A.; Reventos, J.; Domon, B.; Colas, E.; Gil-Moreno, A., Targeted Proteomics Identifies Proteomic Signatures in Liquid Biopsies of the Endometrium to Diagnose Endometrial Cancer and Assist in the Prediction of the Optimal Surgical Treatment. *Clin Cancer Res* **2017,** 23, (21), 6458-6467.
40. Woo, J.; Han, D.; Wang, J. I.; Park, J.; Kim, H.; Kim, Y., Quantitative Proteomics Reveals Temporal Proteomic Changes in Signaling Pathways during BV2 Mouse Microglial Cell Activation. *J Proteome Res* **2017,** 16, (9), 3419-3432.
41. Assiddiq, B. F.; Tan, K. Y.; Toy, W.; Chan, S. P.; Chong, P. K.; Lim, Y. P., EGFR S1166 phosphorylation induced by a combination of EGF and gefitinib has a potentially negative impact on lung cancer cell growth. *J Proteome Res* **2012,** 11, (8), 4110-9.

4

PHOSPHORYLATION RATIO DETERMINATION IN FRESH-FROZEN AND FORMALIN-FIXED PARAFFIN-EMBEDDED TISSUE WITH TARGETED MASS SPECTROMETRY

Lona Zeneyedpour[1], Christoph Stingl[1], Lennard J. M. Dekker[1], Dana A. M. Mustafa[2], Johan M. Kros[2], Theo M. Luider[1]

1. Erasmus MC, Department of Neurology, Rotterdam, The Netherlands
2. Erasmus MC, Department of Pathology, Rotterdam, The Netherlands

Journal of Proteome Research. 2020, 19(10):4179-4190
The Supporting Information is available at https://pubs.acs.org/doi/10.1021/acs.jproteome.0c00354.

ABSTRACT

Formalin-fixed paraffin-embedded (FFPE) tissues are routinely prepared and collected for diagnostics in pathology departments. These are, therefore, the most accessible research sources in pathology archives. In this study we investigated whether we can apply a targeted and quantitative parallel reaction monitoring (PRM) method for FFPE tissue samples in a sensitive and reproducible way. The feasibility of this technical approach was demonstrated for normal brain and glioblastoma multiforme tissues. Two methods were used: PRM measurement of a tryptic digest without phosphopeptide enrichment (Direct-PRM) and after Fe-NTA phosphopeptide enrichment (Fe-NTA-PRM). With these two methods, the phosphorylation ratio could be determined for four selected peptide pairs that originate from neuroblast differentiation-associated protein (AHNAK S5448-p), calcium/calmodulin-dependent protein kinase type II subunit delta (CAMK2D T337-p), eukaryotic translation initiation factor 4B (EIF4B S93-p) and epidermal growth factor receptor (EGFR S1166-p). In normal brain FFPE tissues, the Fe-NTA-PRM method enabled to quantify the targeted phosphorylated peptides with high reproducibility (CV < 14%). Our results indicate that formalin fixation does not impede relative quantification of a phospho-site and its phosphorylation ratio in FFPE tissues. The developed workflow combining these methods opens ways to study archival FFPE tissues for phosphorylation ratio determination in proteins.

Keywords
Phosphoproteomics, PRM, Targeted mass spectrometry, FFPE, Phosphorylation ratio, Quantitative proteomics, Clinical proteomics, Cancer proteomics

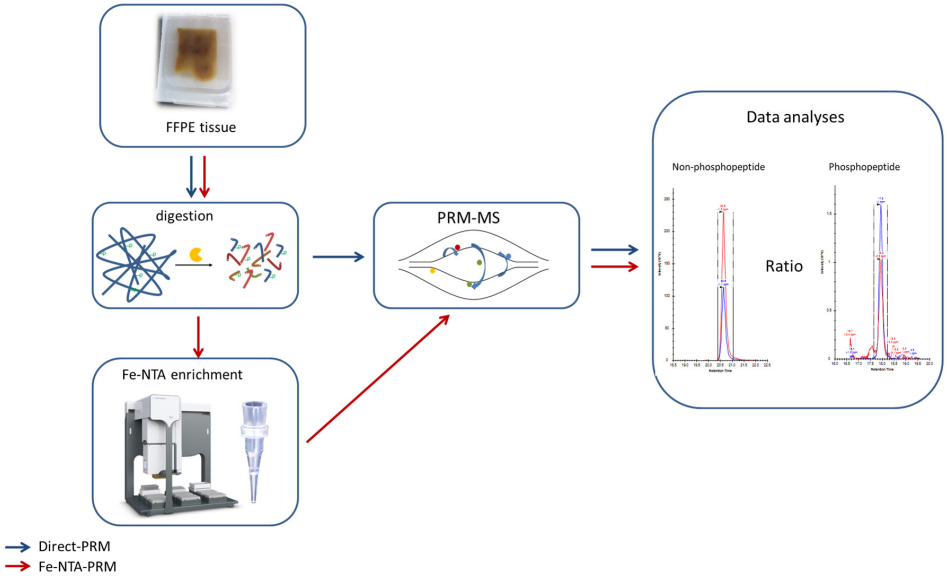

INTRODUCTION

Phosphorylation is a frequent post-translational modification in proteins[1, 2] involved in the regulation of cellular processes, including cell signalling[3, 4]. Many studies have shown that the regulation of phosphorylation in proteins can be derailed in diseases such as cancer[5-8]. Therefore, understanding the mechanisms of protein phosphorylation and dephosphorylation enables to unravel disease processes and generate ideas how to design appropriate drugs[9, 10].

Phosphoproteomics technology has improved from just measuring a few to ten thousands of phosphorylation sites in one sample[7, 11-13]. This has become an advantageous method to investigate phosphorylation sites in addition to antibodies which are only available for a relatively restricted number of phospho-sites. Mass spectrometry has resulted in the identification of unknown phosphorylation sites[14-16]. Phosphopeptide enrichment is essential to this purpose, and different methods such as immobilized metal ion metal affinity chromatography (IMAC), including Fe-NTA, and metal oxide affinity chromatography (MOAC) have been investigated and applied successfully[17-19]. IMAC and MOAC are complementary phosphopeptide enrichment methods and any of these two methods could also be chosen separately[19].

Phosphorylated peptides can be quantified in an absolute way or in relative numbers with targeted MS methods[20, 21]. Progress in high-resolution MS with Orbitrap mass analyzers has led to the parallel reaction monitoring (PRM) method that can outperform other targeted MS methods such as selected reaction monitoring (SRM)[16, 22, 23]. It has been demonstrated that relatively low ng mL^{-1} levels of HSP90α in serum could be measured by PRM combining multi-dimensional chromatography[22].

Formalin-fixed paraffin-embedded (FFPE) tissues are routinely prepared and collected for diagnostics in pathology departments. Therefore, FFPE tissues are the most accessible research source in pathology archives[24, 25]. An accurate MS-based method is essential to apply these valuable resources for proteomics research. Still, FFPE tissues in proteomics studies have been examined less due to covalent cross-links caused by formalin fixation resulting in less protein retrieval[26, 27]. However, chemical solutions exist that can successfully reverse these cross-links[12]. Recent studies about FFPE proteomics and phosphoproteomics have shown results comparable to those from frozen tissues[26-31]. Ostasiewicz and coworkers have shown that the phosphoproteome was preserved in FFPE. Using the filter-aided sample preparation (FASP) method, they were able to analyze phosphopeptides by mass spectrometry and could identify 7,718 phosphopeptides in FFPE tissue with an untargeted approach[11]. From tissue sections mounted on microscope slides, Wakayabashi and coworkers investigated a protein extraction method using

phase transfer surfactants as effective protein-solubilizing reagents[32]. They identified and quantified 1,413 unique phosphopeptides from FFPE murine liver tissue using Stable Isotope Dimethyl Labeling with this untargeted approach. Hembrough and coworkers have examined the clinical utility of targeted mass spectrometry and concluded that targeted mass spectrometry has the potential to serve as complementary method in diagnostics[33, 34].

In our previous study, we used a PRM method in combination with stable isotope labelled peptides in a U87 cell line[35] to determine the percentage of phosphorylation applying TiO_2 phosphopeptide enrichment. Extensive or complex sample processing to accurately calculate the phosphorylation percentage is not required with this method. In the present study we investigated – as the first, to our knowledge – whether we could develop a targeted and quantitative PRM method for FFPE tissue samples in a sensitive and reproducible way. Having combined an existing preparation method[36, 37] for FFPE tissues with this PRM method[35] to quantify phosphorylation ratio of specific phospho-sites in tissue is the novelty of our work. For this work we have used Fe-NTA as phosphopeptide enrichment method. The feasibility of this technological approach was demonstrated for normal brain and glioblastoma multiforme (GBM) tissues.

MATERIALS AND METHODS

Unless mentioned otherwise, all chemicals were purchased from Sigma-Aldrich, (Saint Louis, MO) and all solvents were purchased from Biosolve (Valkenswaard, The Netherlands).

Biological material

To optimize the PRM method, we used three pairs of both FF (fresh-frozen) and FFPE (formalin–fixed, paraffin-embedded) brain tissue from identical brain material. To validate our method, we used three pairs of FF and FFPE GBM tissues. In all experiments, 8 µm slices of FF tissues of the same brain material were compared with 8 µm slices of FFPE tissues. The tissue volume was the same for FF and FFPE tissues Supplemental Table S1 provides information on tissue volumes. The tissues were scanned using a slide scanner (NanoZoomer Digital Pathology System, Hamamatsu, Shizuoka, Japan). Tissue blocks were obtained from the Department of Pathology, Erasmus MC, Rotterdam. The use of patient material was approved by the Institutional Ethics Review Board of Erasmus MC, Rotterdam, the Netherlands (MEC 221.520/2002/262; date of approval 22 July 2003, and MEC-2005-057, date of approval 14 February 2005). Patients gave written consent to use their tissues for research purposes.

Sample preparation for LC-MS measurement

FFPE tissue lysis

Four 8 µm slices of tissues were cut and placed in separate Eppendorf tubes. The tissue was washed twice with 1 ml xylene and subsequently the tissue was rehydrated by two washes of 1 ml of each 100%, 70% and 50% ethanol and water, consecutively. Four hundred µl of 0.1% Rapigest (Waters, Milford, MA) in 300 mM Tris-Base, pH 8.0 was added to each tissue pellet (~500 µg total protein) and disrupted by external sonification for 2 min at 70% amplitude at a maximum temperature of 25°C (Branson, Ultrasonic, Danbury, CT). Samples were then incubated for 90 min at 90°C.

FF tissue lysis

Five to ten 8 µm FF tissue slices (see Table S1) were cut and placed in separate Eppendorf tubes. We used five to ten slices because in the tissue block size differs from that of the FFPE tissues. Four hundred µl of 0.1% Rapigest (Waters) was added to the tissue pellet (~500 µg total protein) and disrupted by external sonification for 2 min at 70% amplitude at a maximum temperature of 25°C (Branson) and incubated for 5 min at 99°C.

In-solution digestion

To the lysates of FF and FFPE tissue, after cooling down from the above-mentioned 90 and 99°C, 20 µl of 100 mM dithiothreitol (DTT) was added and incubated for 30 min at 60°C. Subsequently, 20 µl 300 mM iodoacetamide (IAA) was added and incubated at room temperature for 30 min. Then, 10 µg trypsin (Promega, Madison, WI) was added and incubated overnight at 37°C. After this incubation, 5 µl 50% trifluoroacetic acid (TFA) was added to each sample and centrifuged at 20,000 g. The supernatant of the digested sample was dried using a vacuum centrifuge (Savant SC210A, Thermo Fisher Scientific, Waltham, MA) and stored at -80 °C.

Desalting of peptides and phosphopeptides with automation

For the automated sample processing, an AssayMAP Bravo platform (Agilent technologies, Santa Clara, CA was used. For the phosphopeptide enrichment Fe-NTA cartridges were used. Manufacturer's protocols were applied for all cartridges as described below[38].

Desalting of peptides

Following the manufacturer's peptide cleanup protocol (v2.0)[38], the digested samples were desalted. C18 cartridges were primed with 100 µl 50% ACN /0.1% TFA and equilibrated with loading buffer (0.1% TFA / water). The dried digested tissue was re-suspended in 220 µl peptide mixture of Stable Isotope Labeled (SIL) peptides (see Table 1). Two hundred µl of the resuspended sample was loaded onto the C18 cartridge. The desalted peptides were eluted in 25 µl aquous elution buffer (70% ACN/0.1% TFA) after washing the cartridges with 100 µl loading buffer.

Fe-NTA phosphopeptide enrichment

Using the phosphopeptide enrichment protocol (v2.0)[38], the enrichment was achieved by using 5 µl Fe(III)-NTA cartridges on the AssayMAP Bravo platform. To the 25 µl desalted digested tissue sample, 95 µl 80% ACN/0.1% TFA was added. From this solution, 10 µl was kept to determine the peptide concentration using a quantitative colorimetric peptide assay (Pierce, Thermo Fisher Scientific, Rockford, IL). Fe-NTA cartridges were primed with 100 µl 50% ACN/0.1% TFA and equilibrated with equilibration buffer (80% ACN/0.1% TFA). The desalted digest of tissue samples was loaded onto the cartridges. Phosphopeptides were eluted with 25 µl 1% ammonia after washing the cartridges with 100 µl of the equilibration buffer. The eluted phosphopeptides were dried directly using a vacuum centrifuge. Dried samples were dissolved in 25 µl 0.1% TFA/ 2% ACN and measured by LC-MS.

Sample preparation for Parallel Reaction Monitoring (PRM)

For PRM analyses, four peptide pairs were selected; i.e., a phosphopeptide and its non-phosphorylated counterpart. For absolute quantification, SIL-peptides for these four peptide pairs were purchased (Pepscan, Lelystad, The Netherlands). The SIL-peptides were labeled with lysine-$^{13}C_{6,}$ $^{15}N_2$. The purity of the obtained peptides was >95% and the variation in the concentration was specified as less than 5%. The spiking levels of SIL-peptides in the digested samples were determined based on the measured levels of endogenous peptide in different samples; see Table 1. Using a robotic platform, phosphopeptide enrichment for 96 samples could be done in less than 2 hours, which makes this technology feasible for relative high throughput applications.

Sample preparation and analysis of the calibration curve

One hundred micrograms of digested FF and FFPE brain tissues were dissolved in 100 µl 0.1% TFA/ 2% ACN and spiked with a peptide mixture of 125 fmol/µl of all SIL-peptide calibrators. Eighteen dilutions with 2 fold incremental steps were prepared for both FF and FFPE tissues for non-phosphorylated peptides. For phosphopeptides, phosphopeptide-enriched brain tissue was used as matrix and spiked with a peptide mixture of 1 fmol/µl of all SIL-phosphopeptide calibrators. Five dilutions with 5 fold incremental steps were prepared for both FF and FFPE tissues. For both FF and FFPE brain tissue the dilution series were measured three times with mass spectrometry. Sensitivity was determined for each SIL-peptide separately. The limit of detection (LOD) and the lower limit of quantification (LLoQ) were calculated based on the standard deviation of the non-spiked sample (blank) and linear regression analysis on the slope of the calibrators. We used only calibrators with a CV lower than 20%.

The LOD was defined as (3.3xSD)/slope, and the LLoQ was defined as 3xLOD, according to ICH guidelines (http://www.ich.org).

Data dependent mass spectrometry measurements

Samples were analyzed by nano-LC (Ultimate 3000RS, Thermo Fisher Scientific, Germering, Germany). After preconcentration and washing the samples on a C18 trap column (5 mm × 300 µm internal diameter (ID), Thermo Fisher Scientific), samples were loaded onto a C18 column (PepMap C18, 75 µm ID × 250 mm, 2 µm particle and 100 Å pore size, Thermo Fisher Scientific) using a linear 90 minutes gradient (4-38% ACN/H20; 0.1% formic acid) at a flow rate of 300 nL/min. The separation of the peptides was monitored by a UV detector (absorption at 214 nm). The nano-LC was coupled to an Orbitrap Fusion Lumos (Thermo Fisher Scientific, San Jose, CA, USA). The Orbitrap Fusion Lumos was operated in the data dependent acquisition (DDA) mode. Full scan MS spectra (m/z 375-1,500) in profile mode were acquired in the Orbitrap with a resolution of 120,000 after accumulation of an AGC target of 400,000. A top speed method with a maximum duty cycle of 3 seconds was used. In these 3 seconds the most intense peptide ions from the full scan in the Orbitrap were fragmented by HCD (normalized collision energy 30%) and measured in the iontrap with an AGC target of 10,000. Maximum fill times were 50 ms for the full scans and 50 ms for the MS/MS scans. Precursor ion charge state screening was enabled and only charge states from 2-7 were selected for fragmentation. The dynamic exclusion was activated after the first time a precursor was selected for fragmentation and excluded for a period of 60 seconds using a relative mass window of 10 ppm. Lock mass correction was activated to improve mass accuracy of the survey scan.

The mass spectrometry proteomics data have been deposited to the ProteomeXchange Consortium via the PRIDE[39] partner repository with the dataset identifier PXD017943 and 10.6019/PXD017943.

Quantification-PRM approaches

Previously, we selected the investigated proteins based on their intensity level in a U87 cell line[35]. The selected four peptide pairs originate from AHNAK S5448 (ISAPNVDFNLEGPK) (high intensity), CAMK2D T337 (ESTESSNTTIEDEDVK) (medium intensity), EIF4B S93 (SPPYTAFLGNLPYDVTEESIK) (medium intensity) and EGFR S1166 (GSHQISLDNPDYQQDFFPK) (low intensity), see also Table 1. These four peptide pairs and the established PRM method were used for quantification of phosphorylated and non-phosphorylated forms of these peptides. The stable isotope-labeled forms of these peptides were used as internal standard in the PRM measurements.

To quantify the percentages of phosphorylation of the selected proteins, we used two different sample preparation methods: a) an in-solution digestion (Direct-PRM) and b) an in-solution digestion followed by Fe-NTA enrichment (Fe-NTA-PRM). The two mass spectrometry approaches are displayed in Figure 1; the same setting was used for the two PRM methods. Using Direct-PRM followed by the Fe-NTA-PRM approach, we

calculated the percentages of phosphorylation as well as the amounts in ng protein per 100 µg of total peptide for AHNAK, CAMK2D, EIF4B and EGFR proteins, respectively, for both the phosphorylated and the non-phosphorylated fraction. To determine the biological variation in the same FF and FFPE tissues, each tissue was sequentially sliced, digested and phospho-enriched in triplicate as explained above. Furthermore, with the use of the Fe-NTA-PRM approach, one of the tissues (Ctrl-3) was measured in triplicate to determine the technical variation of the PRM method. The experimental procedure is displayed in Figure 2. To validate the two PRM methods in clinical samples that contain known higher levels of EGFR than normal brain tissue, we selected three pairs of FF and FFPE GBM tissues. Each tissue pair was derived from the same tumor. EGFR is one of the targets for therapy in clinical trials for GBM[40]. Therefore, the of EGFR amplification and expression levels were taken into account in the selection of the GBM tissue. Three tissues have been selected according to clinical and expression data (Supplementary Table S2): tissue-GBM-17 (high level of EGFR), tissue-GBM-11 (medium level of EGFR) and tissue-GBM-21 (low level of EGFR).

Targeted-MS:

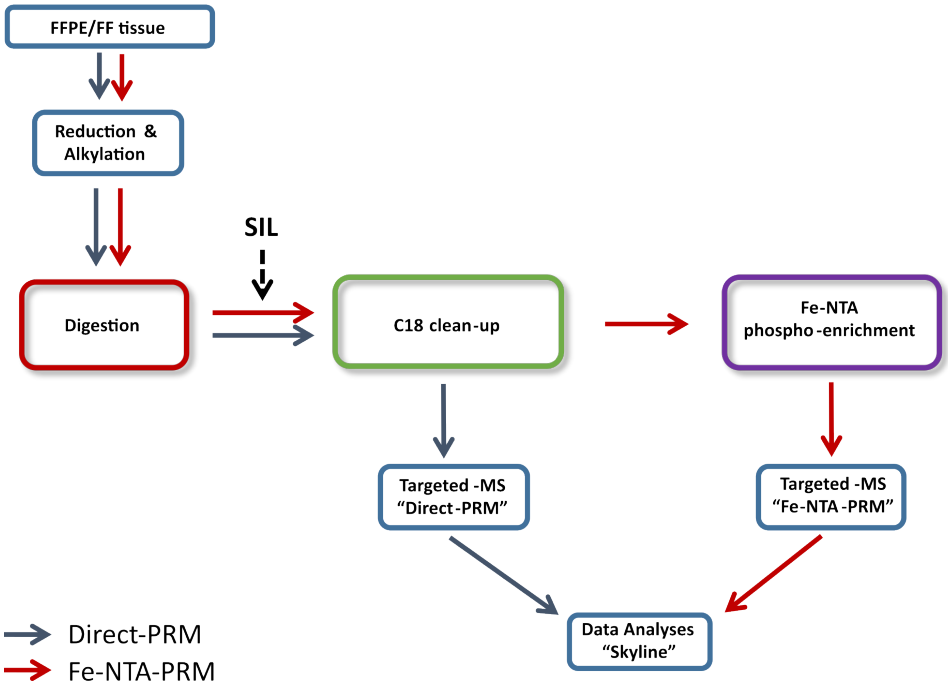

Figure 1: Flowchart of the two PRM methods: Direct-PRM (blue arrows) and Fe-NTA-PRM (red arrows).

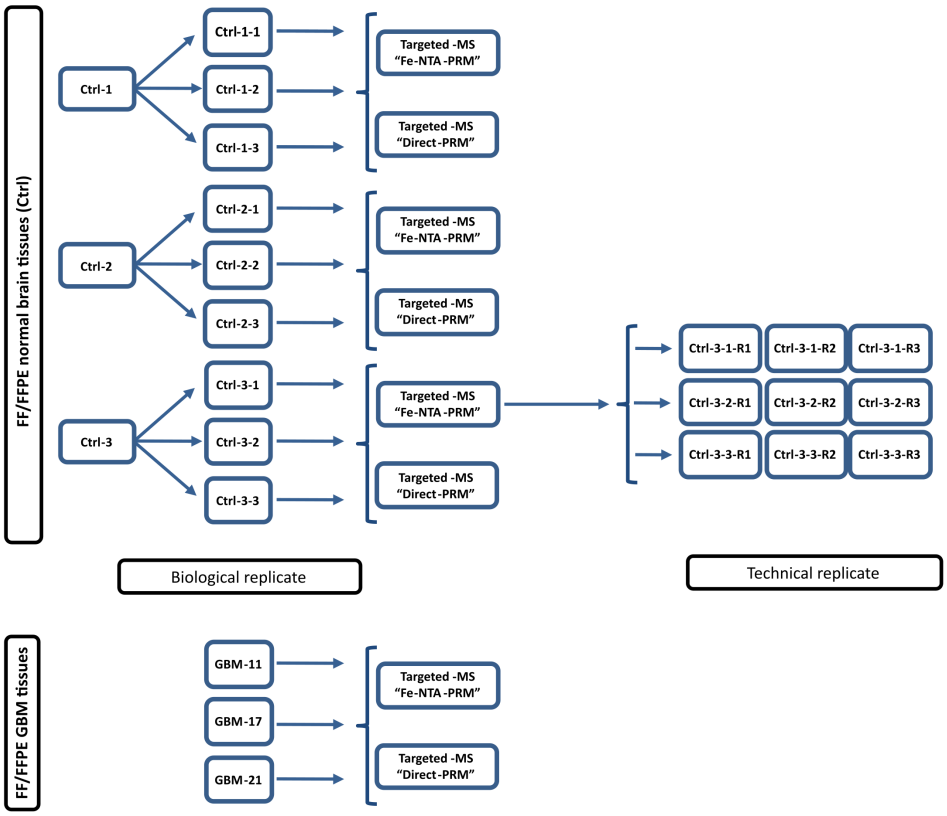

Figure 2: Flowchart of experimental procedures for the FF/FFPE tissues investigated.

PRM measurements

PRM was performed on a nano-LC Orbitrap Q Exactive HF. A shorter 30 minutes gradient was used on the nano-LC system under otherwise identical conditions as for the DDA measurements (90 min). A targeted MS/MS method was developed for 16 peptides (see Table 1). A quadrupole isolation window of 0.7 m/z units was applied, and an Orbitrap resolving power of 120,000 at 200 m/z was configured. An AGC target of 1e6 ions and a maximum fill time of 250 ms were applied. The normalized collision energy was optimized, and the retention time was determined for each peptide, using the SIL-peptides. An optimal normalized collision energy of NCE 20 for AHNAK, CAMK2D and EGFR and 25 for EIF4B selected peptides was used, and a retention time window of 3 minutes was applied for each peptide.

Table 1: Characteristics of peptides selected for targeted PRM approach

Protein	Sequence	Precursor mass	Charge	Extracted fragments	Amount of spiked peptide fmol/100 µg total peptide
AHNAK (S5448)	ISAPNVDFNLEGPK	750.8883	2	y8[+],y11[+],y12[++],y11[++]	-
	ISAPNVDFNLEGP**K**	754.8954			1000
	I**S**APNVDFNLEGPK	790.8714			-
	I**S**APNVDFNLEGP**K**	794.8714			1000
CAMK2D (T337)	ESTESSNTTIEDEDVK	892.3894	2	y6[+],y10[+],y11[+],y12[+]	-
	ESTESSNTTIEDEDV**K**	896.3965			1000
	ESTESSNT**T**IEDEDVK	932.3726		y6[+],y9[+],y11[+],y12[+]	-
	ESTESSNT**T**IEDEDV**K**	936.3797			1000
EGFR (S1166)	GSHQISLDNPDYQQDFFPK	746.015	3	y6[+],y7[+],y10[++],b9[+]	-
	GSHQISLDNPDYQQDFFP**K**	748.6864			1000
	GSHQI**S**LDNPDYQQDFFPK	772.6705			-
	GSHQI**S**LDNPDYQQDFFP**K**	775.3419			1000
EIF4B (S93)	SPPYTAFLGNLPYDVTEESIK	781.0581	3	y10[+],y10[++],b10[+],b11[+]	-
	SPPYTAFLGNLPYDVTEESI**K**	783.7295			2000
	SPPYTAFLGNLPYDVTEESIK	807.7136			-
	SPPYTAFLGNLPYDVTEESI**K**	810.3850			2000

*__Bold and underlined__ is a phosphorylated residue, **Bold** lysine-$^{13}C_6$ $^{15}N_2$

Data Processing and Analysis

From the DDA files, the MS/MS spectra were extracted and converted into mgf files by using MSConvert of ProteoWizard (version 3.0.10444). All mgf files were analyzed using Mascot (version 2.3.02; the Matrix Science, London, UK). Extracted MS/MS data were used in Mascot to perform database searches in the human subset of the uniprot_sprot_2015-11 database (Homo sapiens species restriction; 20,194 sequences). The following settings were used for the database search: a maximum of two miscleavages, oxidation as a variable modification of methionine, carbamidomethylation as a fixed modification of cysteine, and phosphotyrosine, phosphoserine and phosphothreonine as variable modifications. Trypsin was set as enzyme. A peptide mass tolerance of 10 ppm and a fragment mass tolerance of 0.5 Da were allowed. Scaffold software (version 4.8.7, Portland, OR) was used to summarize and filter MS/MS based peptides and protein identifications at an FDR of 1% (peptide and protein level) and to carry out protein grouping.

PRM data analysis

The PRM data was analyzed using the Skyline version 4.2.0.19009, MacCoss Lab Software[41]; fragment ions for each targeted mass were extracted and peak areas were integrated. Based on the peak areas, the ratio between the endogenous peptide and the SIL-peptide was calculated in Excel. The ratio, spiking level of the SIL-peptide and the total peptide concentration determined by the peptide assay were used to calculate the respective protein amount per 100 µg total peptide for each peptide. In addition, the

phosphorylation ratios were calculated using the formula:

$$\frac{\text{Amount of phosphorylated protein*} \times 100}{\text{amount of phosphorylated protein*} + \text{amount of non-phosphorylated protein*}} = \text{ratio phosphorylation (\%)**}$$

**For the targeted phosphorylation site.*
*** This formula assumes that trypsinization of non-phosphorylated proteins is as efficient as trypsinization of phosphorylated proteins. This is a rough assumption because in some instances this can be an effect[42]. If this occurs, then the use of other enzymes and PRM on missed cleavages can overcome such events.*

Statistical comparisons between methods and experimental conditions were performed using a t-test in Excel (p-value < 0.05 considered as significant) and Bland-Altman agreement-analysis using GraphPad Prism statistical software (Prism version 5.01 for Windows, GraphPad Software, La Jolla California USA, www.graphpad.com). Cluster analysis was performed with R 3.4.3 through the Metaboanalyst interface libraries [43]. Venn diagrams were made using Venny 2.1.0 version (https://bioinfogp.cnb.csic.es/tools/venny/index.html).

The mass spectrometry proteomics data have been deposited to the ProteomeXchange Consortium via the PRIDE[39] partner repository with the dataset identifier PXD017943 and 10.6019/PXD017943 for untargeted-MS and PXD017993 and 10.6019/PXD017993.

RESULTS

Untargeted mass spectrometry in normal brain tissue

Using an Orbitrap Fusion Lumos operated in DDA mode, we identified 2,580 proteins and 17,877 peptides in all FF brain samples and 1,616 proteins and 10,122 peptides in all FFPE brain samples. Applying phosphopeptide enrichment, 7,083 phosphopeptides in the FF tissues and 2,874 phosphopeptides in the FFPE tissues were identified. Supplementary Table S3 shows the identified non-phosphorylated and phosphorylated peptides for each tissue.

To determine the biological variation of the same FF and FFPE tissues, each tissue was sequentially sliced, digested and phosphopeptide enriched (using an AssayMAP Bravo platform) in triplicate. After applying phosphopeptide enrichment, the numbers of identified phosphopeptides for each FF and FFPE tissue were on average 4,426 and 1,893, with a mean CV of 5.1% and 21.5%, respectively. Supplemental Table S3 provides detailed information. Figure 3 presents the identified non-phosphoproteins, phosphoproteins, non-phosphopeptides and phosphopeptides in normal brain tissue (A) and GBM (B). In unsupervised hierarchical cluster analysis, too, the FF and FFPE tissues are grouped together (see supplemental Figure 1).

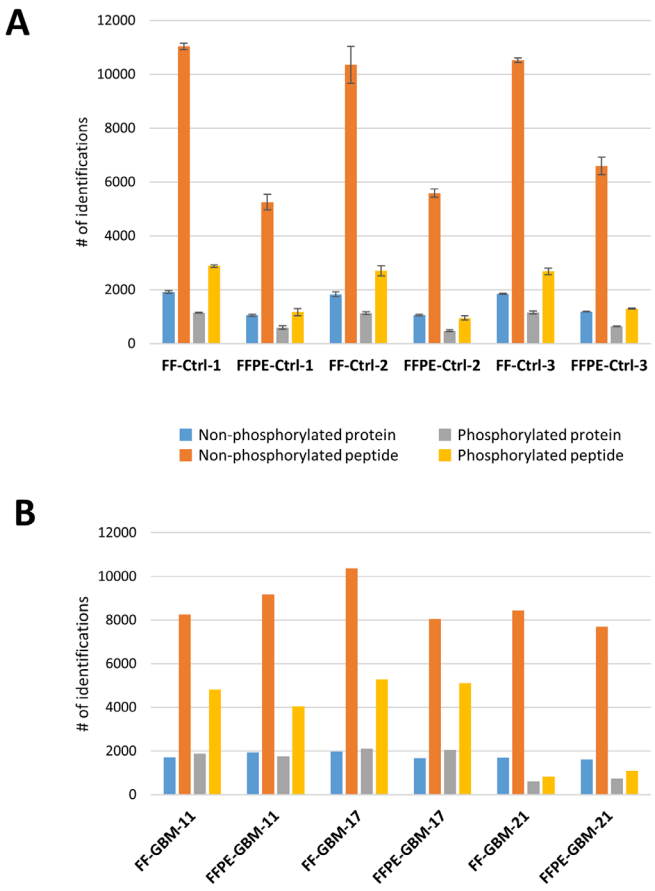

Figure 3: Total identified non-phosphorylated and phosphorylated proteins and peptides in A) normal brain tissue and B) GBM tissue.

After applying phosphopeptide enrichment, one of the three pairs of FF and FFPE tissues (Ctrl-1) was also measured in triplicate. This resulted in respectively a 2.6% and 3% CV for the identified phosphopeptides of FF and FFPE.

Targeted and quantitative mass spectrometry

Calibration curve

To examine the linearity between signal intensity and spiked stable isotope peptide amount, we prepared ten dilutions with two fold incremental steps. The SIL-peptides were diluted into digested tissue lysates (FF and FFPE) as matrix. The calculated R^2 value is for all the selected peptides of AHNAK, CAMK2D and EGFR higher than 0.994. For the EIF4B protein, the calibration curve showed a non-linear behavior if the whole concentration range was used. Therefore, we used a narrower concentration range, in

which EIF4B behaved linearly. Based on these calibration curves, the LOD and LLoQ of all SIL peptides were calculated (see Table 2). The LOD and LLoQ were also calculated with the phosphopeptide-enriched tissue (FF and FFPE) as matrix. This resulted in a much lower LOD and LLoQ compared to the non-phosphorylated (paired) peptides (Table 2). For the EIF4B protein in phosphopeptide-enriched tissue matrix, we could only measure EIF4B at the highest concentration (1.23 ng protein / 100 µg total peptide) of the calibration curve (CV < 20%). Supplementary Table S4 presents the calibration curve and linear regression analysis.

With the use of the Direct-PRM and Fe-NTA-PRM methods, the non-phosphorylated peptide and phosphorylated peptide of these proteins could be quantified. Regarding the EGFR peptide, both the phosphorylated and non-phosphorylated peptides were not detected in the normal brain tissue. It is likely that this is related to the lower amount of EGFR protein in normal brain tissue (Human Protein Atlas available, http://www.proteinatlas.org) than in the U87 cell line measured previously[35].

Biological and technical variations

In the PRM mode, we determined the amounts of selected non-phosphorylated and phosphorylated peptides, and subsequently calculated the phosphorylation ratios. In each FF or FFPE tissue, the calculated phosphorylation ratio had a maximum CV of 14.2% for AHNAK, of 7.3% for CAMK2D, and of 12.3% for EIF4B.

The mean calculated phosphorylation ratio of all three FF tissues is for AHNAK 1.4 ± 0.8%, CAMK2D 3.2 ± 0.2% and EIF4B 9.5 ± 2.6%. These ratios are comparable with the calculated phosphorylation ratios in all three FFPE tissues; for AHNAK 1.1 ± 0.6%, CAMK2D 2.2 ± 0.4% and EIF4B 9.2 ± 0.9 %. The measured concentrations, the CV values and the phosphorylation ratios are depicted in Figure 4 and in supplemental Table S5.

With the use of the Fe-NTA-PRM method, one of the tissues (Ctrl-3) was measured in triplicate to determine the technical variation of the PRM method. CV values of 4.2%, 6.4% and 1.0% were obtained for AHNAK, CAMK2D and EIF4B, respectively. For EGFR, neither the non-phosphorylated nor the phosphorylated peptide could be detected. The measured concentrations, the CV values and the phosphorylation ratios are summarized in Figure 5 and supplemental Table S6.

The calculated amounts of protein (µg) per volume (mm^3) of tissue are given in supplementary Table S1. In all FF tissues, we extracted a higher amount of protein per volume of tissue (range 97.5 to 215 µg / mm^3) compared to FFPE tissue (range 49.4 to 118.8 µg / mm^3), which implied a systematic off set change in relation to the results of PRM measurements.

Table 2: LOD and LLoQ values of spiked SIL-peptides in digested and phosphopeptide-enriched FF and FFPE tissue

Measurement	Matrix***	Applied MS approach	Protein	Peptide	Range spiked SIL peptides (ng protein / 100 µg peptides)	FF (ng / 100 µg total peptide)		FFPE (ng / 100 µg total peptide)	
						LOD	LLoQ	LOD	LLoQ
Calibration curve-1 (18 calibrators)*[1]	**Digested tissue**	**Direct-PRM**	**AHNAK (S5448)**	ISAPNVDFNLEGP**K**	0.12 - 7863.8	4.7	14.1	1.6	4.8
			CAMK2D (T337)	ESTESSNTTIEDEDV**K**	0.011 - 704.6	0.03	0.1	0.01	0.03
			EIF4B[2] (S93)	SPPYTAFLGNLPYDVTEESI**K**	108.0 - 864.4	30.0	90.1	10.8	32.4
			EGFR (S1166)	GSHQISLDNPDYQQDFFP**K**	0.026 - 1678.5	0.4	1.1	0.2	0.6
Calibration curve-2 (5 calibrators)**	**Phosphopeptide-enriched tissue**	**Fe-NTA-PRM**	**AHNAK (S5448)**	I**S**APNVDFNLEGP**K**	0.09 - 11.2	0.01	0.02	0.007	0.020
			CAMK2D (T337)	ESTESSNT**T**IEDEDV**K**	0.01 - 1.0	0.0001	0.0003	0.0001	0.0004
			EIF4B[3] (S93)	**S**PPYTAFLGNLPYDVTEESI**K**	0.01 - 1.23	1.23	1.23	1.23	1.23
			EGFR (S1166)	GSHQI**S**LDNPDYQQDFFP**K**	0.02 - 2.4	0.0004	0.001	0.001	0.002

[1]Only points with a CV less than 20% were used to calculate LOD and LLOQ.
[2]EIF4B peptides showed less sensitivity as the other peptides. Therefore, a smaller range has been used for EIF4B peptides. In this smaller range the peptides behaved linearly.
[3]EIF4B peptides only at the highest concentration (1.23 ng protein / 100 µg peptides) could be measured.
*Two-fold incremental steps
**Five-fold incremental steps
*** Digested tissue was used as matrix for LOD calculation of non-phosphopeptide and phosphopeptide-enriched tissue was used as matrix for LOD calculation of phosphopeptide

Untargeted mass spectrometry in GBM tissues

Using an Orbitrap Fusion Lumos with DDA mode, we could identify in GBM tissue samples on average 2,659 proteins and 15,972 peptides in all FF samples and 2,559 proteins and 15,094 peptides in all FFPE samples. Applying phosphopeptide enrichment resulted in the identification of 8,051 phosphopeptides in FF tissues and 7,344 phosphopeptides in FFPE GBM tissues. Figure 3-B shows the identified proteins and peptides in non-phosphopeptide-enriched samples and in the phosphopeptide enriched samples, (see supplementary Table S7). An unsupervised hierarchical cluster analysis of the identified phosphoproteins resulted in each pair of FF and FFPE GBM tissue grouped together; see supplemental Figure 1. Tissue GBM-21 differs from the other two tissues, this difference might correlate with a higher amount of necrosis in tissue GBM-21 compared to the other GBM samples. Necrosis results in decomposition of dead cells, which potentially leads to a different proteome profile[44].

Targeted and quantitative mass spectrometry

The non-phosphorylated and phosphorylated peptides of AHNAK, CAMK2D, EIF4B and EGFR could be quantified in GBM samples. The calculated non-phosphorylated, phosphorylated and phosphorylation ratios for AHNAK, CAMK2D and EIF4B in FF tissues are comparable with those in FFPE tissues; a t-test did not show significant differences. The measured concentrations, the CV values and the phosphorylation ratios are shown in Supplementary Table S8. EGFR could not be quantified by PRM and shotgun approaches in normal brain tissues, but, as expected, it could be measured in two of the three GBM tissue pairs (GBM-17 and GBM-11).

The measured concentration of EGFR in each GBM tissue varies in line with the clinical and expression data (Supplementary Table S2). The concentration of phosphorylated EGFR for selected phospho-site in FFPE tissues has been calculated as 0.54 ng and 2.03 ng in 100 µg of total peptide in tissues GBM-17 and GBM-11, respectively. The percentages of phosphorylation for the specific EGFR phospho-site is 9.4% (GBM-17) and 4.1% (GBM-11) in the corresponding FFPE tissues (in tissue GBM-21, EGFR as expected could not be detected) and in this regard there were no significant differences between FF and FFPE tissue for the EGFR phospho-site. Figure 4 (A-B) shows the measured concentrations and percentages of phosphorylation for all proteins in different tissues using the Fe-NTA-PRM approach.

Comparison of the measured concentrations by the Direct-PRM and Fe-NTA-PRM methods between all FF and FFPE (normal brain and GBM tissues) in a Bland–Altman plot with a ± 95% confidence interval showed a bias of 7.6% without an observed statistical difference in outcome (Figure 4-C).

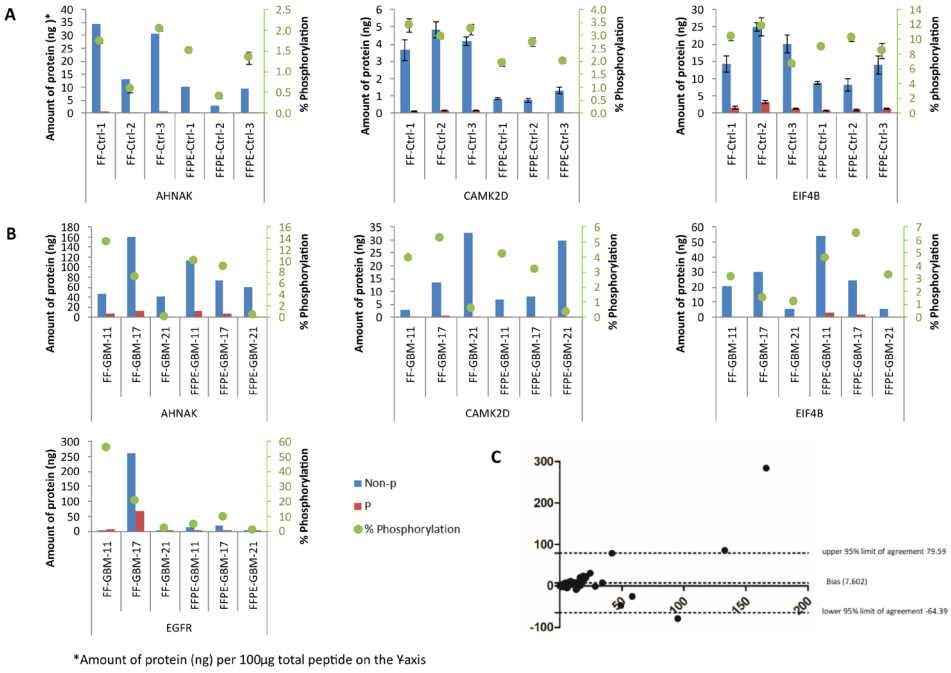

Figure 4: Changes in phosphorylated and non-phosphorylated protein abundance and phosphorylation ratio in. A) normal brain FF and FFPE tissues B) GBM FF and FFPE tissues C) Bland-Altman plot comparing proteins extracted from FFPE and FF tissue.

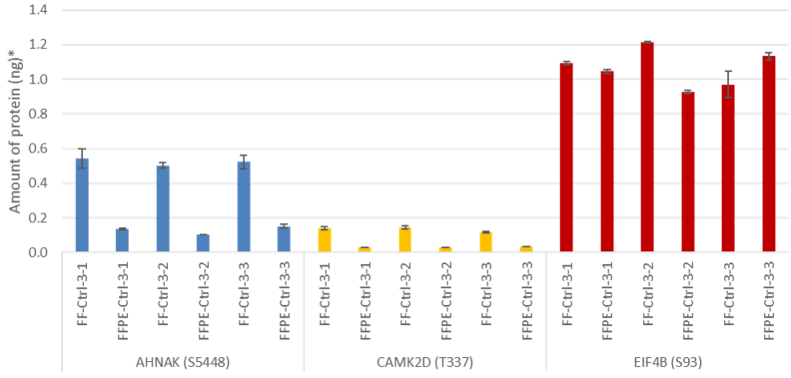

Figure 5: Amount of protein quantified and reproducibility of PRM method in phosphopeptide enriched tissues (technical triplicates).

DISCUSSION

The technical oriented study presented here is novel in that it integrates existing approaches that each works on its own, but have not yet been reported to work integrated for FFPE tissue. We showed the possibility to quantify phosphorylation with PRM in clinical tissue samples and successfully applied a targeted phosphoproteomics PRM method to analyze FFPE and FF of the same brain tissue. Previously, we have shown that this method can be applied to a U87 cell line [35]. This targeted method was performed using high resolution mass spectrometry to accurately determine the phosphorylation percentage of a selected set of phosphorylation sites in a cell lysate. Using the Direct-PRM and Fe-NTA-PRM methods, non-phosphopeptides and phosphopeptides can be measured and the phosphorylation percentage can be calculated.

In the present study we used the same targeted peptides as in the previous study of a U87 cell line (Table 1). The peptides were selected on the basis of their intensities in the U87 cell line. In tissues, the intensities of these peptides were different from those in the U87 cell line. The amount of EGFR in normal brain tissues could not be detected, and therefore EGFR was measured in GBM tissues. EGFR amounts in GBM tissue are often higher since an amplification of this gene in GBM is often observed[40, 45]. Confirmed by clinical and expression data, three GBM tissues with respectively high, medium and low of EGFR RNA expression level, caused by the presence or absence of amplification, were selected and successfully measured.

Regarding the reproducibility and quantitative performance, the results from normal brain FFPE tissues for the CAMK2D and AHNAK proteins were comparable to those measured in the U87 cell line. We could determine the phosphorylation ratio on four selected sites in all three pairs of FF and FFPE tissues with a CV of 4.2% (12% for U87 cell line) and CV of 7.3% (6.4% for U87 cell line) for AHNAK and CAMK2D, respectively. It proves that this PRM method is also applicable and reproducible for FF and FFPE tissues. In GBM tissues, the phosphorylation ratios of the selected proteins could be quantified, and no significant difference in this respect between FF and FFPE tissue for AHNAK, CAMK2D, EIF4B and EGFR proteins was found. In two of three (medium and high) GBM tissues, as expected, EGFR could be detected; see Figure 4-B.

An advantage of the PRM method is that multiple phosphorylation sites in one sample can be investigated simultaneously. The percentages of protein phosphorylation sites can be investigated for more phospho-sites compared to e.g. immunohistochemistry (IHC) using phosphopeptide specific antibodies. In this study we opted to investigate 8 peptides in parallel, but larger numbers are possible. Moreover, less material is needed and measurements can be done in a shorter time than with the traditional methods

(immunohistochemistry/ immunoassay) applied for FFPE.

As described for the non-fixated U87 cell line, the Direct-PRM method can also be applied to FFPE tissues for highly abundant phosphorylation sites, which is easier and faster (30 min gradient time) to apply than the Fe-NTA-PRM approach. However, phosphopeptide enrichment is necessary to reach the required sensitivity for low abundant phosphoproteins. This means that for most phosphopeptides, we need to perform Direct-PRM as well as Fe-NTA-PRM to determine the percentages of phosphorylation.

We compared the DDA method (untargeted method) with our developed PRM (targeted) method for identification of selected peptides in both normal brain and GBM tissues. The numbers of samples in which selected peptides have been identified are displayed in Figure 6. From this figure it can be concluded that with the PRM method the selected proteins could be measured more efficiently and consistently than with the DDA method, a stochastic process based on the probability to detect a specific peptide from a potential larger number of ions.

One of the main challenges in cancer research is heterogeneity of tumor tissues[12, 16]. Our cluster analysis of identified proteins and phosphoproteins revealed that in normal brain tissue all FFPE or FF tissues are grouped together. Consequently, these tissues have the same proteome and phosphoproteome. In GBM samples, however, each pair of FFPE and FF tissues was grouped together. This probably relates to inter tumor tissue heterogeneity for each patient[45]. Furthermore, in normal brain tissue we noticed a smaller difference between the numbers of identified peptides and phosphopeptides in FFPE than in FF tissues. We presumed this is due to a difference in the amount of extracted proteins per mm^3, which in all FF tissues was larger than in FFPE tissues. In GBM tissues, however, these differences in protein amount were more comparable (see Figure 3). In GBM tissues the determined amount of extracted proteins in FF tissues is still larger than in FFPE tissues. Still, the number of identifications is comparable, despite the fact, that FF tissues were smaller in size than the corresponding FFPE tissues (see Figure 7).

Another reason could be the impact of pre-analytical factors on FF and FFPE tissues. FFPE tissues are kept longer at room temperature during preparation in comparison with FF tissues[46, 47]. In addition, FFPE tissues are treated with formalin, water and organic solutions, which may result in less total protein per volume unit in FFPE materials than in FF materials. This feature could explain the lower protein content in FFPE tissue (Table S1). We presume that globular proteins are easier lost than cellular proteins in FFPE, and that this influences to some extent the phosphorylation ratio between different phosphoproteins and the amount of protein per volume unit.

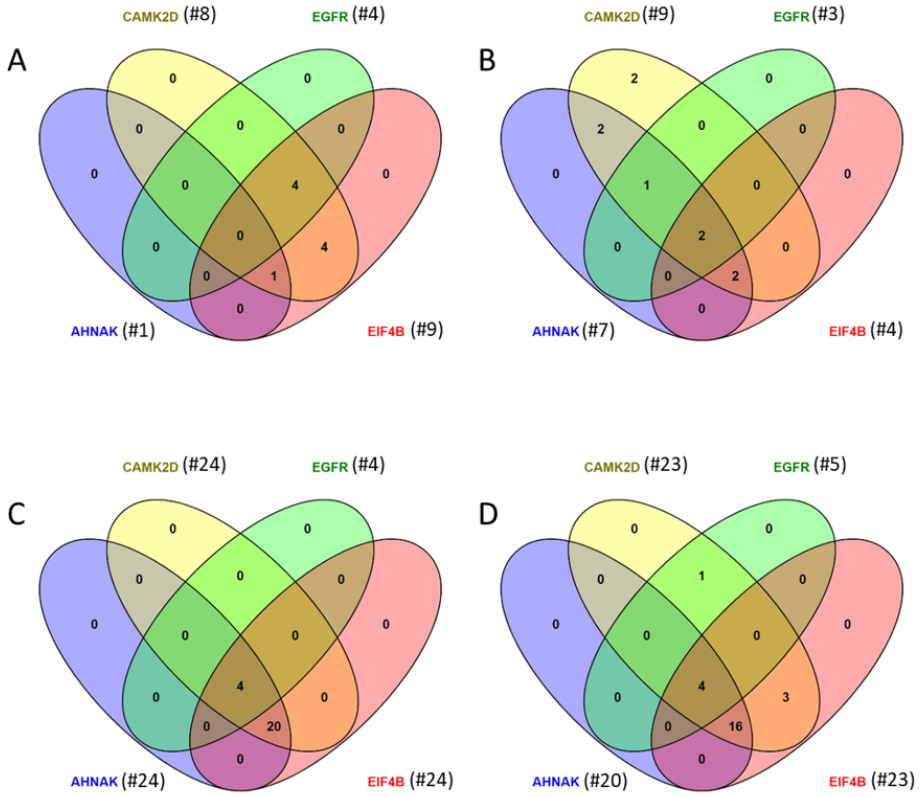

Figure 6: Number of samples both FF and FFPE (n=24) in which selected peptides have been identified in normal brain and GBM tissues. Explanation of the Venn diagram: (A) non-phosphorylated samples measured with DDA mode, (B) phosphorylated samples measured with DDA mode (C) non-phosphorylated samples measured with PRM mode and (D) phosphorylated samples measured with PRM mode. In the PRM method the selected proteins could be most ideally measured. For instance in panel D we could measure 4 samples with all 4 phosphorylated proteins (GBM-11 and GBM-17), 16 samples that had phosphorylated CAMK2D, EIF4B and AHNAK and 3 samples with the combination of phosphorylated CAMK2D and EIF4B. The PRM method showed a better sensitivity than the DDA method for all proteins.

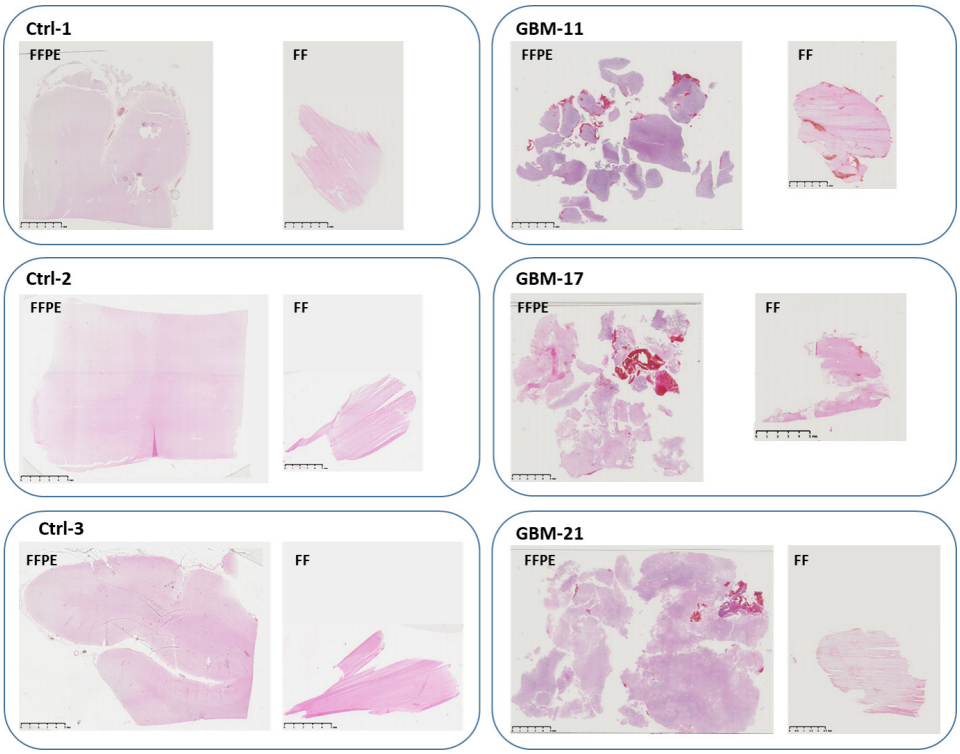

Figure 7: H&E staining of all tissues (unit of ruler is 1 mm except for FF-GBM-21 (0.5 mm))

EGFR is one of the targets for cancer therapy in clinical trials, and many research groups have attempted to improve understanding of the EGFR signaling pathway[40, 45]. Guerin et al. used the PRM method to quantify non-phosphopeptides of EGFR, HER2, HER3 and PTEN proteins (10 peptides) in breast cancer cell lines and frozen breast cancer tissues, including two phosphopeptides of HER2 protein in breast cancer cell lines[48].

In the present study, use of the developed PRM method for FFPE enabled to quantify the phosphorylation percentage of a phospho-site of EGFR in the GBM samples with known amplification of EGFR. We had prior knowledge of EGFR amplification and expression in these samples, and this was confirmed by the data obtained Hembrough and coworkers applied a Liquid Tissue-SRM method on microdissected FFPE tissue and cultured cells to quantify only the non-phosphorylated proteins, and compared the efficacy of this method with that that of IHC. They suggested this MS-based quantitative method for FFPE tissues could be implemented as a method for diagnostics, complementing traditional diagnostic methods such as IHC[33, 34]. While they didn't examine the phosphorylation in FFPE tissue. Wakabayashi and coworkers have shown that a dimethyl labeling untargeted method could be applied in an untargeted way to quantify phosphoproteins in FFPE

tissue [32]. Although the phosphorylation ratio for specific phospho-site is not determined. Our results support that the PRM method allows to sensitively measure diagnostic markers in FFPE tissues: 0.1 pg to 10 ng per 100 µg tissue for both phosphorylated and non-phosphorylated proteins. This method does not require extensive sample preparations such as excessive fractionation, laser capture microdissection (LCM) or gel electrophoresis[26].

CONCLUSIONS

The PRM method is a promising approach to quantify pairs of non-phosphorylated and phosphorylated peptides and to determine the percentage of phosphorylation of specific phospho-sites in biological samples such as FFPE tissue in a multiplex way. From our findings in a sample of four non-phosphopeptides and phosphorylated peptide pairs we conclude that formalin fixation does not impede relative quantification of phospho-sites in FFPE tissues compared to FF materials.

List of supporting information:
Table-S1-Volume and amount of protein of tissues
Table-S2-Clinical and expression data in GBM samples
Table-S3-Identified proteins and peptides in normal brain tissues
Table-S4-PRM technical variation in normal brain tissue
Table-S5-Calibration curves
Table-S6-Overview of concentration, CV values and percentage phosphorylation in normal brain tissue
Table-S7-Identified proteins and peptides in GBM tissues
Table-S8-Overview of concentration, CV values and percentage phosphorylation in GBM tissues
Figure 1: Unsupervised cluster analysis of identified A) non-phosphoproteins and B) phosphoproteins in FF and FFPE tissues

Acknowledgment
The mass spectrometry equipment used for this study was in part financed by the Netherlands Organisation for Scientific Research (NWO) infrastructure grant number 1631. This work has received funding from the Eurostars–2 joint program with cofunding from the European Union Horizon 2020 research and innovation program (Eurostars project 10688 (GlioPhos)).

REFERENCES

1. Hunter, T., Signaling--2000 and beyond. *Cell* **2000,** 100, (1), 113-27.
2. Osinalde, N.; Aloria, K.; Omaetxebarria, M. J.; Kratchmarova, I., Targeted mass spectrometry: An emerging powerful approach to unblock the bottleneck in phosphoproteomics. *J Chromatogr B Analyt Technol Biomed Life Sci* **2017,** 1055-1056, 29-38.
3. Burkhart, J. M.; Gambaryan, S.; Watson, S. P.; Jurk, K.; Walter, U.; Sickmann, A.; Heemskerk, J. W.; Zahedi, R. P., What can proteomics tell us about platelets? *Circ Res* **2014,** 114, (7), 1204-19.
4. Manning, G.; Whyte, D. B.; Martinez, R.; Hunter, T.; Sudarsanam, S., The protein kinase complement of the human genome. *Science* **2002,** 298, (5600), 1912-34.
5. Rikova, K.; Guo, A.; Zeng, Q.; Possemato, A.; Yu, J.; Haack, H.; Nardone, J.; Lee, K.; Reeves, C.; Li, Y.; Hu, Y.; Tan, Z.; Stokes, M.; Sullivan, L.; Mitchell, J.; Wetzel, R.; Macneill, J.; Ren, J. M.; Yuan, J.; Bakalarski, C. E.; Villen, J.; Kornhauser, J. M.; Smith, B.; Li, D.; Zhou, X.; Gygi, S. P.; Gu, T. L.; Polakiewicz, R. D.; Rush, J.; Comb, M. J., Global survey of phosphotyrosine signaling identifies oncogenic kinases in lung cancer. *Cell* **2007,** 131, (6), 1190-203.
6. Wulfkuhle, J. D.; Berg, D.; Wolff, C.; Langer, R.; Tran, K.; Illi, J.; Espina, V.; Pierobon, M.; Deng, J.; DeMichele, A.; Walch, A.; Bronger, H.; Becker, I.; Waldhor, C.; Hofler, H.; Esserman, L.; Investigators, I. S. T.; Liotta, L. A.; Becker, K. F.; Petricoin, E. F., 3rd, Molecular analysis of HER2 signaling in human breast cancer by functional protein pathway activation mapping. *Clin Cancer Res* **2012,** 18, (23), 6426-35.
7. Archer, T. C.; Ehrenberger, T.; Mundt, F.; Gold, M. P.; Krug, K.; Mah, C. K.; Mahoney, E. L.; Daniel, C. J.; LeNail, A.; Ramamoorthy, D.; Mertins, P.; Mani, D. R.; Zhang, H.; Gillette, M. A.; Clauser, K.; Noble, M.; Tang, L. C.; Pierre-Francois, J.; Silterra, J.; Jensen, J.; Tamayo, P.; Korshunov, A.; Pfister, S. M.; Kool, M.; Northcott, P. A.; Sears, R. C.; Lipton, J. O.; Carr, S. A.; Mesirov, J. P.; Pomeroy, S. L.; Fraenkel, E., Proteomics, Post-translational Modifications, and Integrative Analyses Reveal Molecular Heterogeneity within Medulloblastoma Subgroups. *Cancer Cell* **2018,** 34, (3), 396-410 e8.
8. Bode, A. M.; Dong, Z., Post-translational modification of p53 in tumorigenesis. *Nature Reviews Cancer* **2004,** 4, (10), 793-805.
9. Reimand, J.; Wagih, O.; Bader, G. D., The mutational landscape of phosphorylation signaling in cancer. *Scientific Reports* **2013,** 3, 2651.
10. Blom, N.; Sicheritz-Ponten, T.; Gupta, R.; Gammeltoft, S.; Brunak, S., Prediction of post-translational glycosylation and phosphorylation of proteins from the amino acid sequence. *Proteomics* **2004,** 4, (6), 1633-49.
11. Ostasiewicz, P.; Zielinska, D. F.; Mann, M.; Wiśniewski, J. R., Proteome, Phosphoproteome, and N-Glycoproteome Are Quantitatively Preserved in Formalin-Fixed Paraffin-Embedded Tissue and Analyzable by High-Resolution Mass Spectrometry. *Journal of Proteome Research* **2010,** 9, (7), 3688-3700.
12. Maes, E.; Mertens, I.; Valkenborg, D.; Pauwels, P.; Rolfo, C.; Baggerman, G., Proteomics in cancer research: Are we ready for clinical practice? *Crit Rev Oncol Hematol* **2015,** 96, (3), 437-48.
13. Gámez-Pozo, A.; Sánchez-Navarro, I.; Calvo, E.; Díaz, E.; Miguel-Martín, M.; López, R.; Agulló, T.; Camafeita, E.; Espinosa, E.; López, J. A.; Nistal, M.; Vara, J. Á. F., Protein phosphorylation analysis in archival clinical cancer samples by shotgun and targeted proteomics approaches. *Molecular BioSystems* **2011,** 7, (8), 2368-2374.
14. Doll, S.; Gnad, F.; Mann, M., The Case for Proteomics and Phospho-Proteomics in Personalized Cancer Medicine. *Proteomics Clin Appl* **2019,** 13, (2), e1800113.
15. Liu, Y.; Chance, M. R., Integrating phosphoproteomics in systems biology. *Computational and Structural Biotechnology Journal* **2014,** 10, (17), 90-97.
16. Mnatsakanyan, R.; Shema, G.; Basik, M.; Batist, G.; Borchers, C. H.; Sickmann, A.; Zahedi, R. P., Detecting post-translational modification signatures as potential biomarkers in clinical mass spectrometry. *Expert Review of Proteomics* **2018,** 15, (6), 515-535.
17. Montoya, A.; Beltran, L.; Casado, P.; Rodríguez-Prados, J.-C.; Cutillas, P. R., Characterization of a TiO_2 enrichment method for label-free quantitative phosphoproteomics. *Methods (San Diego, Calif)* **2011,** 54, (4), 370-378.
18. Beausoleil, S. A.; Jedrychowski, M.; Schwartz, D.; Elias, J. E.; Villen, J.; Li, J.; Cohn, M. A.; Cantley, L. C.; Gygi, S. P., Large-scale characterization of HeLa cell nuclear phosphoproteins. *Proc Natl Acad Sci U S A* **2004,** 101, (33), 12130-5.
19. Villen, J.; Gygi, S. P., The SCX/IMAC enrichment approach for global phosphorylation analysis by mass spectrometry. *Nat Protoc* **2008,** 3, (10), 1630-8.
20. Lawrence, R. T.; Searle, B. C.; Llovet, A.; Villen, J., Plug-and-play analysis of the human phosphoproteome by targeted high-resolution mass spectrometry. *Nat Methods* **2016,** 13, (5), 431-4.
21. Bourmaud, A.; Gallien, S.; Domon, B., Parallel reaction monitoring using quadrupole-Orbitrap mass spectrometer: Principle and applications. *Proteomics* **2016,** 16, (15-16), 2146-59.
22. Guzel, C.; Govorukhina, N. I.; Stingl, C.; Dekker, L. J. M.; Boichenko, A.; van der Zee, A. G. J.; Bischoff, R. P. H.; Luider, T. M., Comparison of

Targeted Mass Spectrometry Techniques with an Immunoassay: A Case Study for HSP90alpha. *Proteomics Clin Appl* **2018,** 12, (1).
23. Banerjee, S. L.; Dionne, U.; Lambert, J. P.; Bisson, N., Targeted proteomics analyses of phosphorylation-dependent signalling networks. *J Proteomics* **2018,** 189, 39-47.
24. Hood, B. L.; Conrads, T. P.; Veenstra, T. D., Mass spectrometric analysis of formalin-fixed paraffin-embedded tissue: unlocking the proteome within. *Proteomics* **2006,** 6, (14), 4106-14.
25. Ludyga, N.; Grünwald, B.; Azimzadeh, O.; Englert, S.; Höfler, H.; Tapio, S.; Aubele, M., Nucleic acids from long-term preserved FFPE tissues are suitable for downstream analyses. *Virchows Archiv* **2012,** 460, (2), 131-140.
26. Gustafsson, O. J. R.; Arentz, G.; Hoffmann, P., Proteomic developments in the analysis of formalin-fixed tissue. *Biochimica et Biophysica Acta (BBA) - Proteins and Proteomics* **2015,** 1854, (6), 559-580.
27. Piehowski, P. D.; Petyuk, V. A.; Sontag, R. L.; Gritsenko, M. A.; Weitz, K. K.; Fillmore, T. L.; Moon, J.; Makhlouf, H.; Chuaqui, R. F.; Boja, E. S.; Rodriguez, H.; Lee, J. S. H.; Smith, R. D.; Carrick, D. M.; Liu, T.; Rodland, K. D., Residual tissue repositories as a resource for population-based cancer proteomic studies. *Clin Proteomics* **2018,** 15, 26.
28. Flores-Morales, A.; Iglesias-Gato, D., Quantitative Mass Spectrometry-Based Proteomic Profiling for Precision Medicine in Prostate Cancer. *Frontiers in Oncology* **2017,** 7, (267).
29. Guo, T.; Wang, W.; Rudnick, P. A.; Song, T.; Li, J.; Zhuang, Z.; Weil, R. J.; DeVoe, D. L.; Lee, C. S.; Balgley, B. M., Proteome Analysis of Microdissected Formalin-fixed and Paraffin-embedded Tissue Specimens. *Journal of Histochemistry & Cytochemistry* **2007,** 55, (7), 763-772.
30. Holfeld, A.; Valdes, A.; Malmstrom, P. U.; Segersten, U.; Lind, S. B., Parallel Proteomic Workflow for Mass Spectrometric Analysis of Tissue Samples Preserved by Different Methods. *Anal Chem* **2018,** 90, (9), 5841-5849.
31. Longuespee, R.; Alberts, D.; Pottier, C.; Smargiasso, N.; Mazzucchelli, G.; Baiwir, D.; Kriegsmann, M.; Herfs, M.; Kriegsmann, J.; Delvenne, P.; De Pauw, E., A laser microdissection-based workflow for FFPE tissue microproteomics: Important considerations for small sample processing. *Methods* **2016,** 104, 154-62.
32. Wakabayashi, M.; Yoshihara, H.; Masuda, T.; Tsukahara, M.; Sugiyama, N.; Ishihama, Y., Phosphoproteome Analysis of Formalin-Fixed and Paraffin-Embedded Tissue Sections Mounted on Microscope Slides. *Journal of Proteome Research* **2014,** 13, (2), 915-924.
33. Hembrough, T.; Thyparambil, S.; Liao, W.-L.; Darfler, M. M.; Abdo, J.; Bengali, K. M.; Hewitt, S. M.; Bender, R. A.; Krizman, D. B.; Burrows, J., Application of Selected Reaction Monitoring for Multiplex Quantification of Clinically Validated Biomarkers in Formalin-Fixed, Paraffin-Embedded Tumor Tissue. *The Journal of Molecular Diagnostics* **2013,** 15, (4), 454-465.
34. Hembrough, T.; Thyparambil, S.; Liao, W. L.; Darfler, M. M.; Abdo, J.; Bengali, K. M.; Taylor, P.; Tong, J.; Lara-Guerra, H.; Waddell, T. K.; Moran, M. F.; Tsao, M. S.; Krizman, D. B.; Burrows, J., Selected Reaction Monitoring (SRM) Analysis of Epidermal Growth Factor Receptor (EGFR) in Formalin Fixed Tumor Tissue. *Clin Proteomics* **2012,** 9, (1), 5.
35. Dekker, L. J. M.; Zeneyedpour, L.; Snoeijers, S.; Joore, J.; Leenstra, S.; Luider, T. M., Determination of Site-Specific Phosphorylation Ratios in Proteins with Targeted Mass Spectrometry. *J Proteome Res* **2018,** 17, (4), 1654-1663.
36. Kawashima, Y.; Kodera, Y.; Singh, A.; Matsumoto, M.; Matsumoto, H., Efficient extraction of proteins from formalin-fixed paraffin-embedded tissues requires higher concentration of tris(hydroxymethyl)aminomethane. *Clin Proteomics* **2014,** 11, (1), 4.
37. van Huizen, N. A.; Coebergh van den Braak, R. R. J.; Doukas, M.; Dekker, L. J. M.; JNM, I. J.; Luider, T. M., Up-regulation of collagen proteins in colorectal liver metastasis compared with normal liver tissue. *J Biol Chem* **2019,** 294, (1), 281-289.
38. Agilent Workflow Automation for LC/MS: In-Solution Protein Digestion, Peptide Cleanup, and Strong Cation-Exchange Fractionation of Peptides Enabled by AssayMAP Technology. (https://www.agilent.com/cs/library/applications/5991-3602EN.pdf)
39. Perez-Riverol, Y.; Csordas, A.; Bai, J.; Bernal-Llinares, M.; Hewapathirana, S.; Kundu, D. J.; Inuganti, A.; Griss, J.; Mayer, G.; Eisenacher, M.; Perez, E.; Uszkoreit, J.; Pfeuffer, J.; Sachsenberg, T.; Yilmaz, S.; Tiwary, S.; Cox, J.; Audain, E.; Walzer, M.; Jarnuczak, A. F.; Ternent, T.; Brazma, A.; Vizcaino, J. A., The PRIDE database and related tools and resources in 2019: improving support for quantification data. *Nucleic Acids Res* **2019,** 47, (D1), D442-D450.
40. Westphal, M.; Maire, C. L.; Lamszus, K., EGFR as a Target for Glioblastoma Treatment: An Unfulfilled Promise. *CNS drugs* **2017,** 31, (9), 723-735.
41. MacLean, B.; Tomazela, D. M.; Shulman, N.; Chambers, M.; Finney, G. L.; Frewen, B.; Kern, R.; Tabb, D. L.; Liebler, D. C.; MacCoss, M. J., Skyline: an open source document editor for creating and analyzing targeted proteomics experiments. *Bioinformatics* **2010,** 26, (7), 966-8.
42. Dickhut, C.; Feldmann, I.; Lambert, J.; Zahedi, R. P., Impact of digestion conditions on phosphoproteomics. *J Proteome Res* **2014,** 13, (6), 2761-70.

43. Chong, J.; Yamamoto, M.; Xia, J., MetaboAnalystR 2.0: From Raw Spectra to Biological Insights. *Metabolites* **2019,** 9, (3).
44. Marshall, K. D.; Edwards, M. A.; Krenz, M.; Davis, J. W.; Baines, C. P., Proteomic mapping of proteins released during necrosis and apoptosis from cultured neonatal cardiac myocytes. *American journal of physiology Cell physiology* **2014,** 306, (7), C639-C647.
45. An, Z.; Aksoy, O.; Zheng, T.; Fan, Q.-W.; Weiss, W. A., Epidermal growth factor receptor and EGFRvIII in glioblastoma: signaling pathways and targeted therapies. *Oncogene* **2018,** 37, (12), 1561-1575.
46. Gündisch, S.; Annaratone, L.; Beese, C.; Drecol, E.; Marchiò, C.; Quaglino, E.; Sapino, A.; Becker, K.-F.; Bussolati, G., Critical roles of specimen type and temperature before and during fixation in the detection of phosphoproteins in breast cancer tissues. *Laboratory investigation; a journal of technical methods and pathology* **2015,** 95, (5), 561-571.
47. Gundisch, S.; Grundner-Culemann, K.; Wolff, C.; Schott, C.; Reischauer, B.; Machatti, M.; Groelz, D.; Schaab, C.; Tebbe, A.; Becker, K. F., Delayed times to tissue fixation result in unpredictable global phosphoproteome changes. *J Proteome Res* **2013,** 12, (10), 4424-34.
48. Guerin, M.; Goncalves, A.; Toiron, Y.; Baudelet, E.; Pophillat, M.; Granjeaud, S.; Fourquet, P.; Jacot, W.; Tarpin, C.; Sabatier, R.; Agavnian, E.; Finetti, P.; Adelaide, J.; Birnbaum, D.; Ginestier, C.; Charafe-Jauffret, E.; Viens, P.; Bertucci, F.; Borg, J. P.; Camoin, L., Development of parallel reaction monitoring (PRM)-based quantitative proteomics applied to HER2-Positive breast cancer. *Oncotarget* **2018,** 9, (73), 33762-33777.

5

NOVEL ANTIBODY–PEPTIDE BINDING ASSAY INDICATES PRESENCE OF IMMUNOGLOBULINS AGAINST EGFR PHOSPHO-SITE S1166 IN HIGH-GRADE GLIOMA

Lona Zeneyedpour [1], Christoph Stingl [1], Johan M. Kros [2], Peter A. E. Sillevis Smitt [1], and Theo M. Luider [1]

[1] Department of Neurology, Erasmus MC, 3015 GD Rotterdam, The Netherlands
[2] Department of Pathology, Erasmus MC, 3015 GD Rotterdam, The Netherlands

International Journal of Molecular Science. 2022, 23(9):5061
The supporting information can be downloaded at:
https://www.mdpi.com/article/10.3390/ijms23095061/s1.

ABSTRACT

We investigated the feasibility of detecting the presence of specific autoantibodies against potential tumor-associated peptide antigens by enriching these antibody–peptide complexes using Melon Gel resin and mass spectrometry. Our goal was to find tumor-associated phospho-sites that trigger immunoreactions and raise autoantibodies that are detectable in plasma of glioma patients. Such immunoglobulins can potentially be used as targets in immunotherapy. To that aim, we describe a method to detect the presence of antibodies in biological samples that are specific to selected clinically relevant peptides. The method is based on the formation of antibody–peptide complexes by mixing patient plasma with a glioblastoma multiforme (GBM) derived peptide library, enrichment of antibodies and antibody–peptide complexes, the separation of peptides after they are released from immunoglobulins by molecular weight filtration and finally mass spectrometric quantification of these peptides. As proof of concept, we successfully applied the method to dinitrophenyl (DNP)-labeled α-casein peptides mixed with anti-DNP. Further, we incubated human plasma with a phospho-peptide library and conducted targeted analysis on EGFR and GFAP phospho-peptides. As a result, immunoaffinity against phospho-peptide GSHQIS[+80]LDNPDYQQDFFPK (EGFR phospho-site S1166) was detected in high-grade glioma (HGG) patient plasma but not in healthy donor plasma. For the GFAP phospho-sites selected, such immunoaffinity was not observed.

Keywords

Antibodies; tumor-specific antigen; Melon Gel; phospho-proteomics; mass spectrometry

INTRODUCTION

Proteins in tumors may differ from proteins in normal tissue in quantity, amino acid sequence, post-translational modification or three-dimensional structure. These altered properties can potentially lead to the generation of autoantibodies [1]. Recent studies have shown that antibodies against specific tumor-associated antigens are detectable in blood in various types of cancer and could be valuable for monitoring cancer treatment [1–5] and, potentially, generate treatment options.

In eukaryotes, phosphorylation is a common post-translational modification in proteins. Many studies have shown that dysregulation of protein phosphorylation plays an important role in the development of cancer—as comprehensively reviewed by Ardito et al. [6] and Mahoney et al. [7]. Aberrantly phosphorylated peptides can be derived from these dysregulated cell signaling pathways in various cancers and may serve as tumor-specific antigens [7,8]. Antigenic peptides can bind to major histocompatibility complex (MHC) class I and II molecules. MHC-restricted phospho-peptides might be promising targets for cancer immunotherapy [7–10].

Developments in high-resolution mass analyzers have led to progress in targeted mass spectrometry (MS) methods, such as parallel reaction monitoring (PRM) [11,12]. PRM enables absolute and relative quantification of peptides, including phospho-peptides, with high selectivity and sensitivity [13,14]. Mapping of phospho-sites and quantification of the ratio of phosphorylation is possible in both biological and clinical samples, such as fresh-frozen specimen, formalin-fixed paraffin-embedded (FFPE) tissues, cell line cultures and body fluids [15–17].

Several techniques are available to purify immunoglobulins (IgG) from plasma or other body fluids; e.g., ammonium sulfate precipitation and affinity purification using protein A, protein G or ion exchange chromatography [18,19]. In contrast, Melon Gel resin (Thermo Fisher Scientific, Waltham, MA, USA) retains non-IgG proteins and hence allows enrichment of IgG directly from the sample without an extra (acidic) elution step. In this assay, we used this special property of Melon Gel resin to enrich Ig and Ig–peptide complexes that we formed by mixing clinical plasma samples with GBM-tissue-derived peptide libraries.

The aim of the present study was to develop a method to determine the immunoaffinity of plasma IgG against peptide antigens. We evaluated the applicability of this method by detecting the presence of IgG against a tumor-specific EGFR phospho-peptide in plasma from glioma patients.

RESULTS

Detection of Anti-DNP-Bound Peptides with Melon Gel Resin

The feasibility of the Ab–peptide binding assay was first tested by binding and detection of DNP-labeled peptides in the presence of anti-DNP. Selectivity was determined on the basis of both unspecific binding of peptides in the absence of anti-DNP (negative control experiment) and the detection of unlabeled peptides. In both experiments (presence and absence of anti-DNP), Avastin was present as a DNP-unspecific antibody, at a 100-fold higher (based on vendor's specifications) amount than the amount of anti-DNP when present. Selectivity was assessed by comparing the abundances of the individual peptides in the IgG-bound fraction to the abundances of the unbound and filter-bound fractions. In addition to the fractions collected during the assay described in Figure 1, in the feasibility assay we collected two filter-bound fractions, namely the peptides that passed the MW cut-off filter after acidification (FB1) and the peptides retained in the filter device (FB2).

IgG-bound, unbound and filter-bound fractions were analyzed by PRM measurements, whereby 19 alpha-casein peptides (7 of them DNP-labeled) were detected in at least one fraction. The four most abundant DNP-peptides (DNP modifications indicated with the delta mass [+166]) were TK[+166]VIPYVR, LTEEEK[+166]NR, HIQK[+166]EDVPSER and EK[+166]VNELSK, which accounted for 99.0% of the total number (MS response) of DNP-labeled peptides. Further, DNP-labeled peptides were predominately (83.4%) found in IgG-bound (IB) fractions when anti-DNP was present. When no anti-DNP was present, DNP-peptides were found mainly in the unbound (20.3%) and filter-bound (77.9%) fractions, and only to a minor extent in the IgG-bound fraction (1.8%). Unlabeled peptides were, independent of the presence or absence of anti-DNP, predominantly found in unbound (37.8% in the presence and 23.7% in the absence of anti-DNP) and filter-bound (61.5% and 71.4%, respectively) fractions. In IgG-bound fractions, only small numbers of unlabeled peptides were measured (in the presence of anti-DNP = 0.7% and in the absence of anti-DNP = 1.0%). (Figures 2 and S1)

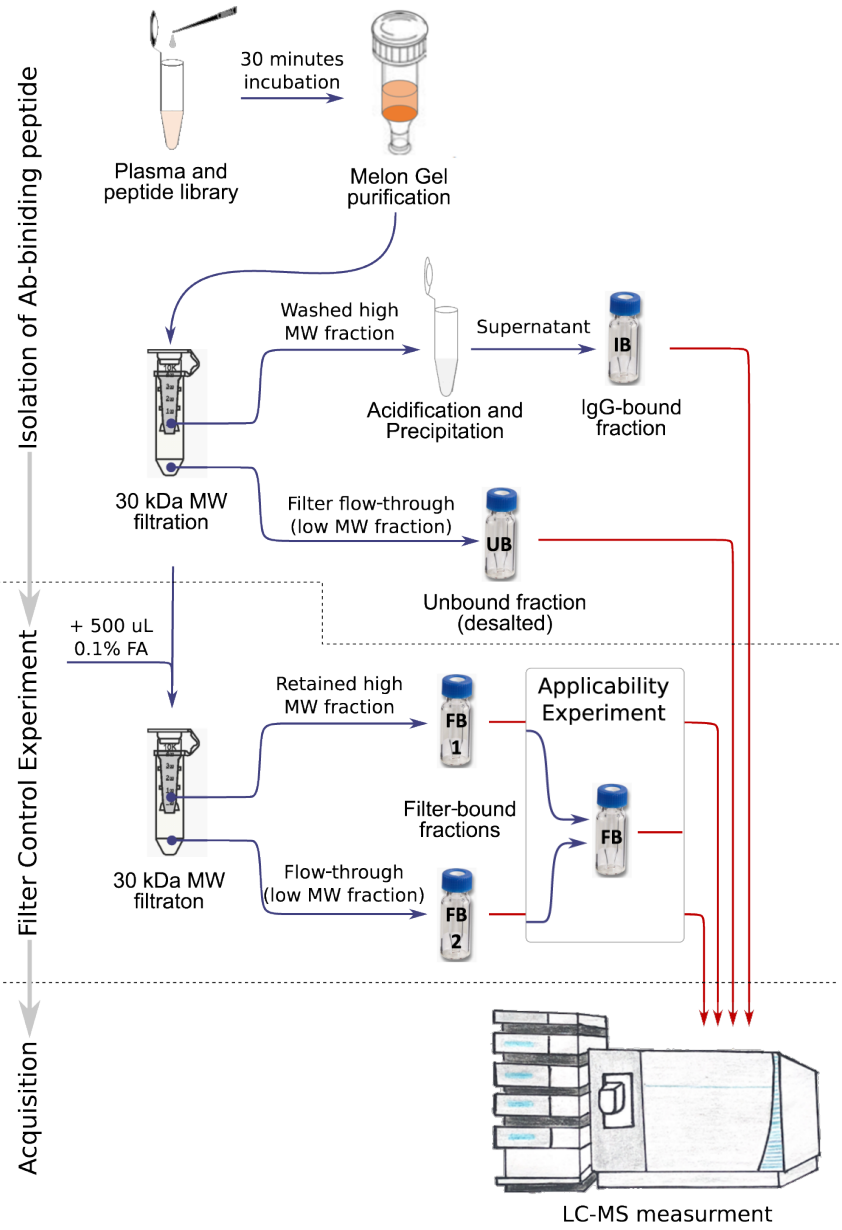

Figure 1. Flowchart of the antibody–peptide binding assay. IgG-bound fraction (IB), unbound fraction (UB) and filter-bound fraction (FB) annotated on LC vials are described in the text. In the feasibility experiment, two filter-bound fractions (high- and low-MW fractions) were collected and analyzed separately. In the applicability experiment, filter-bound fractions FB1 and FB2 were taken together as one filter-bound fraction (FB).

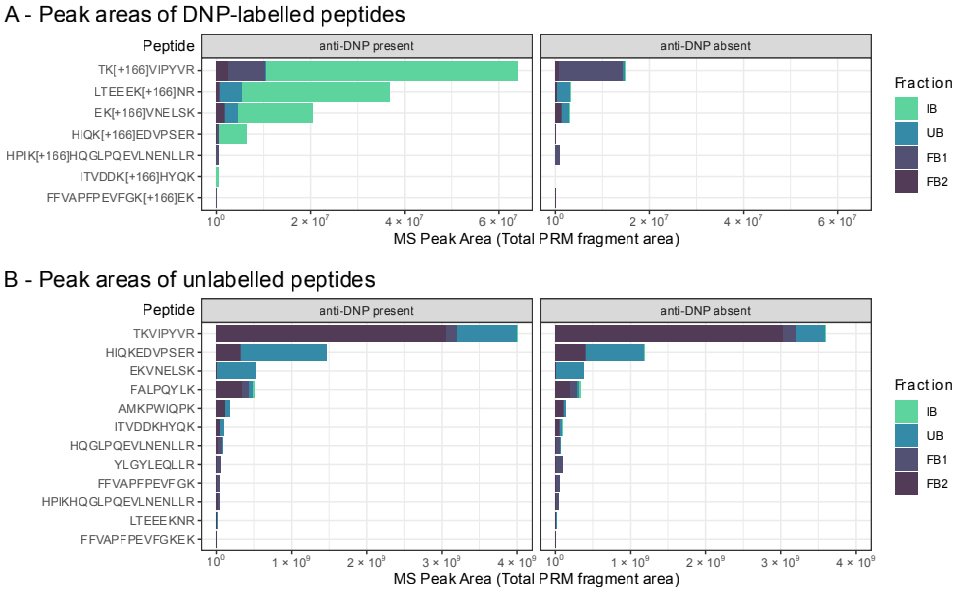

*Figure 2. Bar chart of peak abundances of DNP-labeled peptides (**A**) and unlabeled peptides (**B**).* The peptides were determined in the presence (left) or the absence (right) of anti-DNP. Color of the bars indicate corresponding fractions: IgG-bound fraction (IB), unbound fraction (UB), fraction remaining in the filter (FB1) and passed the MW filter (FB2) after acidification and centrifugation.

Selection of GBM-Associated Phospho-Peptide Antigens

In a previous study [15], we measured the total proteome and phospho-proteome of three GBM and three normal brain tissue (NBT) samples using shotgun proteomics with the aim of demonstrating the phosphorylation ratio in clinically relevant FFPE samples. In total, the bottom-up shotgun analysis of these six samples yielded 7020 phosphorylated, 1234 double-phosphorylated and 252 triple- or higher phosphorylated peptides. Comparing GBM and NBT, 238 of these phospho-peptides were exclusively found in all (3/3) GBM samples, and 2083 phospho-peptides were exclusively found in 2/3 of GBM samples. For the following Ab–peptide binding assay, we considered peptides exclusively found in at least two GBM samples—and thus not in any normal brain tissue—as putatively related to GBM and hence a potential target peptide antigen. Next, we linked the corresponding precursor proteins of these peptides to a well-known association in GBM and, as a result, selected seven GFAP peptides and one EGFR peptide as targets for the Ab–peptide binding assay (Supplementary Table S2) [20–23].

GFAP was the protein with the second highest abundance (spectra counts) in the dataset and was found in all GBM and normal brain tissue (NBT) samples with sequence coverages from 58.8% to 85.6%. Numbers of phospho-sites determined were on average five times higher in GBM samples compared to normal brain tissue (GBM: 13.3 vs. NBT: 2.7). Interestingly, peptides that cover the first 41 amino acids (within the head domain,

amino acids 1–72) and the corresponding phospho-sites were exclusively identified in GBM samples. For the Ab–peptide binding assay, two phospho-peptides of the head domain, three phospho-peptides of the rod domain, and two phospho-peptides of the tail domain were selected as potential epitope targets. Compared to GFAP, EGFR was found in lower abundance (abundance ranked by spectra count of 1089 of 3236 total proteins identified). It was almost exclusively identified in two of the three GBM samples, with sequence coverages from 7.9% to 35.2% and with a total of 17 phospho-sites. The identified phospho-peptides and non-phospho-peptides of EGFR and GFAP are shown in Figure 3.

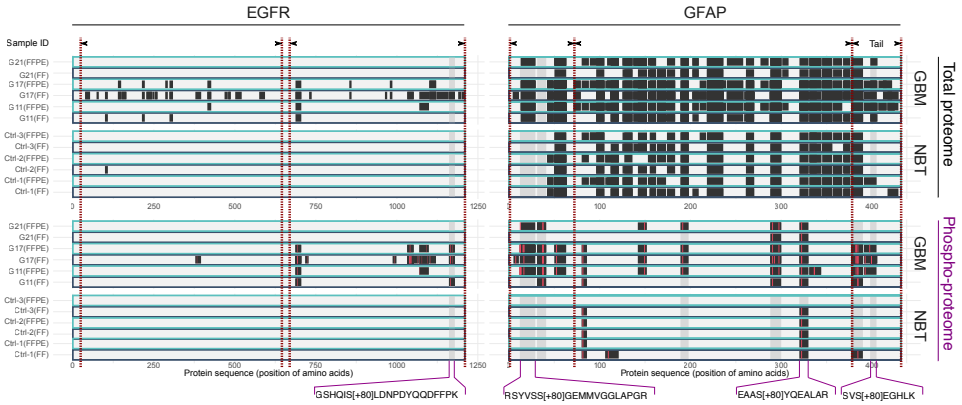

*Figure 3. Sequence coverage and phospho-sites of EGFR (**left**) and GFAP (**right**) identified in the total proteome analysis (top) and phospho-proteome analysis (**bottom**) of 3 glioblastoma multiforme (GBM) and 3 normal brain tissue (NBT) samples.* Results were derived from a publicly available dataset of a previous study (PXD017943). Each sample was prepared and processed in two forms, as fresh frozen tissue (FF, dark blue) and formalin-fixed paraffin-embedded tissue (FFPE, light blue). Dark segments indicate regions covered by peptide identifications, and the red lines mark identified phospho-sites. Gray regions in the sequence mark phospho-peptide targets used for PRM measurements. The four peptides that are annotated at the bottom of the plot were used as epitope-carrying peptide antigens for the Ab–peptide binding assay.

Ab–Peptide Binding Assay on EGFR and GFAP Phospho-Peptides

Performing an Ab–peptide binding assay using HGG and healthy plasma samples and the GBM phospho-peptide library, we detected EGFR phospho-peptide GSHQIS[+80] LDNPDYQQDFFPK (phosphorylation is annotated with the delta mass, [+80]) in three of four IgG-bound fractions of samples incubated with HGG plasma, but not in the corresponding unbound fractions. This result indicates the presence of autoantibodies against EGFR phospho-peptide GSHQIS[+80]LDNPDYQQDFFPK in these three GBM patients. The opposite result was obtained in the donor sample, where the peptide was detected almost exclusively in the unbound fraction (Figure 4). With the use of Avastin as negative control instead of plasma, the EGFR peptide GSHQIS[+80]LDNPDYQQDFFPK

was solely found in the unbound fraction. In two HGG samples, pnop-13 and pnop-30, major proportions (77.9% and 80.1%, respectively) of the peptide were found in the filter-bound fraction. In one of the four samples, pnop-17, the peptide could not be detected in any of the fractions, and consequently a reliable interpretation of the result was not possible for this specific sample; hence, this sample was not further analyzed.

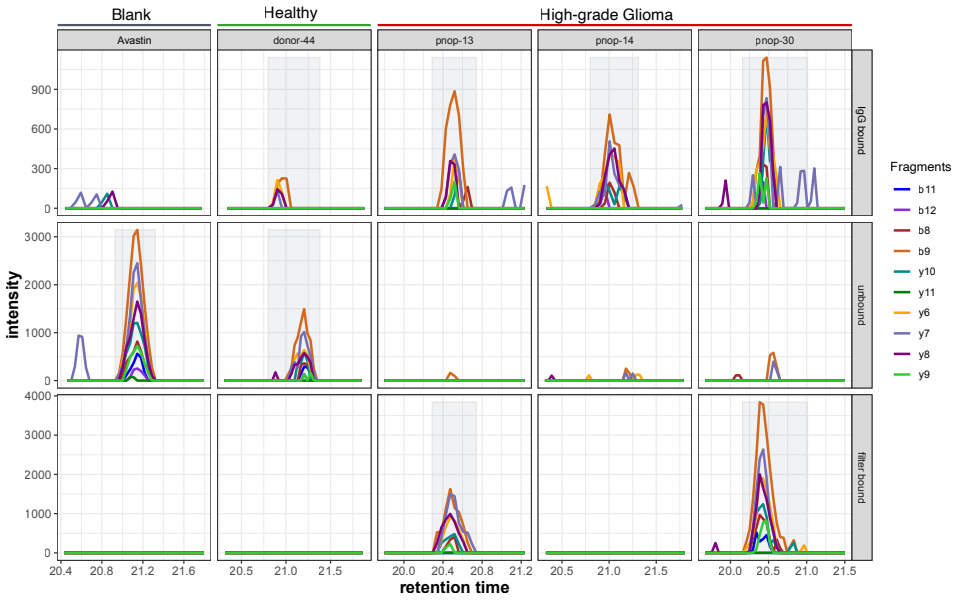

Figure 4. PRM peaks of EGFR peptide GSHQIS[+80]LDNPDYQQDFFPK in the IgG-bound, unbound and filter-bound fractions of one blank sample (Avastin), one healthy control plasma sample and three HGG plasma samples. A fourth HGG plasma sample did show any detectable response of this peptide and was excluded from the analysis (data not shown in figure). Colors in the chromatogram plots indicate the various fragments detected and used for quantification. Gray peak background indicates if a positive peak detection on the basis of at least 3 fragments was achieved.

Furthermore, the IgG binding affinity of the seven GFAP phospho-peptides (Supplementary Table.S2 and Figure S2) was tested analogously to the EGFR phospho-peptide binding assay in five HGG plasma samples and two healthy donor plasma samples. Peptides that were not detected in any fraction (LGPGTRLS[+80]LAR, KIES[+80]LEEEIR, QLQS[+80]LTCDLESLR and ITIPVQT[+80]FSNLQIR) were excluded from further analysis. Three peptides, EAAS[+80]YQEALAR, SVS[+80]EGHLK and RS[+80]YVSSGEMMVGGLAPGR, could be detected reliably in at least one fraction of the assay, whereas peptides were not detected in the IgG-bound fraction in any of the samples, be it HGG or donor plasma. This indicated no detectable quantities of autoantibodies against these three GFAP phospho-peptides.

Mapping of Background and Unspecific Binding Peptides

To determine the background of the Ab–peptide binding assay, we analyzed the IgG-bound fractions (IB) of a total peptide library, in which 4256 peptides were identified and quantified. This library was tested against three samples: (a) Avastin as a blank, (b) HGG plasma and (c) healthy donor plasma. The three IgG-bound fractions were analyzed by an untargeted MS method (DDA), a method that allowed us to obtain a complete overview of the peptides of these samples but offers lower sensitivity than the PRM method used, as described before. Sixty-eight peptides were identified in the blank sample (Avastin) versus 92 and 97 in the HGG plasma and healthy donor plasma samples, respectively. These peptides, in total 127 unique sequences, were grouped depending on whether they were found in the IgG-bound fraction of the blank sample (they were also independently found in a plasma sample, N = 68 peptides), or solely in HGG plasma (N = 12 peptides), or solely in donor plasma (N =13 peptides) or in both plasma samples (N = 34 peptides) (Figure 5 and Supplemental Table S3). Precursor abundances of the peptides in the originating total peptide library were determined by label-free quantitation and assigned, if applicable, to the appropriate division (blank, donor, HGG or donor and HGG). Peptides found in the IgG-bound fractions (IB) were predominantly (100 of 127) also highly abundant in the peptide library (top abundance quartile), which had on average a 10–100-fold higher abundance than the mean abundance of all peptides in the library. Approximately half (56 of 127) of these peptides are derived from high- and middle-abundant plasma proteins (Supplemental Table S3).

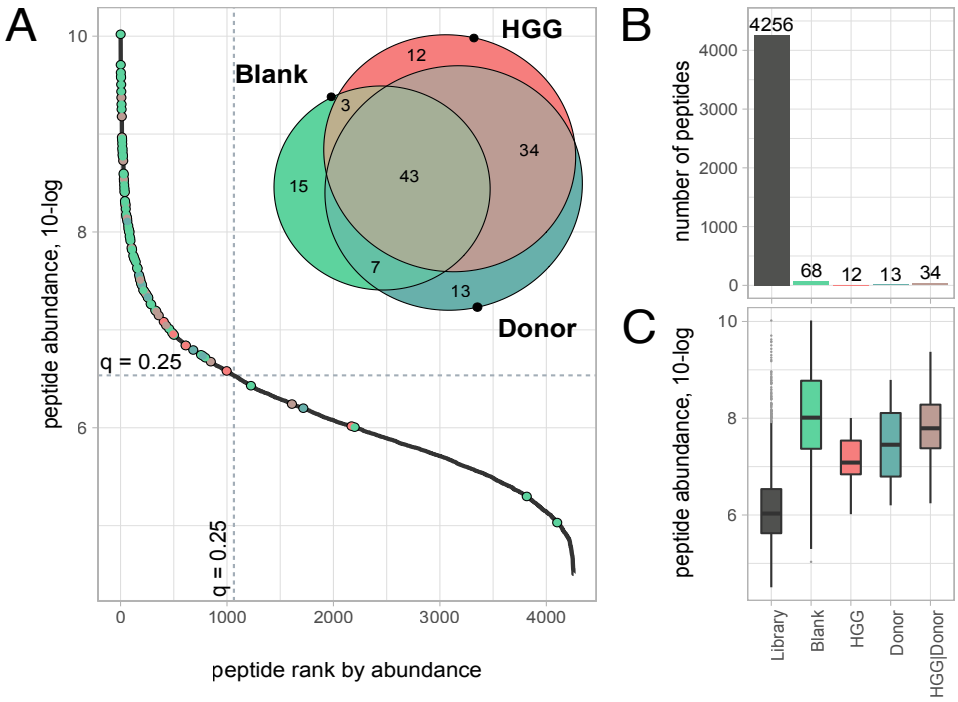

Figure 5. (**A**) Waterfall plot of total peptide library, with (logarithmic) peptide abundance plotted against the peptide abundance rank; peptides identified using shotgun proteomics in the blank sample (Avastin), HGG plasma or donor plasma samples are marked as points, with a color corresponding to the originating sample. Dotted horizontal and vertical lines show the abundance level (6.54) and rank (1065), respectively, of the top peptide abundance quartile. The Venn diagram insert shows the originating sample of the 127 peptides. (**B**) Bar chart of number of peptides identified in the peptide library (gray) and the Ab-binding fraction of an Avastin blank (including peptides that were found in blanks and other samples), donor plasma, HGG plasma and in both, HGG and donor plasma. (**C**) Box-plot of peptide abundances (10-log transformed) of the sets of peptides specified in panel B.

DISCUSSION

We have successfully described an assay to detect peptide antigens through their affinity for circulating antibodies in plasma. In this approach, Ab–peptide complexes are separated from non-IgG proteins and unbound low-molecular-weight peptides by Melon Gel IgG purification and molecular weight filtration. In a second step, these peptide antigens are dissociated from the antibodies by acidification, and the released peptides are separated from the IgG-fraction by acetone precipitation. Finally, sensitive and confident (selective) detection of peptides is accomplished by high-resolution mass spectrometry (parallel reaction monitoring). Hence, the antibodies themselves

are actually not measured directly, but their presence is determined by the detection of corresponding peptide antigens. In practice, the association with a particular type of cancer or stage of disease is determined by the selected set of peptide antigens (peptide library) and antibody samples (e.g., plasma sample). We conducted two experiments to demonstrate the feasibility and applicability of the method.

The IgG purification method plays a central role in this assay, as it allows the enrichment of intact IgG–peptide complexes and ultimately the isolation of the bound peptide antigens. We used Melon Gel IgG purification as it offers several advantages over conventional immunoaffinity methods such as protein A or protein G affinity purification. The actual mechanism of Melon Gel IgG purification is not described in detail in the literature. Basically, Melon Gel binds all non-Ig proteins and allows the IgG fraction to be collected simply in the flow-through. Hence, in contrast to other techniques, an elution step that could potentially affect the integrity of the antibody is not needed, and the purified IgG fraction can be collected directly. The Melon Gel technique does not require immobilization of antibodies and avoids reduction in the site-specific accessibility dependent on the coupling conditions. The free IgG remains more accessible to an antigen than in the case of binding to an immobilized antibody. In addition, upscaling of the Melon Gel method is less limited than in the case of immobilized antibodies. Lopez and coworkers [20] have compared the protein G and the Melon Gel immunoaffinity purification methods and concluded that the elution step at low pH in the protein G affinity method can cause IgG aggregation. As a result, IgG cannot be presumed to be fully native and accessible, as is the case when Melon Gel resin is used to enrich immunoglobulins. Melon Gel IgG purification has been applied successfully to identify disease-related IgG in various clinical body fluids, such as CSF of multiple sclerosis pathology [21–23], serum of lung cancer patients [22] and M-protein serum levels related to a monoclonal gammopathy [23]. In addition to previous studies in which isolation of IgG was performed to identify or quantify IgG, we successfully proved the ability of Melon Gel to enrich intact antibody–peptide antigen complexes.

To examine the feasibility of the method, we first conducted an experiment in which a digest of DNP-labeled α-casein (as antigen) was mixed with anti-DNP. The formed antibody–antigen complexes (of anti-DNP and DNP-labeled peptides) were purified, after which the peptide antigens were isolated and measured. While DNP-labeled peptides were predominantly found in the IgG-bound fractions, just a relatively small proportion (<1%) of unlabeled peptides were found in the IgG-bound fraction. Similarly, when we conducted the experiment without adding anti-DNP, by far the largest number of the peptides detected (>98%) was found in the non-IgG-bound fractions. These results confirm the applicability of the method in this proof of principle. However, not all selected peptides were detected in any of the fractions. Consequentially, both IgG-

bound and non-IgG-bound fractions must be analyzed to obtain reliable readouts of the assay while avoiding false-negative results. To confirm the absence of a detectable specific peptide affinity, the absence of the peptide in the IgG-bound fraction as well as its presence in the unbound-fraction should be confirmed. Correspondingly, to confirm the presence of affinity, detections in the IgG-bound fraction have to be set in relation with detected intensities in the unbound fractions. Analysis of the filter-bound fraction has shown that in addition to the peptide numbers in the IgG-bound and unbound fractions, peptides can be retained on the filter device. Probable reasons for the latter observation are adsorption at the surface of the filter device or incomplete flushing due to the design of the filter device used. To describe this more precisely, in this feasibility experiment a distinction was made between the fraction of peptides released after acidification through the filter (FB2) and peptides retained in the filter device (FB1). Peptides were found in both filter-bound fractions, regardless of whether these peptides were bound to antibodies or not. Therefore, the differentiation into the two filter-bound fractions did not provide any further information about the immuno-specificity of the peptides. In the subsequent experiments, these two filter-bound fractions were replaced with a filter-bound fraction representing a pool of FB1 and FB2. We could not determine if, in the filter-bound fraction, peptides were bound to antibodies or, though probably more unlikely, unspecifically bound to the filter. Consequentially, for the interpretation of the results of the Ab–peptide binding assay, we did not use information about the filter-bound fractions.

To determine the analytical background—in order to be able to differentiate between specific and unspecific binding of peptides—we conducted an Ab–peptide binding experiment using a total peptide library against Avastin (plasma blank), HGG plasma and healthy donor plasma. The resulting IgG-bound fractions were analyzed with the untargeted shotgun proteomics method to acquire an overview of all peptides, both unspecific and IgG-bound. Although less sensitive than the targeted PRM method, the untargeted shotgun method was most suitable for acquiring a comprehensive peptide map of the assay background. Analysis revealed that 68 peptides (out of a total of 4256 peptides in the peptide library) were found in the Avastin blank sample and 59 peptides in the plasma samples. Most of these peptides (99.2%) corresponded with high- or middle-abundant plasma proteins or had high abundance in the peptide library (highest quantile). Therefore, we conclude that the method is sufficiently selective to prevent nonspecific quantitative elution (slip-through) of library peptides and to assess background. Furthermore, the analysis of both fractions, IgG-bound and non-IgG-bound, is a key feature of the analysis in determining high selectivity.

Next, by using plasma samples and the phospho-peptide library derived from glioma tumor tissue, we investigated if the assay was suitable to detect Ab-binding peptides.

Phospho-peptides that carry tumor-specific phospho-sites can be considered a potential novel class of tumor-specific antigens. The phospho-peptide antigens have been less studied than mutated antigens [6–8]. Zarling et al. found that phospho-peptides are presented on various types of cancer cells and recognized by CD8+ T cells, indicating that phospho-peptide antigens are potential targets for immunotherapy.[24] Mohammed and coworkers investigated the effect of conformational changes due to phosphorylation on the antigenic identify and concluded that the phospho-peptide neoantigen RQA_V (covering LSP-1 phospho-S251) might be a valuable candidate for cancer immunotherapy [10]. Engelhard and colleagues investigated the immunogenicity of phospho-peptides from breast cancer antiestrogen resistance 3 ($pBCAR3_{126-134}$) and insulin receptor substrate 2 ($pIRS2_{1097-1105}$) and concluded that the specific immunogenicity observed provides a rationale for immunotherapy targeting phospho-peptides [25].

To prove the applicability of our method, we tested for the presence of antibodies against GBM-associated phospho-peptides in plasma. We selected candidate phospho-peptides antigens from two GBM-associated proteins, EGFR and GFAP, on the basis of data from our previous study that compared GBM and normal brain tissue [15]. EGFR phospho-site S1166 was exclusively detected in GBM tissue samples but not in normal brain tissue. EGFR phospho-site S1166 has been detected by mass spectrometry in various phospho-proteomics studies, listed on PhosphoSitePlus [26]. Moreover, we observed changes in the phosphorylation level for this phospho-site as a result of serum starvation, a process that triggers EGFR phosphorylation [15,16]. Assiddiq and coworkers used multiple reaction monitoring (MRM) in the H838 lung cancer cell line to study the effect of gefitinib on the phospho-sites of the EGFR protein before and after EGF treatment [27]. They concluded that phosphorylation of S1166 could have a negative effect on cell growth and proliferation [27] in this cell line. Whether phosphorylation of S1166 is also involved in growth and proliferation in glioma patients is not reported. Doll et al. detected upregulation of pS1166 (1.6-fold), among other EGFR phospho-sites, in an HRAS-NHA cell line. This cell line was used as a model for primary GBM, and the authors suggested involvement in feedback downregulation of EGFR [28]. We further compared the phosphorylation data from these two studies [27,28] to our results obtained from glioma tissue (this study and [15]). For EGFR, we also found the S/T phospho-peptide (pT693: ELVEPLT[+80]PSGEAPNQALLR) in our dataset (for patient G11 and G17) and additional S/T phospho-peptides of EGFR that were not found in the cell lines. This emphasizes possible differences in the phosphorylation state between cell lines and tumor tissue. Ideally, the effect of a treatment on autoantibodies should be investigated by a separate study, but this would come with difficulties in the clinical implementation. As an alternative, we envision an experiment whereby GBM cell cultures are exposed to patient plasma to determine a possible effect on proliferation.

Seven different GFAP phospho-peptides were selected based on the results of our previous study [15]. Additionally, the literature indicates differences in GFAP between GBM tissue and normal brain tissue, positing, for instance, alternative splicing [29] and that autoantibodies for GFAP exist in pathologies such as paraneoplasm [30]. Higher expression of GFAP in glioblastoma is associated with poor prognosis [31], but little is known about the role of specific phospho-sites of GFAP in glioma. A multitude of GFAP phospho-sites are known, especially in the head domain in which GFAP assembly is regulated by phosphorylation [32]. Interestingly, the phospho-proteomics results of our previous study [15] showed a distinct phosphorylation pattern predominantly identified in the head but also in the tail domain of GFAP.

As a result of both experiments (EGFR and GFAP), we conclude that IgG binding to the EGFR phospho-peptide exists in plasma of glioma patients but not in plasma of healthy donors, and that autoantibodies against EGFR phospho-site S1166 are associated with high-grade glioma. The result of the AB peptide assay for the GFAP peptides suggests that there is no HGG-related immune response to the GFAP phospho-peptides investigated. Only three of the seven GFAP peptide antigens could be successfully analyzed; the other four had to be excluded from analysis because they could not be detected in any of the fractions. Still, these four peptides might have been retained on the Melon Gel if they had not been bound to an antibody. This observation shows to a certain extent the limitation of the assay.

In conclusion, antibody–peptide–antigen complex enrichment with Melon Gel has been applied successfully to investigate disease-related phospho-peptides. The Melon Gel immunoglobulin purification method is a promising technique to detect antibody (IgG)-bound peptides (antigens) in complex peptide libraries. This method has the potential to detect the putative presence of autoantibodies without knowledge of the antigen. We demonstrated a proof of concept for the presence of autoantibodies against the EGFR phospho-peptide S1166 in plasma of high-grade glioma patients. This antibody–peptide binding assay could potentially be further applied for diseases such as autoimmune diseases and for other types of cancer.

MATERIALS AND METHODS

Unless mentioned otherwise, chemicals were purchased from Merck Millipore (Burlington, MA, USA) and solvents for LC-MS from Biosolve (Valkenswaard, The Netherlands).

Biological Material

One fresh-frozen GBM tissue sample served as the basis for the peptide libraries (a total peptide library and a phospho-peptide library, clinical information in Supplementary Table S1) and seven plasma samples from high-grade glioma (HGG) patients and two from healthy donors as source of IgG (Table 1). Two of the plasma samples from HGG patients were taken from the same patient before and after surgery and further therapy. The tissue and the other plasma samples were taken from other, different persons. The use of patient and donor material was approved by the Institutional Ethics Review Board of Erasmus MC, Rotterdam, The Netherlands (MEC 221.520/2002/262; date of approval 22 July 2003, and MEC-2005-057, date of approval 14 February 2005). Patients gave written consent to the use of their tissue or plasma for research purposes.

Preparation of Tissue Peptide Libraries

A total peptide library is a mixture of peptides obtained after digestion of one fresh-frozen GBM tissue, and a phospho-peptide library is a mixture of phospho-peptides obtained after phospho-enrichment of digested fresh-frozen GBM tissue. The GBM tissue sample was cut in five 8 µm fresh-frozen (FF) tissue slices on a microtome and placed in a 1.5 mL tube (Eppendorf). Four hundred µL of 0.1% Rapigest (Waters, Milford, MA, USA) was added to the tissue pellet (~300 µg of total protein) and sonified for 2 min at 70% amplitude at a maximum temperature of 25 °C (Branson Ultrasonics, Danbury, CT, USA) and subsequently heated at 99 °C for 5 min.

Next, the two peptide libraries were prepared from these tissue slices as described in a previous study [15]. In brief, tissue lysate was reduced and alkylated using dithiothreitol (DTT) and iodoacetamide (IAA), respectively. Then, 10 µg of trypsin (Promega, Madison, WI, USA) was added and incubated overnight at 37 °C. After acidification (pH < 2) and centrifugation, the supernatant was stored at 4 °C. Both desalting of the tryptic digests and phospho-peptide enrichment were performed using an AssayMAP Bravo automated platform (Agilent Technologies, Santa Clara, CA, USA) according to the manufacturer's protocols [33]. Peptide concentration of the peptide library was determined with a quantitative colorimetric peptide assay (Pierce, Thermo Fisher Scientific, Rockford, IL, USA).

Table 1. List of plasma samples with clinical data and corresponding use in experiments.

Sample ID	Individual	Age	Gender	Treatment	Molecular Diagnosis	Tumor Type and WHO Classification	Experiment
Donor-44	D1	53	Male	-	-	Healthy	GFAP and EGFR
Donor-45	D2	52	Male	-	-	Healthy	GFAP
Pnop-01	P1	61	Male	Before	IDH-mutant p1p/19q No EGFR amplification	Oligodendroglioma (grade 2)	GFAP
Pnop-02	P1	61	Male	After surgery and therapy	IDH-mutant p1p/19q No EGFR amplification	Oligodendroglioma (grade 2)	GFAP
Pnop-09	P2	47	Female	Before	IDH-mutant No EGFR amplification	Glioblastoma (grade 4)	GFAP
Pnop-13	P3	75	Male	Before	Not available	Glioblastoma (grade 4)	GFAP and EGFR
Pnop-14	P3	75	Male	After surgery and therapy	Not available	Glioblastoma (grade 4)	EGFR
Pnop-17	P4	66	Male	Before	Not available	Glioblastoma (grade 4)	EGFR
Pnop-30	P5	41	Female	Before	p1p/19q	Oligodendroglioma (grade 3)	GFAP and EGFR

Isolation of Immunoglobulin-Binding Peptides

In the first step of the method, plasma samples were mixed with a peptide library and incubated for 30 min at 18 °C to allow possible binding of peptides and antibodies with the corresponding affinity. Next, the non-IgG protein fraction was removed using the Melon Gel IgG Purification Kit (Thermo Fisher Scientific) according to the manufacturer's protocol. The flow-through fraction containing the IgG and IgG–peptide complexes was loaded onto a 30 kDa-molecular-weight (MW) filter device (Amicon, Merck, Burlington, MA, USA), which had been preconditioned for 30 min with 500 µL of 0.02 µg/µL bovine serum albumin (BSA) in phosphate-buffered saline (PBS). The low MW fraction (<30 kDa), containing unbound peptides, was removed by centrifugation (15 min at 20,000g), desalted (removal of PBS), resuspended in 25 µL 0.1% TFA/2% ACN) and stored at 4 °C until LC-MS analysis ("Unbound peptides", Figure 1). The remaining high MW fraction, containing IgGs and IgG–peptide complexes, was washed four times with 500 µL of PBS, and the retained volume (approximately 20–25 µL) was pipetted into a fresh tube and acidified with 1 µL of 50% TFA to dissociate the Ab–peptide complex and to release Ab-bound peptides. Next, acetone precipitation was performed to separate peptides from IgG by addition of 10 sample volumes of ice-cold (–20 °C) acetone, precipitation at –20 °C for 2 h and centrifugation (10 min at 20,000 g). Subsequently, the supernatant, containing the IgG-bound peptides (Figure 1), was dried using a vacuum centrifuge (Savant SC210A, Thermo Fisher Scientific), re-suspended in 25 µL of 0.1% TFA/2% ACN and stored at 4 °C until LC-MS analysis. Additionally, the MW filter device was rinsed with 500 µL of 0.5% formic acid (FA), dried (vacuum centrifugation) and stored at 4 °C until LC-MS analysis to check for "Filter bound peptides" eluted by acidification (Figure 1).

Targeted Parallel Reaction Monitoring (PRM) Measurements

Mass spectrometric measurements were performed on a nano-LC (Ultimate 3000RS, Thermo Fisher Scientific, Germering, Germany) coupled to an Orbitrap tribrid mass spectrometer (Orbitrap Fusion or Orbitrap Fusion Lumos; Thermo Fisher Scientific, San Jose, CA, USA). One half of the volume of each fraction (IgG-bound, unbound and filter-bound) was loaded on a trap column (C18 PepMap, 5 µm particle size, 100 Å pore size, 5 mm × 300 µm, Thermo Fisher Scientific) and desalted for 10 min with 0.1% TFA at a flow rate of 20 µL/min. Next, analytes were eluted from the trap column and separated on an analytical C18 column (PepMap C18, 75 µm ID × 250 mm, 2 µm particle and 100 Å pore size, Thermo Fisher Scientific) using a binary gradient from 4 to 38% solvent B in 30 min, whereby solvent A consists of 0.1% formic in water and solvent B consists of 80% acetonitrile and 0.08% formic acid in water. The flow rate was 300 nL/min and the column temperature 40 °C. For electrospray ionization, nano ESI emitters (New Objective, Woburn, MA, USA) were used at a spray voltage of 1.8 kV. The targeted MS/MS mode had the following settings: 1.6 m/z isolation width, 60,000 Orbitrap resolution, 200,000 automatic gain control and 118 ms maximum injection time. Further peptide

specific settings are listed in Supplementary Table S2. PRM data were processed with the software package Skyline [34]. Peak picking was revised manually, and peptide detection was considered to be valid when consistent peaks of at least three fragments were acquired. Result tables of Skyline were further analyzed and plotted with the statistical software package R [35]. The mass spectrometry proteomics data have been deposited into the ProteomeXchange Consortium via the PRIDE [36] partner repository with the dataset identifier PXD032844 and DOI 10.6019/PXD032844.

Data-Dependent Mass Spectrometry Measurements

For the untargeted LC-MS measurement, we used the same instrumental setting and chromatography method as for the PRM measurements. A data-dependent MS acquisition method was used with an Orbitrap survey scan (range 375–1550 *m*/*z*, resolution of 120,000, AGC target 400,000), followed by consecutively isolation (isolation with 1.6 *m*/*z*), HCD fragmentation (30% normalized collision energy) and ion-trap detection of the peptide precursors detected in the survey scan until a duty cycle time of 3 s was exceeded. Dynamic exclusion was used with 10 ppm mass tolerance and 60 s exclusion duration. The acquired fragment mass spectra were searched against the human subset of the Uniprot database (version 2020-12-12; 20,395 entries) using Mascot (version 2.3.02; Matrix Science, UK) with tryptic cleavage, two missed cleavages allowed, oxidation of Methionine (+15.995 Da) as variable modification and carbamidomethylation of Cysteine (+57.021 Da) as fixed modification, precursor tolerance of 10 ppm and fragment tolerance of 0.5 Da. Search results were post-processed with the software package Scaffold (version 5.1.0, Proteome Software, Portland, OR, USA) to merge the individual search results, conduct protein grouping and calculate protein and peptide identification confidence levels (false discovery rate <1%). The precursor intensities of the identified peptides were determined with the label-free quantitation software package Progenesis QI (Version 2.0; Nonlinear Dynamics, Newcastle-upon-Tyne, UK).

Feasibility Experiments

Following the scheme of the isolation of immunoglobulin-binding peptides, first a feasibility experiment to proof the concept was performed with a hapten (dinitrophenyl, DNP) bound peptide of α-casein specific for a monoclonal antibody (anti-DNP). To partially label α-casein protein with DNP, bovine protein α-casein (0.4 mM, Sigma Aldrich) was incubated with 0.4 mM di-nitrobenzenesulfonic acid in 0.15 M potassium carbonate [37,38]. This partial DNP labeling of lysine moieties was meant to prevent the formation of relatively long tryptic peptides as DNP labeling blocks tryptic cleavage. The sample was acetone-precipitated to remove detergents and reagents, and the protein pellet was digested with trypsin, as described above.

Anti-DNP (Anti-DNP Antibody, clone 9H8.1, Cat# MAB2223, Merck Millipore, Burlington,

MA) and Avastin, to serve as a DNP-unspecific negative control (Roche, Basel, Switzerland), were purchased and stored according to the manufacturer's recommendations. To test the feasibility of the method, digested DNP-labeled α-casein (10 µg), 1 µg of anti-DNP and 100 µg of Avastin were combined and incubated with gentle shaking for 30 min at room temperature. Additionally, the same experiment was conducted without anti-DNP as a negative control experiment to determine unspecific binding of DNP peptides. Isolation of IgG-bound peptides and targeted PRM measurements of DNP-labeled and unlabeled peptides were conducted as described above.

Selection of GBM-Associated Phospho-Peptide Antigens

To select relevant phospho-peptide candidates, we reprocessed a dataset of three GBM samples and three normal brain tissue (NBT) samples from a previous study [15]; the dataset is publicly accessible on ProteomeXchange PRIDE repository with the dataset identifier PXD017943. To compare GBM and NBT, we used data of replicates of both FFPE-embedded and fresh-frozen tissue of each sample. Data were processed by Mascot MS/MS database search and Scaffold post-processing as described above. The final selection of suitable antigen candidates was based on two criteria: (a) the respective phospho-peptides were identified specifically in GBM tissue and (b) the corresponding precursor proteins had a known association with GBM.

Detection of Peptide–Antigen-Binding IgG in Plasma

For each analysis, 10 µg of GBM phospho-peptide library was mixed with 100 µL of plasma containing putative phospho-peptide-binding autoantibodies. As a negative control experiment, instead of plasma, 100 µg of Avastin was added to determine unspecific IgG binding. Isolation of IgG-binding peptides and targeted PRM measurements of EGFR and GFAP phospho-peptides took place analogous to the feasibility experiment described above. To survey the overall detectable peptides and to determine unspecific and specific binding, we performed three additional analyses in which 10 µg of GBM peptide library was mixed with 100 µg of Avastin, 100 µL of HGG plasma or 100 µL of normal plasma. The three samples were processed according to the protocol described above. The IgG-bound fractions and GBM total peptide library were measured by a data-dependent shotgun method described above.

Supplementary Materials

The following supporting information can be downloaded at: www.mdpi.com/xxx/s1. Supplemental Figure S1 Supplemental Figure S2. Supplemental Tables S1-S3.

Author Contributions:

L.Z.: Conceptualization, Methodology, Validation, Formal analysis, Investigation, Writing—Original Draft. **C.S.:** Validation, Formal analysis, Data Curation, Writing—

Original Draft, Visualization. **J.M.K.:** Resources, Writing—Review and Editing. **P.A.E.S.S.:** Resources, Writing—Review and Editing, Supervision. **T.M.L.:** Conceptualization, Methodology, Investigation, Resources, Writing—Review and Editing, Supervision. All authors have read and agreed to the published version of the manuscript.

Funding
This research received no external funding.

Institutional Review Board Statement
The study was conducted in accordance with the Declaration of Helsinky, and approved by the Institutional Review Board of Erasmus MC (MEC 221.520/2002/262; date of approval 22 July 2003, and MEC-2005-057; date of approval 14 February 2005).

Informed Consent Statement
Patients gave written consent to the use of their tissue or plasma for research purposes. Of: Informed consent was obtained from all subjects involved in the study.

Data Availability Statement
The mass spectrometry proteomics data have been deposited into the ProteomeXchange Consortium via the PRIDE partner repository with the dataset identifier PXD032844 and DOI 10.

Acknowledgments
The mass spectrometry equipment used for this study was partly financed by The Dutch Organization for Scientific Research (NWO) under infrastructure grant number 1631. This project received funding from the Eurostars-2 joint program with co-funding from the European Union Horizon 2020 research and innovation program (Eurostars project 10688, GlioPhos).

Conflicts of Interest
The authors declare no conflict of interest.

REFERENCES

1. Tan, H.T.; Low, J.; Lim, S.G.; Chung, M.C.M. Serum autoantibodies as biomarkers for early cancer detection. *FEBS J.* **2009**, *276*, 6880–6904. https://doi.org/10.1111/j.1742-4658.2009.07396.x.
2. Chen, H.; Werner, S.; Tao, S.; Zörnig, I.; Brenner, H. Blood autoantibodies against tumor-associated antigens as biomarkers in early detection of colorectal cancer. *Cancer Lett.* **2014**, *346*, 178–187. https://doi.org/10.1016/j.canlet.2014.01.007.
3. Yao, Y.; Fan, Y.; Wu, J.; Wan, H.; Wang, J.; Lam, S.; Lam, W.L.; Girard, L.; Gazdar, A.F.; Wu, Z.; et al. Potential application of non-small cell lung cancer-associated autoantibodies to early cancer diagnosis. *Biochem. Biophys. Res. Commun.* **2012**, *423*, 613–619. https://doi.org/10.1016/j.bbrc.2012.06.050.
4. Hong, C.-Q.; Weng, X.-F.; Huang, X.-C.; Chu, L.-Y.; Wei, L.-F.; Lin, Y.-W.; Chen, L.-Y.; Liu, C.-T.; Xu, Y.-W.; Peng, Y.-H. A Panel of Tumor-associated Autoantibodies for the Detection of Early-stage Breast Cancer. *J. Cancer* **2021**, *12*, 2747–2755. https://doi.org/10.7150/jca.57019.
5. Rauf, F.; Anderson, K.S.; LaBaer, J. Autoantibodies in Early Detection of Breast Cancer. *Cancer Epidemiol. Biomark. Prev.* **2020**, *29*, 2475–2485. https://doi.org/10.1158/1055-9965.epi-20-0331.
6. Ardito, F.; Giuliani, M.; Perrone, D.; Troiano, G.; Lo Muzio, L. The crucial role of protein phosphorylation in cell signaling and its use as targeted therapy (Review). *Int. J. Mol. Med.* **2017**, *40*, 271–280. https://doi.org/10.3892/ijmm.2017.3036.
7. Mahoney, K.E.; Shabanowitz, J.; Hunt, D.F. MHC Phosphopeptides: Promising Targets for Immunotherapy of Cancer and Other Chronic Diseases. *Mol. Cell. Proteom.* **2021**, *20*, 100112. https://doi.org/10.1016/j.mcpro.2021.100112.
8. Zeneyedpour, L.; Sten-van, T.H.J.; Luider, T. Using phosphoproteomics and next generation sequencing to discover novel therapeutic targets in patient antibodies. *Expert Rev. Proteom.* **2020**, *17*, 675–684. https://doi.org/10.1080/14789450.2020.1845147.
9. Depontieu, F.R.; Qian, J.; Zarling, A.L.; McMiller, T.L.; Salay, T.M.; Norris, A.; English, A.M.; Shabanowitz, J.; Engelhard, V.H.; Hunt, D.F.; et al. Identification of tumor-associated, MHC class II-restricted phosphopeptides as targets for immunotherapy. *Proc. Natl. Acad. Sci. USA* **2009**, *106*, 12073–12078. https://doi.org/10.1073/pnas.0903852106.
10. Mohammed, F.; Stones, D.H.; Zarling, A.L.; Willcox, C.R.; Shabanowitz, J.; Cummings, K.L.; Hunt, D.F.; Cobbold, M.; Engelhard, V.H.; Willcox, B.E. The antigenic identity of human class I MHC phosphopeptides is critically dependent upon phosphorylation status. *Oncotarget* **2017**, *8*, 54160–54172. https://doi.org/10.18632/oncotarget.16952.
11. Peterson, A.C.; Russell, J.D.; Bailey, D.J.; Westphall, M.S.; Coon, J.J. Parallel Reaction Monitoring for High Resolution and High Mass Accuracy Quantitative, Targeted Proteomics. *Mol. Cell. Proteom.* **2012**, *11*, 1475–1488. https://doi.org/10.1074/mcp.o112.020131.
12. Osinalde, N.; Aloria, K.; Omaetxebarria, M.J.; Kratchmarova, I. Targeted mass spectrometry: An emerging powerful approach to unblock the bottleneck in phosphoproteomics. *J. Chromatogr. B Analyt. Technol. Biomed. Life Sci.* **2017**, *1055–1056*, 29–38. https://doi.org/10.1016/j.jchromb.2017.04.026.
13. Lawrence, R.T.; Searle, B.C.; Llovet, A.; Villén, J. Plug-and-play analysis of the human phosphoproteome by targeted high-resolution mass spectrometry. *Nat. Methods* **2016**, *13*, 431–434. https://doi.org/10.1038/nmeth.3811.
14. Banerjee, S.L.; Dionne, U.; Lambert, J.-P.; Bisson, N. Targeted proteomics analyses of phosphorylation-dependent signalling networks. *J. Proteom.* **2018**, *189*, 39–47. https://doi.org/10.1016/j.jprot.2018.02.004.
15. Zeneyedpour, L.; Stingl, C.; Dekker, L.J.M.; Mustafa, D.A.M.; Kros, J.M.; Luider, T.M. Phosphorylation Ratio Determination in Fresh-Frozen and Formalin-Fixed Paraffin-Embedded Tissue with Targeted Mass Spectrometry. *J. Proteome Res.* **2020**, *19*, 4179–4190. https://doi.org/10.1021/acs.jproteome.0c00354.
16. Dekker, L.J.M.; Zeneyedpour, L.; Snoeijers, S.; Joore, J.; Leenstra, S.; Luider, T.M. Determination of Site-Specific Phosphorylation Ratios in Proteins with Targeted Mass Spectrometry. *J. Proteome Res.* **2018**, *17*, 1654–1663. https://doi.org/10.1021/acs.jproteome.7b00911.
17. Zetterberg, H. Review: Tau in biofluids—Relation to pathology, imaging and clinical features. *Neuropathol. Appl. Neurobiol.* **2017**, *43*, 194–199. https://doi.org/10.1111/nan.12378.
18. Bergmann-Leitner, E.S.; Mease, R.M.; Duncan, E.H.; Khan, F.; Waitumbi, J.; Angov, E. Evaluation of immunoglobulin purification methods and their impact on quality and yield of antigen-specific antibodies. *Malar. J.* **2008**, *7*, 129. https://doi.org/10.1186/1475-2875-7-129.
19. Grodzki, A.C.; Berenstein, E. Antibody purification: ammonium sulfate fractionation or gel filtration. *Methods Mol. Biol.* **2010**, *588*, 15–26.
20. Lopez, E.; Scott, N.E.; Wines, B.D.; Hogarth, P.M.; Wheatley, A.K.; Kent, S.J.; Chung, A.W. Low pH Exposure During Immunoglobulin G Purification Methods Results in Aggregates That Avidly Bind Fcγ Receptors: Implications for Measuring Fc Dependent Antibody Functions. *Front. Immunol.* **2019**, *10*, 2415. https://doi.org/10.3389/

fimmu.2019.02415.
21. Singh, V.; Stoop, M.P.; Stingl, C.; Luitwieler, R.L.; Dekker, L.J.; van Duijn, M.M.; Kreft, K.L.; Luider, T.M.; Hintzen, R.Q. Cerebrospinal-fluid-derived Immunoglobulin G of Different Multiple Sclerosis Patients Shares Mutated Sequences in Complementarity Determining Regions. *Mol. Cell. Proteom.* **2013**, *12*, 3924–3934. https://doi.org/10.1074/mcp.m113.030346.
22. Broodman, I.; De Costa, D.; Stingl, C.; Dekker, L.J.M.; van Duijn, M.M.; Lindemans, J.; Van Klaveren, R.J.; Luider, T.M. Mass spectrometry analyses of κ and λ fractions result in increased number of complementarity-determining region identifications. *Proteomics* **2012**, *12*, 183–191. https://doi.org/10.1002/pmic.201100244.
23. Barnidge, D.R.; Dasari, S.; Botz, C.M.; Murray, D.H.; Snyder, M.R.; Katzmann, J.A.; Dispenzieri, A.; Murray, D.L. Using Mass Spectrometry to Monitor Monoclonal Immunoglobulins in Patients with a Monoclonal Gammopathy. *J. Proteome Res.* **2014**, *13*, 1419–1427. https://doi.org/10.1021/pr400985k.
24. Zarling, A.L.; Polefrone, J.M.; Evans, A.M.; Mikesh, L.M.; Shabanowitz, J.; Lewis, S.T.; Engelhard, V.H.; Hunt, D.F. Identification of class I MHC-associated phosphopeptides as targets for cancer immunotherapy. *Proc. Natl. Acad. Sci. USA* **2006**, *103*, 14889–14894. https://doi.org/10.1073/pnas.0604045103.
25. Engelhard, V.H.; Obeng, R.C.; Cummings, K.L.; Petroni, G.R.; Ambakhutwala, A.L.; Chianese-Bullock, K.A.; Smith, K.T.; Lulu, A.; Varhegyi, N.; Smolkin, M.E.; et al. MHC-restricted phosphopeptide antigens: Preclinical validation and first-in-humans clinical trial in participants with high-risk melanoma. *J. Immunother. Cancer* **2020**, *8*, e000262. https://doi.org/10.1136/jitc-2019-000262.
26. Hornbeck, P.V.; Zhang, B.; Murray, B.; Kornhauser, J.M.; Latham, V.; Skrzypek, E. PhosphoSitePlus, 2014: Mutations, PTMs and recalibrations. *Nucleic Acids Res.* **2015**, *43*, D512–D520. https://doi.org/10.1093/nar/gku1267.
27. Assiddiq, B.F.; Tan, K.Y.; Toy, W.; Chan, S.P.; Chong, P.K.; Lim, Y.P. EGFR S1166 Phosphorylation Induced by a Combination of EGF and Gefitinib Has a Potentially Negative Impact on Lung Cancer Cell Growth. *J. Proteome Res.* **2012**, *11*, 4110–4119. https://doi.org/10.1021/pr3002029.
28. Doll, S.; Urisman, A.; Oses-Prieto, J.A.; Arnott, D.; Burlingame, A.L. Quantitative Proteomics Reveals Fundamental Regulatory Differences in Oncogenic HRAS and Isocitrate Dehydrogenase (IDH1) Driven Astrocytoma. *Mol. Cell. Proteom. MCP* **2017**, *16*, 39–56. https://doi.org/10.1074/mcp.m116.063883.
29. Uceda-Castro, R.; van Asperen, J.V.; Vennin, C.; Sluijs, J.A.; van Bodegraven, E.J.; Margarido, A.S.; Robe, P.A.J.; van Rheenen, J.; Hol, E.M. GFAP splice variants fine-tune glioma cell invasion and tumour dynamics by modulating migration persistence. *Sci. Rep.* **2022**, *12*, 424. https://doi.org/10.1038/s41598-021-04127-5.
30. Cirkel, A.; Wandinger, K.-P.; Ditz, C.; Leppert, J.; Hanker, L.; Cirkel, C.; Neumann, A.; Brocke, J.; Höftberger, R.; Komorowski, L.; et al. Paraneoplastic encephalomyeloradiculits with multiple autoantibodies against ITPR-1, GFAP and MOG: Case report and literature review. *Neurol. Res. Pract.* **2021**, *3*, 48. https://doi.org/10.1186/s42466-021-00145-w.
31. Ahmadipour, Y.; Gembruch, O.; Pierscianek, D.; Sure, U.; Jabbarli, R. Does the expression of glial fibrillary acid protein (GFAP) stain in glioblastoma tissue have a prognostic impact on survival? *Neurochirurgie* **2020**, *66*, 150–154.
32. Inagaki, M.; Imakamura, Y.; Takeda, M.; Nishimura, T.; Inagaki, N. Glial Fibrillary Acidic Protein: Dynamic Property and Regulation by Phosphorylation. *Brain Pathol.* **1994**, *4*, 239–243. https://doi.org/10.1111/j.1750-3639.1994.tb00839.x.
33. Agilent. Workflow Automation for LC/MS: In-Solution Protein Digestion, Peptide Cleanup, and Strong Cation-Exchange Fractionation of Peptides Enabled by AssayMAP Technology. Available online: https://www.agilent.com/cs/library/applications/5991-3602EN.pdf (accessed on 16 March 2016).
34. MacLean, B.; Tomazela, D.M.; Shulman, N.; Chambers, M.; Finney, G.L.; Frewen, B.; Kern, R.; Tabb, D.L.; Liebler, D.C.; MacCoss, M.J. Skyline: An open source document editor for creating and analyzing targeted proteomics experiments. *Bioinformatics* **2010**, *26*, 966–968. https://doi.org/10.1093/bioinformatics/btq054.
35. R Core Team. R: A language and environment for statistical computing. R Foundation for Statistical Computing, Vienna. 2013. Available online: https://www.R-project.org/ (accessed on 22 April 2022).
36. Perez-Riverol, Y.; Csordas, A.; Bai, J.; Bernal-Llinares, M.; Hewapathirana, S.; Kundu, D.J.; Inuganti, A.; Griss, J.; Mayer, G.; Eisenacher, M.; et al. The PRIDE database and related tools and resources in 2019: Improving support for quantification data. *Nucleic Acids Res.* **2019**, *47*, D442–D450. https://doi.org/10.1093/nar/gky1106.
37. van Duijn, M.M.; Dekker, L.J.; Zeneyedpour, L.; Smitt, P.A.; Luider, T.M. Immune Responses Are Characterized by Specific Shared Immunoglobulin Peptides That Can Be Detected by Proteomic Techniques. *J. Biol. Chem.* **2010**, *285*, 29247–29253. https://doi.org/10.1074/jbc.m110.139071.
38. Hay, F.C.; Westwood, O.M. *Practical Immunology*; Blackwell Publishing Company: Oxford, UK, 2008; pp. 115–162.

6

GENERAL DISCUSSION

GENERAL DISCUSSION

Application of mass spectrometry to detect tumor-specific antigens

The immune system can recognize tumor-specific antigens such as somatic mutation-derived antigens (neoantigens) and post-translationally modified antigens (1, 2) in tumor cells. The recent detection of these tumor-specific antigens is of high interest for the development of antigen-targeted cancer immunotherapies (3-5).

In cancer research, neoantigens can be identified using DNA or RNA high-throughput sequencing data obtained from tumor tissue and mostly normal tissue. Next to these genomic and transcriptomic workflows, proteomic- and phosphoproteomic workflows can be applied to identify mutated proteins and post-translational modifications associated with cancer (6-8).

In **Chapter 2**, we discussed applying MS to identify disease-specific neoantigens in clinical samples. The isocitrate dihyrogenase (IDH1) protein served as example. The IDH1 protein has a mutation at the primary sequence position 132, where an arginine (R) is most often replaced by a histidine (H). This point mutation has been frequently detected in glioma, cholangiocarcinoma and chondrosarcoma; and at much lower frequency in many other cancers, including lung carcinoma. The substitution of an amino acid in the primary sequence of a peptide causes variation in mass between the mutated peptide and the normal peptide. This variation can be detected using MS. This possibility to sensitively investigate mass variations in neoantigens is of high interest and applicable to diverse diseases. In addition to other available genomic and transcriptomic methods, the MS-based method opens a new way to detect neoantigens. It can be applied to monitor neoantigens in an early stage, and can be of use in designing therapies such as cancer immunotherapy. The application of neoantigens in cancer vaccines has been examined in clinical studies (5, 9-12). These cancer vaccines mostly can be classified into peptide-based vaccines, nucleic acid (DNA/mRNA) vaccines and dendritic cell (DC)-based vaccines—as comprehensively reviewed by Zhao et al. (4). Therefore, targeting neoantigens could be a promising approach for cancer immunotherapy (4, 12).

Determination of the phosphorylation percentage of protein phospho-sites with MS

In diseases, and especially in cancer, phosphorylation is dysregulated (13). Therefore, there is a large interest in studying potential changes in the phosphoproteome as a result of disease (14). We developed a method that uses targeted MS with high resolution to accurately determine the phosphorylation percentage of protein phospho-sites in cell lysates. Using stable isotope labeled (SIL) peptides, we were able to determine the phosphorylation percentages of targeted phospho-sites. Using a parallel reaction monitoring (PRM) approach, we applied two types of measurement—direct-PRM and

TiO_2-PRM—to measure the non-phosphorylated peptide and the phosphorylated counterpart, respectively (see also **Chapter 3**). Our results show that targeted non-phosphorylated and associated phosphorylated peptides can be measured with a high degree of reproducibility (CV < 10%). We found that the percentage of phosphorylation can vary, largely depending on the protein identified. Most of the proteins that were phosphorylated had on average a phosphorylation percentage of 6.5%, although outliers of more than 21% were observed. Still, proteins phosphorylated for 100% at a certain phospho-site were not detected. Because we did not observe a degradation of synthetic phosphopeptides spiked to the samples, we could rule out that low percentage phosphorylation was caused by, for instance, phosphatase activity during sample preparation. This method to determine a precise phosphorylation percentage in cell lines and tissues can also be applied for absolute quantification of phosphopeptides and to determine the phosphorylation ratios of specific peptides without using antibodies, labeling strategies, phosphatase treatment, or complex fractionation steps during sample preparation (15-19). Phosphoproteomics has resulted in complementary knowledge about new phospho-sites compared to antibodies directed to specific phospho-sites (20). Using a MS-based approach, we identified still unknown phospho-sites without the need of pre-existing knowledge about phospho-sites (21). Moreover, many studies (22-24) have shown that inconsistent antibody validation can be a bottleneck in clinical research. Therefore, precise antibody characterization remains a topic of concern in research (25).

Multiplex analysis enables to analyze multiple targets (analytes) in a robust, affordable and reproducible way. In both research- and clinical settings, multiplex analysis can be used to obtain better understanding of disease mechanisms, or for biomarker discovery, diagnostics, biomarker monitoring and drug studies (26-29). The Enzyme-linked Immunosorbent Assay (ELISA) is a well-established example of the quantification of proteins in clinical applications (30, 31). Proteomics allows for analyzing multiple targets in one run (32). Targeted-MS methods such as PRM can be applied to analyze multiple proteins and phosphoproteins in a single run. One of the most important advantages of PRM is the possibility to measure in parallel a larger number of peptides and their fragmented transitions. However, we should take into account that the number of peptides that can be monitored simultaneously (using PRM) has its limits (as a rule of thumb 50 to 100 peptides) (33, 34). Furthermore, technological improvement in liquid chromatography-mass spectrometry (LC-MS) in combination with retention time scheduling made it possible to measure 30–40 peptides in a fully automated single run in our experiments. The increased retention time reproducibility of LC systems and developments in MS acquisition and analysis software (automated retention time adjustments or triggered-PRM methods (35, 36)) can even further increase this number, as several research groups have shown (37-39). Therefore, it is possible to monitor phosphorylation in a selected pathway for multiple targets in a single PRM run.

This feature can promote the use of mass spectrometers for clinical applications as a multiplex platform – next to other multiplex assay possibilities (30).

Furthermore, the PRM approach examined in **Chapter 3** was used to determine the phosphorylation percentage of protein phospho-sites in other biological samples. We used formalin-fixed paraffin embedded (FFPE) and fresh-frozen (FF) normal brain tissue and glioblastoma multieforme (GBM) tissue of the same individual, respectively (**Chapter 4**). Before applying PRM, we compared the proteome and phosphoproteome profiling obtained from data-dependent acquisition (DDA) measurements of the corresponding FFPE and FF tissues. The cluster analysis of DDA measurements of these FFPE and FF tissues showed that the identified proteins and the phosphoproteins in normal brain tissue are grouped together. In GBM tissues, however, each pair of FFPE and FF tissues was grouped together. This clustering of the same tissue type probably relates to specific proteins in normal tissue and specific individual tumor tissue heterogeneity (40). Variations in protein identification might result from the probability that the GBM tissues obtained during surgical resection are different from normal brain tissue obtained at autopsy due to post mortem delay and prolonged formalin fixation. FFPE and FF sample preparations gave a corresponding result. We concluded that FFPE and FF tissue material can be compared in such a way that the fixation method does not have a large effect on variability between the FF and FFPE tissues.

To determine the technical feasibility of the PRM approach for targeted quantification of phosphopeptides in FFPE tissue, we integrated the existing sample preparation method with an optimized PRM approach for these paired FFPE and FF tissues (**Chapter 4)**. Our results show that PRM allows to sensitively measure diagnostic markers in FFPE tissues – 0.1 pg to 10 ng per 100 µg protein obtained from brain tissue for both phosphorylated and non-phosphorylated proteins – without applying extensive sample preparations such as excessive fractionation. The analyses of four non-phosphopeptides and phosphorylated peptide pairs of tissues revealed that formalin fixation does not form an obstacle to determine of the phosphorylation percentage of protein phospho-sites in FFPE tissues compared to FF tissues. We conclude that the developed PRM approach can be successfully applied to determine the phosphorylation percentage for specific phosphopeptides in different clinical samples.

Development of a novel antibody-peptide binding assay indicates the presence of immunoglobulins against EGFR phospho-site S1166 in high-grade glioma

Specific phosphopeptides from cancer-related phosphoproteins can be considered tumor-specific antigens, and could serve as valuable candidate targets for cancer-immunotherapy (2, 41). In **Chapter 5** we performed an antibody peptide antigen complex enrichment with Melon Gel resin to examine, with the use of the PRM method,

the presence of autoantibodies specific for disease-related phosphopeptides applying. Melon Gel resin has the ability to bind all serum proteins except immunoglobulin G (IgG), thereby facilitating its enrichment. The exact chemical operation of Melon Gel resin (a registered trademark of Thermo Fisher Scientific) has not been released. Yet, it was not previously reported that Melon Gel can also be used for antibody peptide antigen complex enrichment. Apparently, also antibodies bound to their peptide-antigen are not bound to the Melon Gel resin and can be collected in the flow-through after immunopurification. The main advantage of using Melon Gel resin is that the antibodies do not need pre-purification with binding to the antigen. Thus, an elution step is not needed; and the binding capacity is not limited by binding of the antigen to a surface (bead or well-plate). Furthermore, after Melon Gel resin treatment, IgG would remain fully native and accessible (42).

To demonstrate the applicability of the developed antibody-peptide assay, we tested in plasma the presence of antibodies against GBM-associated phosphopeptides. Based on results from our previous study (**Chapter 4**), we selected candidate phosphopeptides antigens from two GBM-associated proteins, namely epidermal growth factor receptor (EGFR) and glial fibrillary acidic protein (GFAP). We determined the presence of autoantibodies against an EGFR specific phosphopeptide, phosphopeptide GSHQIS[+80]LDNPDYQQDFFPK containing a phospho-site at position 1166 of the primary structure (S1166). This Ab-peptide binding assay was conducted using a phosphopeptide library made from glioma tissue with a targeted PRM readout. We found that EGFR (S1166) showed reactivity to an autoantibody present in plasma samples of two high-grade glioma patients (HGG) and not to Avastin (an irrelevant antibody blank) nor to healthy donor plasma. Furthermore, this binding assay was performed similarly for seven peptides from GFAP in five HGG plasma samples and two healthy donor plasma samples. Only three of seven phosphopeptides (EAAS[+80]YQEALAR, SVS[+80]EGHLK, and RS[+80]YVSSGEMMVGGLAPGR) could be successfully analyzed. Reactivity to an autoantibody was not observed for these GFAP phospho-sites.

To study the background of the assay, we performed an Ab-peptide binding experiment using a total peptide library with a shotgun approach to measure as many peptides as possible. We determined this background using Avastin, one HGG plasma sample and one healthy donor plasma sample. Approximately, 1% of the total peptide library (4,256) were detected in the Avastin blank sample and in each glioma and healthy donor samples. Most of these peptides (99.2%) corresponded with high or middle-abundant plasma proteins, or were highly abundant in the peptide library.

In conclusion, this Ab-peptide binding assay has been successfully applied to investigate the presence of autoantibodies reactive with HGG-related phosphopeptides.

Perspectives

The PRM approach described in this thesis is a relatively fast method to directly quantify phosphopeptides in one run, in contrast to methods which need prolonged and extra sample preparation before measurements, such as excessive fractionation, laser capture microdissection (LCM), or gel electrophoresis. The PRM approach enabled absolute quantification of phosphopeptides in cell lines and tissues with the use of SIL peptides, too. This method allows determining the percentage of phosphorylation of specific phospho-sites in biological samples such as FFPE and FF tissues in a multiplex way. FFPE tissues are the most accessible research sources in pathology archives. Therefore, this MS approach offers interesting possibilities to compare different proteins and their phosphorylation within these tissues.

Phosphorylation plays an important role in cell signaling. In disease – and in particular in cancer – this process is derailed. Our PRM approach can potentially be used for studies in which the activity of a specific pathway is monitored by protein abundance and site-specific phosphorylation ratios of targeted proteins of the chosen pathway in different diseases. (43).

Immunopurification with the use of Melon Gel resin enabled us to directly purify a peptide antigen antibody complex from plasma of HGG patients (see **Chapter 5**). This approach could potentially provide a method of discovering neoantigens and tumor-specific antigens that generate autoantibodies. In addition, it could be applied for a wide range of diseases, besides cancer, in which antibodies are involved, such as autoimmune disorders.

One of the advantages of this method is that both the antigens and antibody-parts of the antibody peptide antigen complex can be measured directly using MS.

Because of the novelty of these antigens, the sequences of these antigens are not always directly available in common protein databases. Therefore, customizing protein databases using proteomics and genomics data (proteogenomics) will provide possibilities to identify these antigens. If genomic information is present, it would be possible to affinity enrich and sequence autoantibodies using these antigens. The identification of specific autoantibodies and the corresponding antigens in patients with an autoimmune disease or cancer can be of interest for diagnosis, prognosis (44-46), drug targeting (47) and for unraveling an underlying mechanism of disease. Using this newly developed method, we can discover novel disease-associated autoantibodies and antigens, which indeed will open new ways for future diagnostic methods and developments in therapeutic interventions.

REFERENCES

1. Benvenuto, M.; Mattera, R.; Masuelli, L.; Tresoldi, I.; Giganti, M. G.; Frajese, G. V.; Manzari, V.; Modesti, A.; Bei, R., The crossroads between cancer immunity and autoimmunity: antibodies to self antigens. *Front Biosci (Landmark Ed)* **2017,** 22, 1289-1329.
2. Mahoney, K. E.; Shabanowitz, J.; Hunt, D. F., MHC Phosphopeptides: Promising Targets for Immunotherapy of Cancer and Other Chronic Diseases. *Mol Cell Proteomics* **2021,** 20, 100112.
3. Zhu, Y.; Liu, J., The Role of Neoantigens in Cancer Immunotherapy. *Frontiers in Oncology* **2021,** 11, (3396).
4. Zhao, X.; Pan, X.; Wang, Y.; Zhang, Y., Targeting neoantigens for cancer immunotherapy. *Biomarker Research* **2021,** 9, (1), 61.
5. Topalian, S. L.; Depontieu, F. A.; Hunt, D. F.; Shabanowitz, J.; Qian, J.; Engelhard, V. H.; Zarling, A. L., Phosphopeptides as melanoma vaccines. In Google Patents: 2016.
6. Johanns, T. M.; Bowman-Kirigin, J. A.; Liu, C.; Dunn, G. P., Targeting Neoantigens in Glioblastoma: An Overview of Cancer Immunogenomics and Translational Implications. *Neurosurgery* **2017,** 64, (CN_suppl_1), 165-176.
7. Ostasiewicz, P.; Zielinska, D. F.; Mann, M.; Wiśniewski, J. R., Proteome, Phosphoproteome, and N-Glycoproteome Are Quantitatively Preserved in Formalin-Fixed Paraffin-Embedded Tissue and Analyzable by High-Resolution Mass Spectrometry. *Journal of Proteome Research* **2010,** 9, (7), 3688-3700.
8. Maes, E.; Mertens, I.; Valkenborg, D.; Pauwels, P.; Rolfo, C.; Baggerman, G., Proteomics in cancer research: Are we ready for clinical practice? *Crit Rev Oncol Hematol* **2015,** 96, (3), 437-48.
9. Abbaspour, M.; Akbari, V., Cancer vaccines as a targeted immunotherapy approach for breast cancer: an update of clinical evidence. *Expert Rev Vaccines* **2022**, 1-17.
10. Richard, G.; Princiotta, M. F.; Bridon, D.; Martin, W. D.; Steinberg, G. D.; De Groot, A. S., Neoantigen-based personalized cancer vaccines: the emergence of precision cancer immunotherapy. *Expert Rev Vaccines* **2021**, 1-12.
11. Lau, S. P., Autologous dendritic cells pulsed with allogeneic tumor cell lysate induce tumor-reactive T-cell responses in pancreatic cancer patients: a phase I study. *european journal of cancer* **2022**.
12. Lau, S. P.; Klaase, L.; Vink, M.; Dumas, J.; Bezemer, K.; van Krimpen, A.; van der Breggen, R.; Wismans, L. V.; Doukas, M.; de Koning, W.; Stubbs, A. P.; Mustafa, D. A. M.; Vroman, H.; Stadhouders, R.; Nunes, J. B.; Stingl, C.; de Miranda, N. F. C. C.; Luider, T. M.; van der Burg, S. H.; Aerts, J. G.; van Eijck, C. H. J., Autologous dendritic cells pulsed with allogeneic tumour cell lysate induce tumour-reactive T-cell responses in patients with pancreatic cancer: A phase I study. *European Journal of Cancer* **2022,** 169, 20-31.
13. Singh, V.; Ram, M.; Kumar, R.; Prasad, R.; Roy, B. K.; Singh, K. K., Phosphorylation: Implications in Cancer. *Protein J* **2017,** 36, (1), 1-6.
14. Cohen, P., Protein kinases — the major drug targets of the twenty-first century? *Nature Reviews Drug Discovery* **2002,** 1, (4), 309-315.
15. Vanmechelen, E.; Vanderstichele, H.; Davidsson, P.; Van Kerschaver, E.; Van Der Perre, B.; Sjögren, M.; Andreasen, N.; Blennow, K., Quantification of tau phosphorylated at threonine 181 in human cerebrospinal fluid: a sandwich ELISA with a synthetic phosphopeptide for standardization. *Neuroscience Letters* **2000,** 285, (1), 49-52.
16. Palmisano, G.; Parker, B. L.; Engholm-Keller, K.; Lendal, S. E.; Kulej, K.; Schulz, M.; Schwämmle, V.; Graham, M. E.; Saxtorph, H.; Cordwell, S. J.; Larsen, M. R., A Novel Method for the Simultaneous Enrichment, Identification, and Quantification of Phosphopeptides and Sialylated Glycopeptides Applied to a Temporal Profile of Mouse Brain Development*. *Molecular & Cellular Proteomics* **2012,** 11, (11), 1191-1202.
17. Hogrebe, A.; von Stechow, L.; Bekker-Jensen, D. B.; Weinert, B. T.; Kelstrup, C. D.; Olsen, J. V., Benchmarking common quantification strategies for large-scale phosphoproteomics. *Nature Communications* **2018,** 9, (1), 1045.
18. Urban, J., A review on recent trends in the phosphoproteomics workflow. From sample preparation to data analysis. *Analytica Chimica Acta* **2021**, 338857.
19. Linke, D.; Koudelka, T.; Becker, A.; Tholey, A., Identification and relative quantification of phosphopeptides by a combination of multi-protease digestion and isobaric labeling. *Rapid Communications in Mass Spectrometry* **2015,** 29, (10), 919-926.
20. Low, T. Y.; Mohtar, M. A.; Lee, P. Y.; Omar, N.; Zhou, H.; Ye, M., Widening the Bottleneck of Phosphoproteomics: Evolving Strategies for Phosphopeptide Enrichment. *Mass Spectrom Rev* **2021,** 40, (4), 309-333.
21. van der Mijn, J. C.; Labots, M.; Piersma, S. R.; Pham, T. V.; Knol, J. C.; Broxterman, H. J.; Verheul, H. M.; Jiménez, C. R., Evaluation of different phospho-tyrosine antibodies for label-free phosphoproteomics. *J Proteomics* **2015,** 127, (Pt B), 259-63.
22. Egelhofer, T. A.; Minoda, A.; Klugman, S.; Lee, K.; Kolasinska-Zwierz, P.; Alekseyenko, A. A.; Cheung, M. S.; Day, D. S.; Gadel, S.; Gorchakov, A. A.; Gu, T.; Kharchenko, P. V.; Kuan, S.; Latorre, I.; Linder-Basso, D.; Luu, Y.; Ngo, Q.; Perry, M.; Rechtsteiner, A.; Riddle, N. C.; Schwartz, Y. B.; Shanower, G. A.; Vielle, A.; Ahringer, J.; Elgin, S. C.; Kuroda, M. I.; Pirrotta, V.; Ren, B.; Strome, S.; Park, P. J.; Karpen, G. H.; Hawkins, R. D.; Lieb,

J. D., An assessment of histone-modification antibody quality. *Nat Struct Mol Biol* **2011,** 18, (1), 91-3.
23. Baker, M., Reproducibility crisis: Blame it on the antibodies. *Nature* **2015,** 521, (7552), 274-6.
24. Colwill, K.; Renewable Protein Binder Working, G.; Gräslund, S., A roadmap to generate renewable protein binders to the human proteome. *Nat Methods* **2011,** 8, (7), 551-8.
25. Taussig, M. J.; Fonseca, C.; Trimmer, J. S., Antibody validation: a view from the mountains. *N Biotechnol* **2018,** 45, 1-8.
26. Robinson, R. A.; Amin, B.; Guest, P. C., Multiplexing Biomarker Methods, Proteomics and Considerations for Alzheimer's Disease. *Adv Exp Med Biol* **2017,** 974, 21-48.
27. Gao, J.; Garulacan, L. A.; Storm, S. M.; Opiteck, G. J.; Dubaquie, Y.; Hefta, S. A.; Dambach, D. M.; Dongre, A. R., Biomarker discovery in biological fluids. *Methods* **2005,** 35, (3), 291-302.
28. Tezel, G., Multiplex protein analysis for the study of glaucoma. *Expert Rev Proteomics* **2021,** 18, (10), 911-924.
29. Chen, J. Q.; Wakefield, L. M.; Goldstein, D. J., Capillary nano-immunoassays: advancing quantitative proteomics analysis, biomarker assessment, and molecular diagnostics. *J Transl Med* **2015,** 13, 182.
30. Van Gool, A.; Corrales, F.; Čolović, M.; Krstić, D.; Oliver-Martos, B.; Martínez-Cáceres, E.; Jakasa, I.; Gajski, G.; Brun, V.; Kyriacou, K.; Burzynska-Pedziwiatr, I.; Wozniak, L. A.; Nierkens, S.; Pascual García, C.; Katrlik, J.; Bojic-Trbojevic, Z.; Vacek, J.; Llorente, A.; Antohe, F.; Suica, V.; Suarez, G.; t'Kindt, R.; Martin, P.; Penque, D.; Martins, I. L.; Bodoki, E.; Iacob, B. C.; Aydindogan, E.; Timur, S.; Allinson, J.; Sutton, C.; Luider, T.; Wittfooth, S.; Sammar, M., Analytical techniques for multiplex analysis of protein biomarkers. *Expert Rev Proteomics* **2020,** 17, (4), 257-273.
31. Ling, M. M.; Ricks, C.; Lea, P., Multiplexing molecular diagnostics and immunoassays using emerging microarray technologies. *Expert Rev Mol Diagn* **2007,** 7, (1), 87-98.
32. Lin, T. T.; Zhang, T.; Kitata, R. B.; Liu, T.; Smith, R. D.; Qian, W. J.; Shi, T., Mass spectrometry-based targeted proteomics for analysis of protein mutations. *Mass Spectrom Rev* **2021**, e21741.
33. Amodei, D.; Egertson, J.; MacLean, B. X.; Johnson, R.; Merrihew, G. E.; Keller, A.; Marsh, D.; Vitek, O.; Mallick, P.; MacCoss, M. J., Improving Precursor Selectivity in Data-Independent Acquisition Using Overlapping Windows. *Journal of The American Society for Mass Spectrometry* **2019,** 30, (4), 669-684.
34. Dekker, L. J. M.; Verheul, C.; Wensveen, N.; Leenders, W.; Lamfers, M. L. M.; Leenstra, S.; Luider, T. M., Effects of the IDH1 R132H Mutation on the Energy Metabolism: A Comparison between Tissue and Corresponding Primary Glioma Cell Cultures. *ACS omega* **2022,** 7, (4), 3568-3578.
35. Gallien, S.; Bourmaud, A.; Kim, S. Y.; Domon, B., Technical considerations for large-scale parallel reaction monitoring analysis. *J Proteomics* **2014,** 100, 147-59.
36. Escher, C.; Reiter, L.; MacLean, B.; Ossola, R.; Herzog, F.; Chilton, J.; MacCoss, M. J.; Rinner, O., Using iRT, a normalized retention time for more targeted measurement of peptides. *Proteomics* **2012,** 12, (8), 1111-21.
37. Gallien, S.; Kim, S. Y.; Domon, B., Large-Scale Targeted Proteomics Using Internal Standard Triggered-Parallel Reaction Monitoring (IS-PRM). *Mol Cell Proteomics* **2015,** 14, (6), 1630-44.
38. Martinez-Garcia, E.; Lesur, A.; Devis, L.; Cabrera, S.; Matias-Guiu, X.; Hirschfeld, M.; Asberger, J.; van Oostrum, J.; Casares de Cal, M.; Gómez-Tato, A.; Reventos, J.; Domon, B.; Colas, E.; Gil-Moreno, A., Targeted Proteomics Identifies Proteomic Signatures in Liquid Biopsies of the Endometrium to Diagnose Endometrial Cancer and Assist in the Prediction of the Optimal Surgical Treatment. *Clin Cancer Res* **2017,** 23, (21), 6458-6467.
39. Woo, J.; Han, D.; Wang, J. I.; Park, J.; Kim, H.; Kim, Y., Quantitative Proteomics Reveals Temporal Proteomic Changes in Signaling Pathways during BV2 Mouse Microglial Cell Activation. *J Proteome Res* **2017,** 16, (9), 3419-3432.
40. An, Z.; Aksoy, O.; Zheng, T.; Fan, Q.-W.; Weiss, W. A., Epidermal growth factor receptor and EGFRvIII in glioblastoma: signaling pathways and targeted therapies. *Oncogene* **2018,** 37, (12), 1561-1575.
41. Zeneyedpour, L.; Sten-van, T. H. J.; Luider, T., Using phosphoproteomics and next generation sequencing to discover novel therapeutic targets in patient antibodies. *Expert Rev Proteomics* **2020,** 17, (9), 675-684.
42. Lopez, E.; Scott, N. E.; Wines, B. D.; Hogarth, P. M.; Wheatley, A. K.; Kent, S. J.; Chung, A. W., Low pH Exposure During Immunoglobulin G Purification Methods Results in Aggregates That Avidly Bind Fcγ Receptors: Implications for Measuring Fc Dependent Antibody Functions. *Front Immunol* **2019,** 10, 2415.
43. Kolch, W.; Halasz, M.; Granovskaya, M.; Kholodenko, B. N., The dynamic control of signal transduction networks in cancer cells. *Nat Rev Cancer* **2015,** 15, (9), 515-27.
44. Imafuku, Y.; Omenn, G. S.; Hanash, S., Proteomics approaches to identify tumor antigen directed autoantibodies as cancer biomarkers. *Dis Markers* **2004,** 20, (3), 149-53.
45. Caron, M.; Choquet-Kastylevsky, G.; Joubert-Caron, R., Cancer immunomics using autoantibody signatures for biomarker discovery. *Mol Cell Proteomics* **2007,** 6, (7), 1115-22.
46. Heo, C. K.; Bahk, Y. Y.; Cho, E. W., Tumor-associated autoantibodies as diagnostic and prognostic biomarkers. *BMB Rep* **2012,** 45, (12), 677-85.

47. Music, M.; Prassas, I.; Diamandis, E. P., Optimizing cancer immunotherapy: Is it time for personalized predictive biomarkers? *Crit Rev Clin Lab Sci* **2018,** 55, (7), 466-479.

7

SUMMARY
SAMENVATTING

SUMMARY

This thesis focuses on the identification and detection of phosphopeptides with the use of mass spectrometry (MS), mainly with parallel reaction monitoring (PRM). The PRM method is a high resolution and accurate targeted-MS based method that can be applied in an Orbitrap mass spectrometer. The Orbitrap mass analyzer allows the in parallel detection of multiple target product ions in one run.

In Chapter 2, one of the clinical applications of proteomics has been discussed. Due to recent developments in MS it is possible to detect somatic mutations in peptides and proteins. In this review, the possible relation between lung cancer and chronic obstructive pulmonary disease (COPD) as pre-stage of lung cancer is discussed. In lung cancer a number of these mutations are known. The risk of lung cancer is eight times higher in COPD patients. An assumption could be that COPD could be considered as a pre-stage of lung cancer. Using MS, investigating these known lung cancer-related mutations in COPD could be used to explore this possibility.

Post-translationally modified proteins such as phosphoproteins can be detected with MS. **Chapter 3** describes a targeted MS method to determine a site-specific phosphorylation ratio in phosphoproteins. Two PRM approaches – direct-PRM (tryptic digested samples measured with PRM) and TiO_2-PRM (phospho-enriched sample using TiO_2 cartridges after digestion and measured with PRM) – were applied to quantify the phosphorylation ratio for three phospho-sites in neuroblast differentiation-associated protein (AHNAK S5480-p), calcium/calmodulin-dependent protein kinase type II subunit delta (CAMK2D T337-p), and epidermal growth factor receptor (EGFR S1166-p). These two approaches were applied on U87 cells (a glioblastoma cell line). A reproducible phosphorylation percentage of 7.3, 2.5 and 11.5% could be determined for all three phosphopeptides AHNAK, CAMK2D and EGFR, respectively, and CV values for phosphorylation percentage of 12.0, 6.4 and 13.1% for the entire approach were obtained, respectively. To validate the PRM approaches, a cell-culture experiment was performed in which U87 cells were deprived from medium containing serum, which allows examining the effect of serum starvation on the phosphorylation ratio. For both EGFR and AHNAK, analyses revealed statistically significant changes in phosphorylation levels due to serum starvation (p value < 0.05). The PRM method can be multiplexed to measure different phosphopeptide targets in one run.

Formalin-fixed paraffin-embedded (FFPE) tissues are valuable research sources. In medical centers, such tissues are regularly prepared and collected for diagnostic purposes. Therefore, FFPE tissues are the most available biological sources in pathology archives. In **Chapter 4**, the same PRM strategies as in **Chapter 3** were used to determine

the site-specific phosphorylation ratio in proteins in FFPE and corresponding FF tissue. Using these two strategies, the phosphorylation ratio could be determined for four selected peptide pairs that originate from the same selected proteins in **Chapter 3** and in addition the eukaryotic translation initiation factor 4B (EIF4B S93-p). In normal brain tissue and glioblastoma multiforme tissue, the PRM method allowed to sensitively measure diagnostic markers in FFPE tissues: 0.1 pg to 10 ng per 100 µg tissue protein for both phosphorylated and non-phosphorylated proteins. In each FF or FFPE tissue, the calculated phosphorylation ratio had a maximum CV of 14.2% for AHNAK, of 7.3% for CAMK2D, and of 12.3% for EIF4B. On the basis of the obtained results in a sample of four non-phosphopeptides and phosphorylated peptide pairs, we concluded that formalin fixation does not interrupt or inhibit relative quantification of phospho-sites in FFPE tissues compared to FF materials. This developed PRM method can be successfully applied to the most accessible archival material, FFPE tissues, to determine the phosphorylation ratio in proteins.

Specific phosphopeptides in cancer-related phosphoproteins can be considered as a possible novel class of tumor-associated antigens. In **Chapter 5**, we investigated an antibody-peptide assay which indicates the presence of a specific autoantibody against a potential phospho-bound antigen (EGFR) by enriching the antibody-peptide complex using Melon Gel resin. Our goal was to find tumor-specific phosphopeptides that can raise autoantibodies that are detectable in plasma of glioma patients using MS. As proof of concept, we successfully applied the method to dinitrophenyl (DNP) labelled α-casein mixed with anti-DNP antibodies. Subsequently, we incubated patient samples (plasma) with a peptide library (i.e., a tryptic phosphopeptide fraction of tumor tissue) followed by Melon Gel immunopurification and separation of IgG bound peptides. We selected one EGFR and 7 GFAP phosphopeptides as targets for the Ab-peptide binding assay. The selected EGFR phosphopeptide was GSHQIS[+80]LDNPDYQQDFFPK (phosphorylated S1166-p). Autoantibodies binding this phosphopeptide were detected in plasma from high-grade glioma (HGG) patients but not in healthy donor plasma. No autoantibodies reactive with any of the 7 GFAP phosphopeptides were detected in HGG plasma.

In conclusion, we developed an IgG purification method using Melon Gel resin that allows separation of IgG bound peptides followed by detection of the antibody bound peptides with MS applying a shotgun and PRM method. This approach can be used to study antigens including phosphopeptides in diseases such as cancer and autoimmune diseases.

SAMENVATTING

Dit proefschrift beschrijft hoe fosfopeptiden geïdentificeerd en gedetecteerd kunnen worden met behulp van massaspectrometrie (MS), voornamelijk door parallelle reactie monitoring (PRM). De PRM methode is een nauwkeurige MS methode met hoge resolutie die kan worden toegepast in een Orbitrap massaspectrometer. De Orbitrap maakt het mogelijk om meerdere product ionen in één run parallel te detecteren en te kwantificeren.

In **Hoofdstuk 2** wordt één van de klinische toepassingen van proteomics beschreven. Recente ontwikkelingen in MS maken het mogelijk om somatische mutaties in peptiden en eiwitten te detecteren. In dit hoofdstuk wordt de mogelijke relatie tussen longkanker en chronische obstructieve longziekte (COPD) als een voorstadium van kanker besproken. Een aantal van deze mutaties zijn in longkanker te vinden. Het risico om longkanker te krijgen is acht keer hoger in COPD patiënten. Men kan veronderstellen dat COPD kan worden beschouwd als een voorstadium van longkanker. Door gebruik te maken van MS kunnen deze bekende longkanker-gerelateerde mutaties in COPD worden onderzocht.
Posttranslationeel gemodificeerde eiwitten, zoals fosfo-eiwitten kunnen met MS worden gedetecteerd. **Hoofdstuk 3** beschrijft een MS methode om een plaats specifieke fosforylering ratio in fosfo-eiwitten te bepalen. Twee PRM methodes – directe PRM (tryptisch gedigesteerde monsters) en TiO_2-PRM (fosfo-verrijkt monster gebruikmakend van TiO_2 cartridges na digestie) – zijn toegepast om de fosforylering ratio te kwantificeren voor drie fosforyleringsplaatsen in neuroblast differentiation-associated protein (AHNAK S5480-p), calcium/calmodulin-dependent protein kinase type II subunit delta (CAMK2D T337-p), and epidermal growth factor receptor (EGFR S1166-p). Voor beide methodes werden U87 cellen gebruikt (een glioblastoma cellijn). Voor alle drie fosfopeptiden AHNAK, CAMK2D en EGFR was het mogelijk een reproduceerbaar fosforylering percentage van, respectievelijk, 7.3, 2.5 en 11.5% te bepalen. Voor deze fosforyleringsplaatsen werd een CV (relatieve variatie) van, respectievelijk, 12.0, 6.4 en 13.1% verkregen. Om validatie van deze PRM methodes mogelijk te maken werd een experiment uitgevoerd waarin serum uit het medium van U87 cellen werd gehaald om het effect te meten van het afsterven van cellen op de fosforylering ratio. Zowel voor EGFR als voor AHNAK werden statistisch significante veranderingen in fosforylering niveaus waargenomen als gevolg van de afwezigheid van serum (p waarde < 0.05). De PRM methode maakt het mogelijk om door een multiplex meting meerdere fosfopeptiden in één keer te meten.

Formaline gefixeerd in paraffine ingebed (FFPE) weefsel is een waardevolle bron voor research. In ziekenhuizen wordt dergelijk weefsel regelmatig gebruikt voor diagnostische doeleinden en daarna verzameld voor onderzoeksdoeleinden. FFPE weefsel is daarom

het meest aanwezig in pathologie archieven. In **Hoofdstuk 4** wordt dezelfde PRM strategie toegepast als in **Hoofdstuk 3** teneinde de plaats specifieke fosforylering ratio van eiwitten in FFPE en overeenkomend FF weefsel te bepalen. Gebruik makend van dezelfde strategieën kon de fosforylering ratio worden bepaald voor vier geselecteerde peptiden uit dezelfde eiwitten als in **Hoofdstuk 3** en eveneens voor de eukaryotic translation initiation factor 4B (EIF4B S93-p). In normaal hersenweefsel en in glioblastoma weefsel was het mogelijk met de PRM methode diagnostische markers in FFPE weefsel gevoelig te meten: 0.1 pg tot 10 ng per 100 µg weefsel eiwit voor zowel gefosforyleerde als voor niet-gefosforyleerde eiwitten. De berekende fosforylering ratios in elk FF of FFPE weefsel hadden een maximum CV van 14.2% voor AHNAK, 7.3% voor CADMK2D en 12.3% voor EIF4B. Op basis van de behaalde resultaten in een monster van vier niet-fosfopeptiden en fosfo-gerelateerde peptiden kunnen wij concluderen dat formaline fixatie de relatieve kwantificering van fosforyleringsplaatsen in FFPE weefsel niet verstoord of geremd heeft in vergelijking tot FF materiaal. Om de fosforyleringsratio in eiwitten te bepalen kan deze ontwikkelde PRM methode succesvol worden toegepast in toegankelijke FFPE archieven.

Specifieke fosfopeptiden in kanker-gerelateerde eiwitten kunnen als een mogelijke nieuwe groep van tumor-geassocieerde antigenen worden beschouwd. In **Hoofdstuk 5** hebben wij een antilichaam-peptide methode onderzocht waarin de aanwezigheid van een specifiek antilichaam tegen een mogelijk fosfo-gebonden antigen (EGFR) wordt aangetoond door het antilichaam-peptide complex te verrijken met Melon Gel™ resin. Wij beoogden in de massaspectrometer tumor-specifieke fosfopeptiden te vinden die autoantilichamen induceren in plasma van glioma patiënten. Om dit te bewijzen hebben wij deze methode succesvol toegepast bij dinitrophenyl (DNP) gelabeld α-casein gemengd met anti-DNP antilichamen. Vervolgens hebben wij plasma monsters geïncubeerd met een weefselbibliotheek van peptiden (i.e. een tryptische fosfopeptide fractie van tumorweefsel) gevolgd door immunopurificatie en scheiding van IgG-gebonden peptiden. Wij selecteerden één EGFR en zeven GFAP fosfo-peptiden om de Ab-peptide gebonden methode toe te passen. De geselecteerde EGFR fosfopeptide was GSHQIS[+80]LDNPDYQQDFFPK (gefosforyleerd S1166-p). Autoantilichamen die zich binden aan deze fosfopeptide werden gevonden in plasma van patiënten met glioma (HGG), maar niet in gezond donor plasma. In HGG plasma werden geen autoantilichamen gevonden die met één van de zeven GFAP fosfopeptiden reageerden.

Concluderend, wij hebben een IgG zuivering methode met Melon Gel™ ontwikkeld die het mogelijk maakt om IgG gebonden peptiden te isoleren, gevolgd door detectie van deze antilichaam-gebonden peptiden gebruikmakend van MS met toepassing van een shotgun en PRM methode. Deze benadering kan worden gebruikt om antigenen te bestuderen, evenals fosfopeptiden in ziektes zoals kanker en auto-immuunziektes.

A

AKNOWLEDGEMENTS
LIST OF PUBLICATIONS
PHD PORTFOLIO
BIOGRAPHY

ACKNOWLEDGEMENTS

Het is zover. Het is mij gelukt om mijn doel te bereiken. Dit proefschrift is mede mogelijk gemaakt door de medewerking van vele collega's en dierbaren en ik ben blij dat ik de kans krijg om deze mensen te bedanken.

Mijn co-promotor dr. Luider, beste Theo, ik ben ontzettend dankbaar voor alle mogelijkheden die je mij hebt geboden. Het begon met jouw telefoontje voor de kerst in 2008 waarin ik hoorde dat ik was aangenomen. Het is het beste kerstcadeau die ik ooit heb gekregen en het heeft mijn leven een totaal andere richting gegeven door de weg naar het onderzoek te openen. Naast onze werk-gerelateerde besprekingen heb ik veel genoten van onze gesprekken over de Nederlandse taal en geschiedenis.

Mijn promotor prof. dr. Sillevis Smitt, beste Peter, ik wil je bedanken voor de mogelijkheid om mijn PhD onderzoek binnen de afdeling Neurologie uit te voeren.

Beste prof. dr. Gooijer, beste Cees, ik ben heel dankbaar voor de mogelijkheid die ik heb gekregen om gedurende zes maanden in jouw groep onderzoek te doen.

Graag wil ik de promotiecommissie bedanken voor het lezen en beoordelen van dit proefschrift.

Aan alle co-auteurs, mede door jullie bijdrage is dit proefschrift tot stand gekomen. Dank voor de prettige samenwerking.

Beste Christoph, dank voor alle leerzame en leuke samenwerking vanaf de eerste dag. We hebben samen heel veel MS metingen gedaan en de laatste publicatie was één van de vruchten daarvan. Je bent ook bezig met je promotieonderzoek en ik wens je heel veel succes.

Beste Martijn, dankzij jouw brede kennis over biochemie en immunologie kon ik bij jou terecht met vragen over antilichamen en je was altijd bereid om deze vragen te beantwoorden. Dank daarvoor.

Beste Coskun, behalve werkbesprekingen, vooral over weefsels, hadden we ook altijd leuke gespreken op het gebied van cultuur en taal.

Beste Peter (Burgers), je bent inmiddels met pensioen, maar je komt af en toe naar onze afdeling. Je was één van de eerste collega's die ik heb ontmoet en je was altijd bereid om mijn vragen op het gebied van MS te beantwoorden.

Dear Dana, I am very happy that I met you at Erasmus MC. You always offered help and encouraged me to go on. Besides that, I enjoyed many conversations in our mother language.

Beste Eric, jouw aanwezigheid betekende voor mij dat IT problemen verleden tijd zijn. Dank dat je altijd bereid was deze problemen op te lossen.

Beste Lennard, Linda, Nick, Marina, Diana, Somayya, Marcel (Stoop), Dominque, Ingrid, Sadaf, Vaibhav, Giovanny, Azadeh, Gero, Roland, Yesim en alle andere oud collega's en stagiaires, ook jullie wil ik bedanken voor alle medewerking, leuke discussies en gezellige borrels en congressen.

Beste collega's van de groep neuro-oncologie, Pim, Mariska, Iris en Maurice voor jullie hulp tijdens het gebruik van onze gezamenlijke lab faciliteiten.

Van de afdeling Pathologie, beste Marcel (van der Weiden) en Thierry, bedankt voor jullie hulp bij het snijden van de weefselcoupes.

Beste dr. van Sten, beste Jenny, dank dat je samen met Roos naast mij wil staan als mijn paranimf. Ontzettend bedankt voor jouw onvoorwaardelijk hulp.

Beste Nederlandse familie, beste Oma en Esther, onze vriendschap is in de loop van de tijd alleen maar sterker geworden. Ik ben heel dankbaar voor jullie aanwezigheid in ons leven.

Lieve mama en baba, Lieve Hona, Feryal, Meysoun en Reza dank voor jullie steun. Ik weet dat jullie heel trots op me zijn.

Lieve Hamid, dit proefschrift is eigenlijk ook van jou. Dank voor jouw steun, geduld en begrip tijdens mijn promotieonderzoek. Dank voor je vertrouwen in mij. Lieve Roos, jij ook heel veel dank voor je begrip. Ik vind het ontzettend leuk dat je tijdens promotie naast mij staat. Jij houdt van biologie en misschien ga je ooit jouw eigen onderzoekstraject volgen. Mama is trots op je. Ik ben heel blij en dankbaar voor jullie aanwezigheid in mijn leven. Ik hou ontzettend van jullie.

LIST OF PUBLICATIONS

Zeneyedpour L, Stingl C, Kros JM, Sillevis Smitt, PAE, Luider TM. Novel antibody-peptide binding assay indicates presence of immunoglobulins against EGFR phospho-site S1166 in high-grade glioma, Int. J. Mol. Sci. 2022, 23(9):5061.

Zeneyedpour L, Stingl C, Dekker LJM, Mustafa DAM, Kros JM, Luider TM. Phosphorylation Ratio Determination in Fresh-Frozen and Formalin-Fixed Paraffin-Embedded Tissue with Targeted Mass Spectrometry. J Proteome Res. 2020, 19(10):4179-4190.

Zeneyedpour L, Dekker LJM, van Sten-van T Hoff JJM, Burgers PC, Ten Hacken NHT, Luider TM. Neoantigens in Chronic Obstructive Pulmonary Disease and Lung Cancer: A Point of View. Proteomics Clin Appl. 2019, 13(2):e1800093.

Dekker LJM, **Zeneyedpour L**, Snoeijers S, Joore J, Leenstra S, Luider TM. Determination of Site-Specific Phosphorylation Ratios in Proteins with Targeted Mass Spectrometry. J Proteome Res. 2018, 17(4):1654-1663.

Mustafa DAM, Saida L, Latifi D, Wismans LV, de Koning W, **Zeneyedpour L**, Luider TM, van den Hoogen B, van Eijck CHJ. Rintatolimod Induces Antiviral Activities in Human Pancreatic Cancer Cells: Opening for an Anti-COVID-19 Opportunity in Cancer Patients? Cancers (Basel). 2021, 13(12):2896.

Zeneyedpour L, Sten-van T Hoff J, Luider T. Using phosphoproteomics and next generation sequencing to discover novel therapeutic targets in patient antibodies. Expert Rev. Proteomics. 2020, 17(9):675-684.

Nascimento-Carvalho GC, Nascimento-Carvalho EC, VanDuijn MM, Ramos CL, Vilas-Boas AL, Moreno-Carvalho OA, **Zeneyedpour L**, Ferwerda G, de Groot R, Luider TM, Nascimento-Carvalho CM. Cerebrospinal fluid immunoglobulins are increased in neonates exposed to Zika virus during foetal life. J Infect. 2020, 80(4):419-425.

Rodríguez-Blanco G, **Zeneyedpour L**, Duijvesz D, Hoogland AM, Verhoef EI, Kweldam CF, Burgers PC, Smitt PS, Bangma CH, Jenster G, van Leenders GJLH, Dekker LJM, Luider TM. Tissue proteomics outlines AGR2 AND LOX5 as markers for biochemical recurrence of prostate cancer. Oncotarget. 2018, 9(92):36444-36456.

Mustafa DAM, Pedrosa RMSM, Smid M, van der Weiden M, de Weerd V, Nigg AL, Berrevoets C, **Zeneyedpour L**, Priego N, Valiente M, Luider TM, Debets R, Martens JWM, Foekens JA, Sieuwerts AM, Kros JM. T lymphocytes facilitate brain metastasis of breast

cancer by inducing Guanylate-Binding Protein 1 expression. Acta Neuropathol. 2018, 135(4):581-599.

Venkatesan S, Hoogstraat M, Caljouw E, Pierson T, Spoor JK, **Zeneyedpour L**, Dubbink HJ, Dekker LJ, van der Kaaij M, Kloezeman J, Berghauser Pont LM, Besselink NJ, Luider TM, Joore J, Martens JW, Lamfers ML, Sleijfer S, Leenstra S. TP53 mutated glioblastoma stem-like cell cultures are sensitive to dual mTORC1/2 inhibition while resistance in TP53 wild type cultures can be overcome by combined inhibition of mTORC1/2 and Bcl-2. Oncotarget. 2016, 7(36):58435-58444.

Hassing RJ, Goessens WH, **Zeneyedpour L**, Sultan S, van Kampen JJ, Verbon A, van Genderen PJ, Hays JP, Luider TM, Dekker LJ. Detection of amino acid substitutions in the GyrA protein of fluoroquinolone-resistant typhoidal Salmonella isolates using high-resolution mass spectrometry. Int J Antimicrob Agents. 2016, 47(5):351-6.

Singh V, Stingl C, Stoop MP, **Zeneyedpour L**, Neuteboom RF, Smitt PS, Hintzen RQ, Luider TM. Proteomics urine analysis of pregnant women suffering from multiple sclerosis. J Proteome Res. 2015, 14(5):2065-73.

Maat P, VanDuijn M, Brouwer E, Dekker L, **Zeneyedpour L**, Luider T, Smitt PS. Mass spectrometric detection of antigen-specific immunoglobulin peptides in paraneoplastic patient sera. J Autoimmun. 2012, 38(4):354-60.

Dekker LJ, **Zeneyedpour L**, Brouwer E, van Duijn MM, Sillevis Smitt PA, Luider TM. An antibody-based biomarker discovery method by mass spectrometry sequencing of complementarity determining regions. Anal Bioanal Chem. 2011, 399(3):1081-91.

VanDuijn MM, Dekker LJ, **Zeneyedpour L**, Smitt PA, Luider TM. Immune responses are characterized by specific shared immunoglobulin peptides that can be detected by proteomic techniques. J Biol Chem. 2010, 285(38):29247-53.

PhD PORTFOLIO

Name PhD student:	Lona Zeneyedpour
	Erasmus MC department: Neurology
PhD period:	September 2017 – September 2022
Promotor:	Prof. Dr. P.A.E. Sillevis Smitt
Co-promotor:	Dr. T.M. Luider

Conferences (19.6 ECT)

Year	Topic	ECTs
2010	American Society of Mass spectrometry	2.1
2011	Late summer practical proteomics seminar	1.3
2012	6th Summer School Mass Spectrometry in Biotechnology and Medicine	2.4
2012	American Society of Mass spectrometry	2.1
2014	American Society of Mass spectrometry	2.1
2016	American Society of Mass spectrometry	2.1
2016	Landelijke werkgroep neuro-oncologie (LWNO) annual meeting	1.3
2017	Human Proteome Organization	2.1
2020	American Society of Mass spectrometry	2.1
2017-2022	JNI lectures + oral	2.0

Courses (8.15 ECT)

Year	Topic	ECTs
2010	ASMS-Mass Spectrometry of peptides and proteins	0.6
2010	Workshop Photoshop and Illustrator CS5	0.25
2011	The basic introduction course on SPSS	0.6
2012	ASMS-Case studies in quantitative proteomics	0.6
2013	The workshop on Microsoft Excel 2010: Basic	0.3
2014	The workshop on Microsoft Excel 2010: Advanced	0.4
2014	ASMS-Practical LC-MS Troubleshooting	0.6
2015	Course in English biomedical writing and communication	3.0
2016	The course on R	1.4
2016	The workshop Ingenuity pathway analysis (IPA)	0.5
2020	Research integrity	0.3

Teaching (12 ECT)

Year	Topic	ECTs
2020	Department research presentation	2.0
2020	Supervision Bachelor internship	4.0
2021	Supervision Bachelor internship	4.0
2017-2022	General training students	2.0

BIOGRAPHY

Lona Zeneyedpour was born on 7th of June, 1972 in Ahvaz, located in Southwestern Iran. Despite the Iran-Iraq war (1980-1988) she has completed her secondary school in 1990. One year later she started with her study Chemistry at Shahid Chamran University, Ahvaz. In 1995, she received her bachelor's degree in Pure Chemistry. In 1997, she moved to Tehran to start her Master study. In 1999, she obtained her Master degree in Inorganic Chemistry entitled: "Synthesis and structure determination of new complexes based on cadmium nitrate" at Iran University of Science & Technology, Tehran. During this period, two new complexes $[Cd(MeUrea)_6](NO_3)_2$ and $[Cd(phen)_2](NO_3)_2$ were synthesized and their structures were determined by single-Crystal X-ray diffraction method.

In 2000, she immigrated to the Netherlands and settled in Delft to begin a new life. On March 2008, she worked for six month at the Vrije Universiteit Amsterdam, as a guest researcher, in the group of Analytical Chemistry and Applied Spectroscopy under supervising of Prof. Cees Gooijer. In 2009, she started working as a research technician in the Maarten van Sten laboratory at the Neurology department, Erasmus MC. She participated in many proteomics-related projects. In 2017, she got the opportunity to continue her education (her ambition) to start a PhD project under guidance of Prof. Dr. Peter A.E. Sillevis Smitt and Dr. Theo M. Luider. Her PhD project was focused on glioblastoma, the characterization of phosphopeptide identification in this tumor and the possibility that auto-antibodies can develop to tumor-specific phosphopeptides found in her study.

During a Dutch language course in 2003 in The Hague, she met Hamidreza Moradi with whom she is blissfully married and they are the proud parents of their daughter Roos.